Master's thesis

NTNU
Norwegian University of Science and Technology
Faculty of Natural Sciences
Department of Biotechnology and Food Science

Martha Grøndahl

Cytocompatibility and Functionalization of Nanocellulose for Bone Tissue Engineering Applications

Master's thesis in Chemical Engineering and Biotechnology
Supervisor: Kristin Syverud, Ellinor Bævre Heggset, Ahmad Rashad and Berit Løkensgård Strand
June 2019

NTNU
Norwegian University of Science and Technology

PFI
PART OF RI.SE

Martha Grøndahl

Cytocompatibility and Functionalization of Nanocellulose for Bone Tissue Engineering Applications

Master's thesis in Chemical Engineering and Biotechnology
Supervisor: Kristin Syverud, Ellinor Bævre Heggset, Ahmad Rashad and Berit Løkensgård Strand
June 2019

Norwegian University of Science and Technology
Faculty of Natural Sciences
Department of Biotechnology and Food Science

NTNU
Norwegian University of
Science and Technology

Preface

This master thesis was conducted as a part of the study program 'Chemical Engineering and Biotechnology' at the Department of Biotechnology and Food Science at the Norwegian University of Science and Technology (NTNU). The master thesis was a continuation of a specialization project conducted autumn 2018 and both the master and specialization project were performed in collaboration with RISE PFI. Some parts of this master thesis were written for the specialization project report. This includes most parts of Section 1, while for the other parts this applies to, I have chosen to continuously specify if the text was obtained from the specialization project report.

I would like to thank my supervisors at RISE PFI, Ellinor Bævre Heggset and Kristin Syverud. I am very thankful that they entrusted me with this work and their help throughout the process. I am also greatful that they made this work possible by introducing me to their contacts in both France and Bergen. On that notion, I would like to thank Julien Bras and Bastien Michel for welcoming me to LGP2 in Grenoble and for teaching me about grafting of β-Cyclodextrin to nanocellulose. I would also like to thank my co-supervisor Ahmad Rashad from the Department of Clinical Dentistry, University of Bergen. I am grateful for everything he taught me, both in the laboratory and during the writing process. I would like to thank Berit Løkensgård Strand for being my co-supervisor from NTNU. I have greatly appreciated her feedback and thoughts on my work. Last but not least, I would like to thank Per Olav Johnsen, Johnny Kvakland Melbø and Birgitte Hjelmeland McDonagh for their technical support.

Abstract

In the following master thesis, surface properties of nanocellulose gels as a scaffold material were explored for bone tissue engineering (BTE) applications. Nanocellulose is a material of great interest within many applications, where attractive properties within BTE include the possibility of forming strong gels and porous structures, and more importantly, nanocellulose is non-toxic and non-immunogenic inside the human body.

2,2,6,6-Tetramethylpiperidinyloxy (TEMPO)-mediated oxidation is a way of introducing carboxylate and aldehyde functional groups on the surface of cellulose fibers. It is considered as a promising route to customize the properties of nanocellulose gels. One of the main goals for this master thesis was to evaluate the effect of the aldehyde groups introduced on cellulose nanofibrils (CNFs) by TEMPO-mediated oxidation, on the cytocompatibility of CNFs in regards to *in vitro* cell viability, morphology, proliferation and osteogenic differentiation. TEMPO-oxidized CNFs without aldehyde groups were obtained by two different treatments; either through $NaClO_2$-oxidation or $NaBH_4$-reduction. The cytocompatibility studies were performed by culturing rat bone marrow stem cells (rBMSCs) on nanocellulose coated tissue culture plates (TCPs) where cells cultured on uncoated TCPs were used as controls.

Another goal for this master thesis was to characterize the nanocellulose materials used for the cytocompatibility studies. A spectrophotometric method was used to confirm the differences in aldehyde contents for the three different CNF samples, in addition, other material properties were characterized, such as the carboxyl content, degree of fibrillation, ζ-potential, contact angle and protein adsorption properties. A bacterial nanocellulose (BNC) sample was also included in the cytocompatibility studies, in order to compare the CNF qualities towards a material which have shown good properties as a scaffold material for different tissue engineering applications. Material properties of the BNC sample were therefore also evaluated.

The characterization of the TEMPO-oxidized quality (TO-CNF), TEMPO-oxidized and further oxidized quality (TO-O-CNF) and TEMPO-oxidized and further reduced quality (TO-R-CNF) showed that neither the TO-O-CNF or TO-R-CNF samples contained detectable amounts of aldehyde groups. The BNC sample showed no traces of aldehyde groups either, while the TO-CNF sample contained 280 ± 14 μmol/g aldehyde groups. The TO-O-CNF sample contained the highest amount of carboxyl groups (992 ± 24 μmol/g), followed by TO-CNF (804 ± 3 μmol/g) and TO-R-CNF (675 ± 14 μmol/g). The TO-O-CNF quality was significantly less fibrillated compared to the other two CNF samples. The ζ-potentials of the three CNF qualities in water were similar to each other, while the BNC sample had a lower ζ-potential compared to the CNF qualities. The BNC sample also had a lower water contact angle compared to the CNF samples, in addition to poorer protein adsorption properties when 10 % FBS in α-MEM medium was used as a protein solution.

The cytocompatibility of the CNF qualities in regards to cell viability and morphology were similar to each other and to the control group. All CNF qualities supported limited cell proliferation and osteogenic differentiation when compared to the control group. However, they still showed similar properties to each other, which implies that it does not make a difference if the aldehyde groups are removed from TEMPO-oxidized CNFs. The BNC material was not

toxic to the cells, however, the CNF samples provided a better surface for early cell attachment and morphology. In addition, the CNF qualities provided better surfaces for cell mineralization.

The last main goal was to functionalize TEMPO-oxidized CNFs by β-cyclodextrin (βCD) grafting. For clarification, grafting is used to describe either covalent or non-covalent binding of βCD to the CNFs. For nanocellulose scaffolds, growth factor (GF) availability at the site of tissue regeneration can be achieved by incorporating GFs in the scaffold material. This can be achieved by grafting the scaffold with βCD and further use the βCD to encapsulate other GFs. Determining a method to functionalize βCD to TEMPO-oxidized CNFs was not completed. Fourier transform infrared spectroscopy (FTIR) analysis could indicate the presence of grafted βCD after certain treatments. However, new grafting and verification methods should be tested.

Sammendrag

I denne masteroppgaven er overflateegenskaper til nanocellulosegeler som armering (scaffold) innenfor benvevsregenererings (BVR) applikasjoner utforsket. Nanocellulose er et materiale av stor interesse innenfor mange applikasjoner, der de mest ettertraktede egenskapene innenfor BVR inkluderer evnen til å danne sterke geler, porøse strukturer samt at nanocellulose er ikke-toksisk og kan unngå immunologiske reaksjoner *in vivo*.

2,2,6,6-Tetramethylpiperidinyloxy (TEMPO)-katalysert oksidering er en måte å introdusere karboksyl- og aldehyd-grupper på overflaten av cellulosefiber. TEMPO-oksidering er ansett som en lovende måte å tilpasse egenskapene til nanocellulosegeler. Et av hovedmålene med denne masteroppgaven var å evaluere effekten av aldehydgrupper introdusert på cellulose nanofibriller (CNF) ved TEMPO-katalysert oksidering, med fokus på cytokompatibiliteten til CNF i forbindelse med *in vitro* cellelevedyktighet, morfologi, vekst og osteogen differensiering. TEMPO-oksidert CNF uten aldehydgrupper ble produsert ved bruk av to ulike metoder; enten $NaClO_2$-oksidering eller $NaBH_4$-reduksjon. Cytokompatibilitetsstudiene ble utført ved å kulturere stamceller fra benmargen til rotter i kulturplate-brønner dekket med nanocellulose. Celler dyrket direkte i kulturplate-brønnene uten nanocellulose ble brukt som kontrollgrupper.

Et annet mål med masterprosjektet var å karakterisere nanocellulosematerialene som ble brukt i cytokompatibilitetsstudiet. En spektrofotometrisk metode ble brukt for å bekrefte ulikheter i aldehydinnhold for de tre CNF-prøvene produsert. I tillegg ble andre egenskaper med CNF-kvalitetene karakterisert, deriblant karboksylinnhold, fibrilleringsgrad, ζ-potensiale, kontaktvinkel og proteinadsorberingsegenskaper. En prøve med bakteriell nanocellulose (BNC) ble også inkludert i cytokompatibilitetsstudiene, for å ha mulighet til å sammenligne CNF-prøvene med et materiale som har vist gode egenskaper som scaffoldmateriale innenfor ulike vevsregenereringsapplikasjoner. Materialegenskaper for BNC-prøven ble derfor også evaluert.

Karakteriseringen av den TEMPO-oksiderte kvaliteten (TO-CNF), TEMPO-oksiderte og videre oksiderte kvaliteten (TO-O-CNF) og TEMPO-oksiderte og videre reduserte kvaliteten (TO-R-CNF) viste at verken TO-O-CNF eller TO-R-CNF inneholdt målbare mengder av aldehydgrupper. BNC-prøven inneholdt heller ingen spor av aldehydgrupper, mens TO-CNF-prøven inneholdt 280 ± 14 μmol aldehyd/g. Når det gjelder karboksyllinnhold hadde TO-O-CNF-prøven det høyeste innholdet (992 ± 24 μmol/g), etterfulgt av TO-CNF (804 ± 3 μmol/g) og TO-R-CNF (675 ± 14 μmol/g). TO-O-CNF-kvaliteten var betydelig mindre fibrillert i forhold til de to andre CNF-kvalitetene. ζ-potensialet til de tre CNF-kvalitetene i vann var tilsvarende hverandre, mens BNC-prøven hadde lavere ζ-potensiale. BNC-prøven hadde også lavere kontaktvinkel, målt med vann, i forhold til CNF-prøvene, samt dårligere proteinadsorberingsegenskaper når 10 % FBS i α-MEM medium ble brukt som proteinløsning.

Cytokompatibiliteten til CNF-kvalitetene med tanke på cellelevedyktighet og morfologi var tilsvarende hverandre, samt kontrollgruppen. Når det gjaldt cellevekst og celledifferensiering viste CNF-kvalitetene derimot dårligere egenskaper sammenlignet med kontrollgruppen. De tre CNF-kvalitetene viste totalt sett lignende egenskaper, noe som tyder på at fjerning av aldehydgrupper fra TEMPO-oksidert CNF har liten effekt. BNC-materialet viste ingen toksiske egenskaper, men sammenlignet med CNF-kvalitetene viste det seg at BNC-prøven hadde

dårligere evne til å stimulere normal binding av cellene til BNC-overflaten, inkludert normal cellemorfologi. I tillegg stimulerte CNF-prøvene cellemineralisering i større grad enn BNC-prøven.

Det siste hovedmålet med masteroppgaven var å funksjonalisere TEMPO-oksidert CNF ved å kovalent binde, eller absorbere, β-cyklodekstrin (βCD). Motivasjonen for å oppnå βCD bundet til CNF er at βCD kan innkapsle andre molekyler som vekstfaktorer (VFer). Det kan sikre at VFer er tilgjengelig på vevsregenreringsområdet der scaffold-materialet er, som vil være nyttig ettersom VFer ofte kreves for å danne nytt vev. Å finne en metode for å oppnå βCD bundet til TEMPO-oksidert CNF ble ikke fullført. Fourier transform infrarød spektroskopi (FTIR) indikerte βCD bundet til CNF-materialet etter enkelte behandlinger. Likevel bør andre metoder for å oppnå βCD bundet til CNF, samt andre metoder for å verifisere dette undersøkes.

Contents

List of Figures

List of Tables

List of abbreviations and symbols

AFM	Atomic Force Microscopy
ALP	Alkaline phosphatase
ARS	Alizarin red S
ATR	Attenuated total reflection
βCD	β-cyclodextrin
BNC	Bacterial nanocellulose
BSA	Bovine serum albumin
(B)TE	(Bone) tissue engineering
CD	Cyclodextrin
CNCs	Cellulose nanocrystals
CNFs	Cellulose nanofibrils
COH	Aldehyde groups
COO^-	Carboxylate groups
DAPI	4,6-diamidino-2-phenylindole
DMSO	Dimetylsulfoxid
ECM	Extracellular matrix
FBS	Fetal bovine serum
FTIR	Fourier Transform Infrared
HPH	High-pressure homogenisation
KI	Potassium iodide
LDH	Lactate dehydrogenase
L/D	Live/dead
NMR	Nuclear Magnetic Resonance
NS	Not significant
OH	Hydroxyl groups
ON	Over night
PBS	Dulbecco's Phosphate Buffered Saline

$\mathbf{R}_a$	Average surface roughness
(r)BMSC	(rat) Bone marrow mesenchymal stem cells
$\mathbf{R}_f$	Residual fiber fraction
RH	Relative humidity
R-oven	Regular oven
RT	Room temperature
SD	Standard deviation
SDS	Sodium dodecyl sulfate
SPR	Specialization project report
TCP	Tissue culture plate
TEMPO	2,2,6,6-Tetramethylpiperidinyloxy
TTC	2,3,5-Triphenyltetrazolium chloride
TTF	1,3,5-Triphenyltetrazolium formazan
V-oven	Vacuum oven
(W)CA	Water contact angle
XPS	X-ray photoelectron spectroscopy
η	Viscosity
$\dot{\gamma}$	Shear rate
τ	Shear stress
θ	Water contact angle

1 Background and aim

Disease and injury often lead to the need of repairing or replacing tissues [1]. If repair is no option, the typical treatment today would be to remove the tissue, and if possible, replace it. Some tissues can be transplanted from one place of a patient's body to another, however, an external donor is often required. In the US alone there were over hundred thousand people on the national transplant list of 2017, waiting to receive new tissues. In addition, 20 people die each day waiting for a transplant, in the US [2].

Alternatively, the field of tissue engineering aims to create new tissues. This is done by combining scaffolds, stem cells and growth factors, and in this project, one aim has been to explore three different nanocellulose qualities with differences in surface chemistry, as possible scaffold materials for bone tissue engineering (BTE) applications. The master project has been performed in collaboration with RISE PFI, as a continuation of the NORCEL project. The NORCEL project had, amongst others, a vision of exploring the use of nanocellulose as a scaffold material in tissue engineering (TE) applications.

In a study by Rashad and co-workers, funded by the NORCEL project, two types of nanocellulose with different surface chemistry were produced [3]. The cytocompatibility of the materials was tested, with respect to cytotoxicity, cell attachment, proliferation, morphology and migration. One of the materials from that study, a TEMPO-oxidized nanocellulose quality, showed promising characteristics as a scaffold material [3]. However, previous studies have shown that cell response to aldehyde groups can be negative [4]. Therefore it has been wanted to test if the cytocompatibility of TEMPO-oxidized wood based nanocellulose can be even better with the aldehyde groups removed. This master project has aimed to investigate the effect of aldehyde groups on TEMPO-oxidized cellulose fibers, on cell responses. The effect of aldehyde groups were investigated by comparing the cytocompatibility of a TEMPO-oxidized nanocellulose quality with two additional nanocellulose qualities where the aldehyde groups had been removed by two different chemical treatments following the TEMPO-oxidation. These treatments, $NaClO_2$-oxidation or $NaBH_4$ reduction, converted the aldehyde groups to carboxyl or hydroxyl groups, respectively. Before conducting the cytocompatibility study, another aim of the master thesis was to characterize the nanocellulose qualities produced, in order to confirm their differences in surface functional groups, as well as investigate other possible differences between the materials.

A third aim of the master project was to investigate grafting of β-cyclodextrin to a TEMPO-oxidized nanocellulose quality. This grafting has been performed in collaboration with Julien Bras and Bastien Michel from LGP2 in Grenoble, France. β-cyclodextrin grafted to nanocellulose can be an efficient way to encapsulate hydrophobic growth factors or other molecules that can improve the properties of possible nanocellulose scaffolds.

2 Introduction

This master thesis is a continuation of a specialization project conducted autumn 2018. A report was submitted from the work conducted in the specialization project and several topics presented in the introduction-section for that report are relevant in this master thesis too. These sections have been included, to a greater or lesser extent. Sub-section 2.1 are included from the specialization project report (SPR), however the last paragraph discussing the materials researched for BTE applications is new. Sub-section 2.2 is also copied from the SPR, while sub-section 2.3 is included with new information added. In section 2.4, theory behind the methods used to characterize the nanocellulose-samples are included. The theory behind electric conductivity titration, viscosity and degree of fibrillation was written for the SPR.

2.1 Tissue engineering

Tissue engineering refers to the practise of restoring or improving damaged tissues or whole organs, by combining scaffolds, stem cells and growth factors [5]. In this project, the focus on tissue engineering is from a scaffold surface perspective, where the role of the scaffold is to create an appropriate 3D environment for tissue regeneration [1].

In vivo, the extracellular matrix (ECM) provides a support for the surrounding cells, in addition, the ECM is essential for cell morphogenesis and regeneration of tissues [6]. Mimicking the in vivo environment responsible for regeneration of tissues is therefore an important part of tissue engineering [5]. The ECM is non-cellular and comprise the organic matter found between most cells of multicellular organisms. The ECM structure is highly complex and varies from tissue to tissue, however, the major classes of ECM components are collagens, glycoproteins and proteoglycans [6]. Instead of trying to reproduce the ECM by combining ECM components, tissue engineering focuses on getting cells to bind to the scaffold material and further produce the ECM themselves, with support and guidance from the scaffold [5]. When ECM formation is in progress, the scaffold material should degrade to avoid inhibition of ECM formation.

A number of key properties are important for scaffold materials, such as biocompatibility, degradability, mechanical properties, scaffold architecture and manufacturing technology [1]. Biocompatibility of the scaffold material is crucial, however, as stated by David F. Williams; 'There is no such thing as a biocompatible material' [7]. By this, Williams argues that the word 'biocompatibility' should not be used as a material property, because it will depend amongst others, on the application for the material. However, the term will be used in this report, for simplicity reasons, but a clarification of which properties this includes for a scaffold material used in tissue engineering applications is as follows: the material must allow cells to grow and proliferate normally on or in the material. In addition, the material must not induce an immune reaction if implemented in the body. The term cytocompatibility is also frequently used in the report to describe materials which do not induce any cytotoxic effects, allow cell attachment, promote normal cell morphology and differentiation when the cells are interaction with the material.

Degradability is important to enhance ECM formation. It is therefore important that scaffold degradation products are non-toxic [1]. The mechanical properties of the scaffold material are also of importance, both to enhance and guide cell growth, as well as being practical to handle and produce. The material must amongst other allow diffusion of cell nutrients, waste products and allow vascularisation [5], which also are important aspects of scaffold architecture. The last key property, manufacturing technology, involves the commercial aspect; the material must be cost effective and the production must be possible to scale-up [1].

The surface properties of scaffolds can affect all the above mentioned key properties of scaffolds. Surface properties include amongst others surface functional groups, roughness, water contact angle (WCA) and protein adsorption properties. In a study by Rashad and colleagues, the effect of surface functional groups on fibroblasts were observed. A carboxymethylated CNF hydrogel adversely influenced the morphology of the cells and limited their spreading, while typical behavior was observed for cells cultured on CNF surfaces containing carboxyl and aldehyde groups [3]. Functional groups present on scaffold surfaces can also affect the surface charge, WCA and protein adsorption properties which further can influence cellular interaction [8]. In addition, functional groups can affect mechanical properties such as material stiffness through providing groups that can crosslink with other crosslinking agents and form stable gels [5]. Functional groups can also affect cellulose degradability, where e.g. periodate oxidized cellulose (chemical treatment which leads to breakage of the bond between C2 and C3 and formation of aldehyde groups at these positions in the glucose residues of the cellulose chain [9]) have been shown to be degradable *in vitro* and in rats, by Singh and colleagues [10].

Regarding surface roughness, Khang et al. reported that surfaces with subnano, nano and sub-micron features can selectively induce osteogenic differentiation of BMSCs [11]. Surface roughness can also influence WCA [12] and furthermore influence cell adhesion properties [13]. When it comes to protein adsorption properties of scaffold surfaces, it is important that the surfaces adsorb cell adhesive proteins in order for the cells to attach to the scaffold surface. The complexity of protein adsorption onto material surfaces will be further discussed in Section 2.4.8.

Tissue engineers have over the time tried to make scaffolds of different types of materials. There are advantages and disadvantages with the materials and some are better for certain tissue engineering applications compared to others. A scaffold system must thus match the specific tissue engineering application [14]. Ceramics, polymerics and composites constitute groups of materials that have been studied for BTE [1]. Ceramics such as coralline and hydroxyapatite (HA) show similar properties as bone with regard to high compressive strength and ductility [15]. However, there are limitations to the materials; they are often brittle [1]. Several polymers have also been investigated for BTE applications, such as the naturally derived polymers fibrin, hyaluronic acid, chitosan and collagen. Synthetically derived polymers include polyanhydried, polylactic acid and polycaprolactone [15]. General advantages with the natural polymers for BTE are that they are not toxic, show low immunogenicity and they promote bone repair. Disadvantages include uncontrolled degradation rate and low mechanical stability [15]. For the synthetic polymers, the degradation rate are more easily controlled, in addition the polymers can often be produced at low costs. Drawbacks for this group of polymers are that the materials show decreased possibility of supporting cell attachment and growth, compared to the natural

polymers [15]. Last but not least, composites are hybrids consisting of two or more materials, each with specific advantageous properties and some drawbacks. In general, composite scaffolds have problems with biocompatibility, degradation or both [1]. A material frequently investigated today for BTE applications is the natural polymer cellulose, which have promising properties as a scaffold material.

2.2 Cellulose

Cellulose is the most abundant organic polymer on earth, as it is an essential component of plant cell walls. Cellulose has a simple primary structure; it is a linear, unbranched polymer of D-glucose units linked together by β-(1-4)-glycosidic bonds. As can be seen from Figure 1, every second glucose unit is rotated 180°. Thus, the repeating unit in a cellulose chain is the cellobiose residue [16]. The cellulose structure is stabilised by the presence of hydrogen bonds, shown in the figure. Hydrogen bonds will also form between individual cellulose chains, forming *sheets* [16]. Van der Waals forces between the cellulose sheets form crystalline cellulose, making the cellulose even more stable to degradation [17].

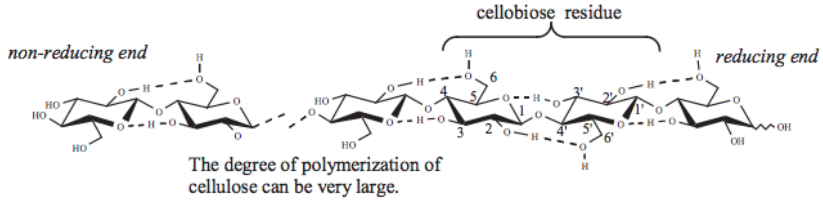

Figure 1: Chemical structure of cellulose built up by the repeating cellobiose residue. Figure collected from [16].

Cellulose is not a continuous crystalline polymer; there exist regions of higher order of crystallinity, as well as amorphous regions [18]. In some regions, long, relatively narrow sheets form bundles known as fibrils. The length and size of such fibrils vary between different tissues and organisms, but a common suggestion for plant cell walls is that one fibril contains about 36 cellulose chains [16]. Such a fibril is shown in Figure 2 with a width of around 3 nm. The length of the fibril will be longer than a single cellulose chain, as several cellulose chains overlap. In literature, suggested cellulose chain length is between 5-7 μm, while the fibril length can exceed 40 μm [16]. Fibrils can also form fibrilar aggregates, see Figure 2.

Cellulose and its derivatives are common materials within biomedical applications, including wound healing, blood coagulant, artificial kidney membranes and as implant material [19]. Cellulose have several appealing properties for biomedical applications, such as the non-toxicity, it can easily be modified to get appropriate properties for different applications and, of course, the abundance of the material. For tissue engineering applications, the focus is on a particular type of cellulose, namely nanocellulose. The properties of nanocellulose are further explained in the next section.

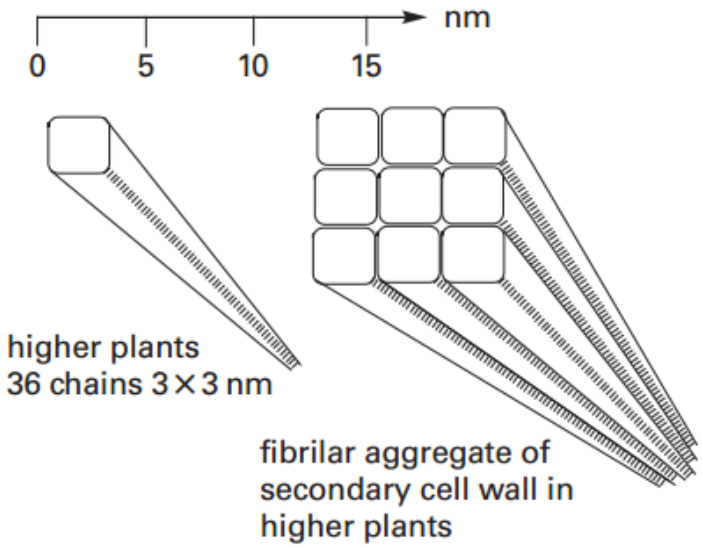

Figure 2: About 36 cellulose chains form crystalline fibril structures, which further can form fibrilar aggregates. Figure collected from [16].

2.3 Nanocellulose

Nanocellulose is a wide term for cellulose fibrils with widths in the nanometre range [20]. The nanocellulose family is generally separated in three groups: cellulose nanofibrils (CNFs), cellulose nanocrystals (CNCs) and bacterial nanocellulose (BNC). Both CNFs and CNCs are mainly derived from wood and plants, while BNC is synthesized by bacteria. CNFs and CNCs can further be distinguished by production methods [20]. A specific type of CNFs have been investigated in this project (wood-based TEMPO-oxidised pretreated quality) and compared to a BNC sample. General properties of CNFs and BNC will therefore be the topic for further discussion, while readers interested in CNC-properties are referred to scientific literature [20].

2.3.1 CNFs

Generally, CNFs are produced by using special separation methods or chemical treatments on the cellulose material before mechanical fibrillation through high-pressure homogenization (HPH) [21]. One of the most common HPH setups is shown in Figure 3 and includes a stream of liquid cellulose (pulp fibers) forced through a narrow valve at high pressure. This causes high shear stress on the material and results in fibrillated cellulose [22]. Depending on pretreatment and fibrillation conditions, cellulose with nanofibrils of different widths can be produced where there in general are two levels; one ranging from 15-20 nm and one from 3-5 nm [20]. Fibrillation can thus separate the cellulose material into individual fibrils and smaller fiber fragments.

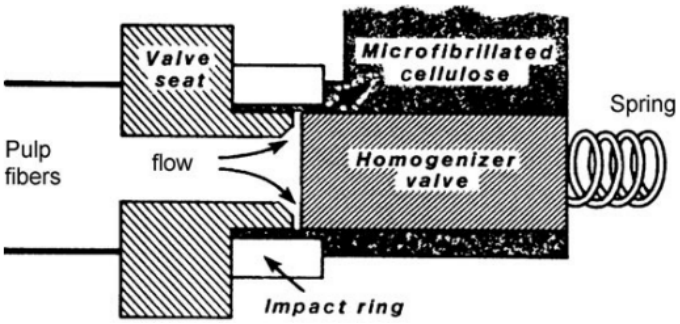

Figure 3: Schematic illustration of a high-pressure homogenizer. The figure is collected from [20].

2.3.2 BNC

BNC is a specific type of cellulose, produced by bacteria. The most studied cellulose-producing bacteria are *Gluconacetobacter xylinus*, however, the ability to produce cellulose is found in other microorganisms, such as other species of the *Gluconacetobacter* genus and *Agrobacterium tumefaciens* [23]. The bacteria polymerize glucose units before secreting the cellulose chains. When the chains are secreted, different cellulose chains will be organized in highly crystalline arrangement through hydrogen bonds and van der Waals forces [23].

Bacterial cellulose is different compared to plant derived cellulose in several aspects; e.g. plant cellulose has a different fiber structure with larger fibers compared to BNC (Figure 4), in addition, BNC is produced in a pure form without lignin and hemicellulose which are present in plant pulp [23]. The average diameter of bacterial fibrils range from 20-100 nm [20].

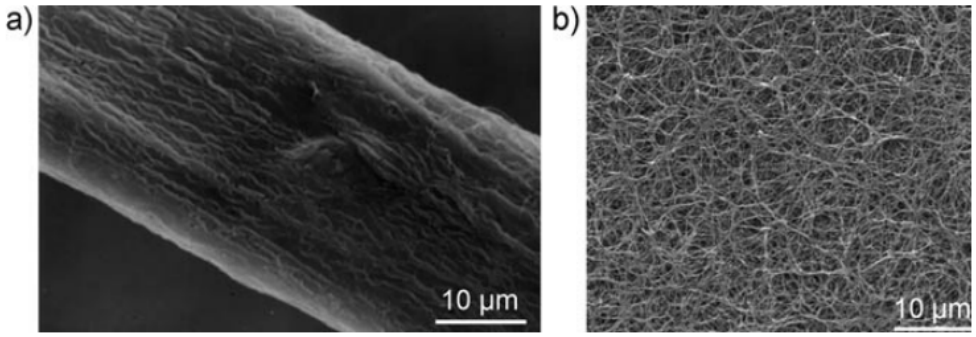

Figure 4: Electron micrographs of fibers of a) common pulp from plant cellulose and b) bacterial cellulose. The figure is collected from [20].

2.3.3 Nanocellulose in tissue engineering

As a scaffold material, nanocellulose has several attractive properties, such as high surface area, good rheological properties, as well as generally biocompatible and non-toxic. In addition, in a world where the demands for products made from renewable and sustainable, non-petroleum based products are increasing, nanocellulose is advantageous [24]. Nanocellulose can also form

hydrogels with high water content [5], where hydrogels are considered as promising scaffold materials [3]. Hydrogels are polymer networks that can store large amounts of water, without dissolving in water [14]. Several biopolymers can form hydrogels such as alginate and chitosan, where hydrogels generally show promising properties as scaffolds within tissue engineering applications as they mimic the extracellular matrix [25]. Nanocellulose can form reversible gels at low solid content, held together by hydrogen bonding and van der Waals forces between hydroxyl groups and individual cellulose chains. The stability of nanocellulose gels can be increased by crosslinking using di- or trivalent ions [5]. This will be possible for chemically modified nanocellulose containing increased amounts of surface charges. Permanent nanocellulose hydrogels can be formed by covalently crosslinking the fibrils in the nanocellulose material to particles such as polyethyleneimine and poly N-isopropylacrylamide-co-allylamine-co-methylenebisacrylamide [26].

In addition to mimick the ECM, hydrogels in tissue engineering applications are beneficial due to the high water content. As the scaffold material shall enhance ECM formation, it is important that the material is not in the way of the tissue formation. A stiff material with high water content decrease material consumption and ensures that little solid material is present, inhibiting ECM formation.

Biocompatibility is a key property for scaffold materials. Native cellulose is considered safe, however, this does not necessarily imply that nanocellulose is non-toxic. As many chemical variations of nanocellulose can be produced, each of these must be tested for toxic effects if they are ever to be used for tissue engineering applications. By now, several different types of nanocelluloses have been tested for cytotoxic effects, using different cell types for the testing, and generally both CNFs and BNC do not induce cytotoxic effects towards cells [5, 23]. Cells must also be able to grow and proliferate normally on or within the scaffold material, which similarly as toxicity must be evaluated for every CNF/BNC quality.

Other key properties for scaffold materials include degradability, scaffold architecture and manufacturing technology. The latter property, manufacturing technology, will again depend on the type of CNFs/BNC. However, it exists commercial production of fibrillated cellulose at Borregaard, in Sarpsborg, confirming that high-volume production technology is available [27]. Cost-efficient, high-volume production of BNC are facing challenges today due to high growth medium costs which represents approximately 30 % of the total production cost [23].

When it comes to degradability, both cellulose and nanocellulose can be degraded by enzymes called cellulases, and the degradation products are non-toxic sugar compounds (glucose) [28]. As cellulases are not produced by animal cells, nanocellulose will not degrade if implanted in a human body. However, this can be exploited, where cellulases can be added with the scaffold material, in an appropriate amount, to get a controlled degradation [29]. Regarding scaffold architecture, both CNFs and BNC can form porous structures allowing diffusion of cell nutrients and waste products, and vascularisation. Such porous structures can be made using e.g. cryogelation or freeze-drying [5].

A last property of nanocelluloses that makes it a particularly interesting material in tissue engineering applications, is the fact that the surface chemistry of the material easily can be changed

by chemical modifications [5]. This is usually done before fibrillation, as many chemical modifications can ease the fibrillation process and thus decrease energy consumption. An example is the introduction of charged groups on the surface of the fibrils [20]. Chemical modifications can also alter the cyto- and biocompatibility of the material. A chemical modification of great interest is TEMPO-mediated oxidation which will be further discussed in the next section.

2.3.4 Chemical modification of cellulose

One of the main impediments for commercial production of CNFs is the high energy consumption of homogenization. Pretreating the cellulose before homogenization can be a way to reduce the fibrillation cost, in addition, chemical modifications can give CNFs and BNCs with various properties [20].

TEMPO-mediated oxidation

TEMPO (2,2,6,6-Tetramethylpiperidinyloxy) is a chemical with the formula $(CH_2)_3(CMe_2)_2NO$. It is used as a catalyst in oxidation reactions, and the structure of TEMPO as well as the reaction mechanism of TEMPO-mediated oxidation of alcohols is shown in Figure 5. TEMPO-mediated oxidation can be performed on cellulose materials, and will result in selective oxidation of the C6 alcohol on the glucose units, to carboxylate and aldehyde groups [30]. In addition to decreasing energy consumption during fibrillation [20], TEMPO-oxidised CNFs show promising features within tissue engineering applications. The introduction of carboxylate (COO^-) and aldehyde (COH) groups makes it possible to form stable CNFs hydrogels by covalent crosslinking. Different crosslinker molecules can be used which give CNFs varying properties [31].

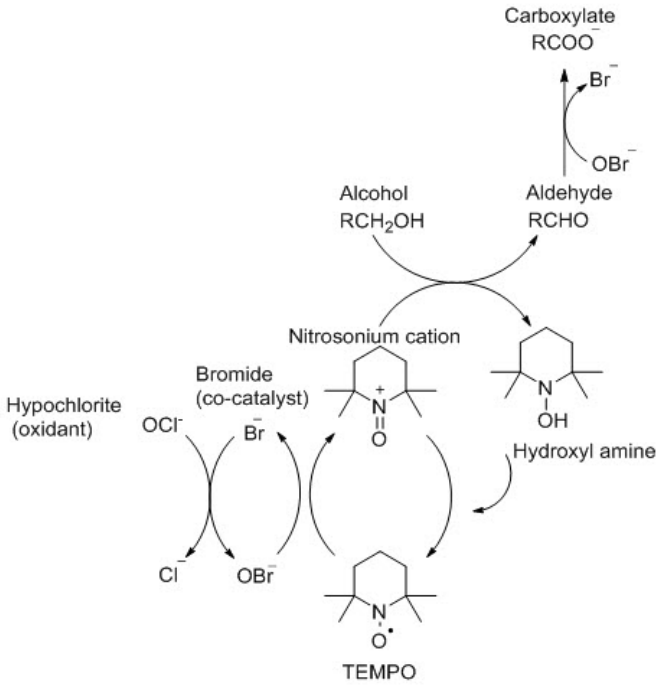

Figure 5: The mechanism of TEMPO-mediated oxidation of alcohols. Figure collected from [32].

Selective oxidation or reduction of aldehyde groups in TEMPO-oxidised cellulose
TEMPO-mediated oxidation introduces both carboxylate and aldehyde groups to C6 of the glucose units in the cellulose chains [33]. The aldehyde groups can be removed by oxidation to carboxylate groups using e.g. $NaClO_2$, or reduction to alcohols using e.g. $NaBH_4$ [34].

$NaBH_4$ is a relatively mild reducing agent, implying that it can only reduce the aldehydes in the TEMPO-oxidised material, not the carboxylate groups [35]. The reaction mechanism of the reduction of aldehydes to alcohols by the use of $NaBH_4$ is shown in Figure 6. $NaClO_2$ also reacts selectively [34], by the reaction mechanism shown in Figure 7.

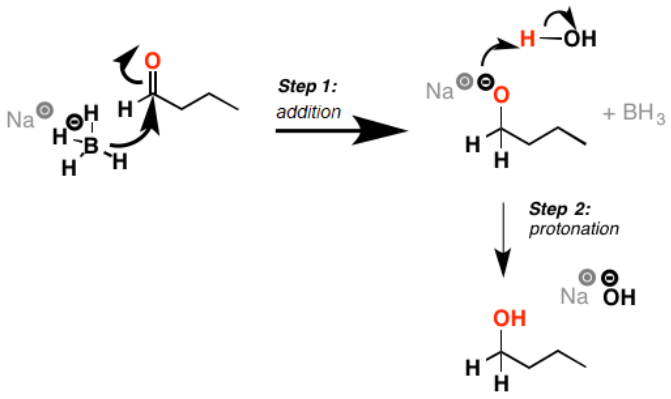

Figure 6: Reaction mechanism for the reduction of an aldehyde to an alcohol, using $NaBH_4$. Figure collected from [36].

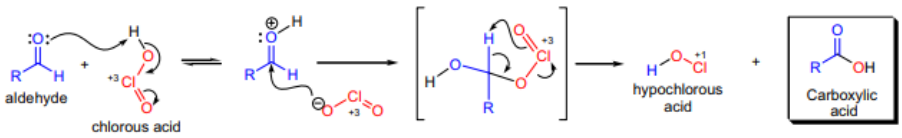

Figure 7: Reaction mechanism for the oxidation of an aldehyde to a carboxylic acid group, using $NaClO_2$. Figure collected from [37], as a part of a bigger reaction mechanism.

2.4 Characterization of nanocellulose

2.4.1 Carboxylate content

Electric conductometric titration is a method that can be used to measure the carboxylate content in TEMPO-oxidised cellulose [33]. A solution containing the cellulose sample of interest, along with excess of strong acid, is titrated against a strong base. A general conductivity curve is shown in Figure 8, and as can be seen from the figure; the titration can be divided into different phases. Between points A and B, phase 1, the strong base reacts with the strong acid and the conductivity decrease. Between points B and C, phase 2, it is assumed that there are no strong acid left, and the strong base neutralises the carboxylic acid groups on the cellulose. At point C, it is assumed that all carboxylic acid groups are neutralised. As such, between points C and D, phase 3, the conductivity increases as a result of excess strong base in the solution.

An additional assumption needed to calculate the carboxylate content is that only carboxylic acid groups are being neutralized between points B and C. The amount of carboxylate groups is equal to the amount of strong base used to neutralize the carboxylic acid groups (on a molar basis), thus the amount of base added during phase 2. How to calculate this is shown in Appendix A.1.

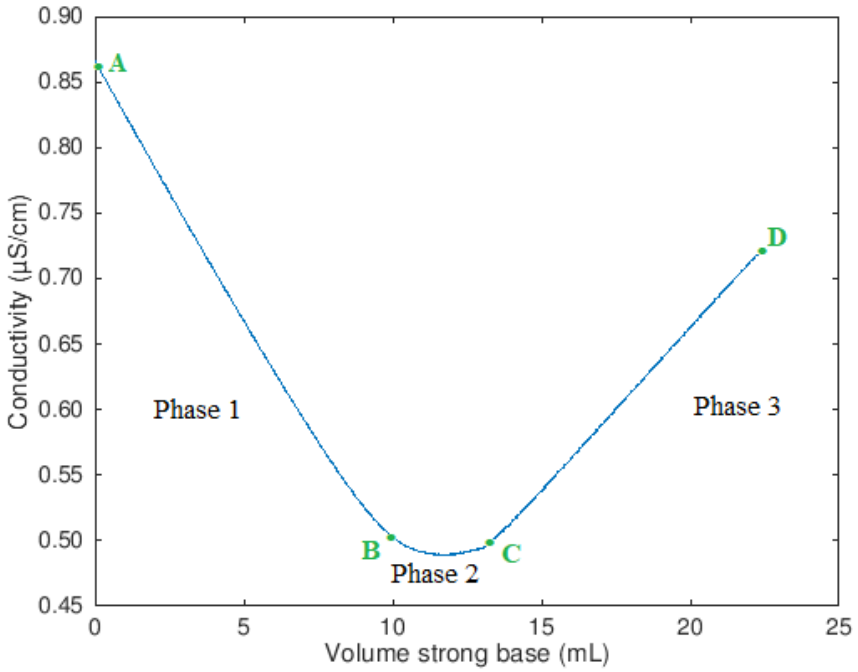

Figure 8: A conductivity curve where a CNF sample dissolved in an aqueous solution has been titrated against a strong base. The mixture was initially at pH 2.5-3, strong acid were used to lower the pH.

2.4.2 Aldehyde content

The aldehyde content of a nanocellulose sample can be determined by a spectrophotometric method, where the oxidation of aldehydes leads to the reduction of 2,3,5-Triphenyltetrazolium chloride (TTC) to the red compound 1,3,5-Triphenyltetrazolium formazan (TTF) under alkaline conditions [38]. The amount of aldehyde groups in an unknown sample can be determined from a calibration curve prepared with e.g glucose as a substrate.

2.4.3 Viscosity

Rheology is the study of how liquids or viscoelastic materials respond to applied stress, and rheometres are used to study rheological properties of materials [39]. It is important that nanocellulose for tissue engineering applications has the right rheological properties. CNFs form gels at low concentrations in water, however, upon increased shear stress, the gels show shear-thinning behavior [20]. This is beneficial in industrial processing, especially within coating applications. In addition, 3D printing of CNF hydrogels to personalised scaffolds is of great interest, and the shear thinning behavior makes printing of the materials easier [5].

A rheological property easily evaluated is the viscosity of a material. Viscosity is defined as a material's internal resistance to flow [39]. Different viscometers can be used to measure the viscosity of a material, and the type of measurement and type of viscometer used will influence the result [17]. By evaluating the viscosity of a material when different forces are applied, the shear thinning behavior of the substance can be evaluated.

One mode for measuring viscosity is by rotational viscometers, and a commonly used rheological device is the Brookfield viscometer [39]. The device uses an internal spring, which measures torque, connected to a spindle which rotates at selected speed (rpm) in the sample. Viscous samples will increase the torque on the spindle, which is registered by the apparatus. The torque can be used to calculate the shear stress, τ, on the spindle surface, by Equation (1), where M is the torque, h_s is the height of the spindle and R_s is the radius of the spindle [39].

$$\tau = \frac{M}{2\pi h_s R_s} \tag{1}$$

The shear rate, $\dot{\gamma}$, can also be approximated at the spindle surface as long as $R_c/R_s \leq 1.1$, where R_c is the radius of the container the sample is placed in, by Equation (2). In Equation (2), ω is the rotational speed of the spindle [39].

$$\dot{\gamma} = \frac{\omega R_s}{R_c - R_s} \tag{2}$$

The shear stress and shear rate can further be used to calculate the viscosity, η, of the sample, through Equation (26), which is the definition of viscosity [17].

$$\eta = \frac{\tau}{\dot{\gamma}} \tag{3}$$

2.4.4 Degree of fibrillation

For clarification, both residual fiber content and degree of fibrillation are used to describe how fibrillated a material is. However, the terms describe how fibrillated a material is from opposite directions; a high residual fiber content implies a low degree of fibrillation.

The size of wood cellulose fibers is at the macro-scale, with lengths typically ranging from 1-3 mm and widths of about 10-50 μm [40]. During fibrillation processes such as homogenization, many of the fibers will be fibrillated to fibrils, however, the mixture will be inhomogenous and contain fibers and residual fibers [41]. Nanocellulose has several potential applications ranging outside the field of TE applications, such as an additive in paper and barrier in food packing applications. The different applications can benefit from different amounts of residual fibres in the CNF materials [40]. Evaluation of how the degree of fibrillation affects the material properties can be of substantial economic interest as fibrillation processes generally are expensive [20].

Fiber analysis
The amount of residual fibers can be estimated for a nanocellulose suspension, e.g. by the use of a fiber analyzer such as the Fiber Tester 912 Plus apparatus. The apparatus reports amongst others the number of fiber residues detected, n, their mean length, l and mean width, b. As shown in Equation (4), b can be used to calculate the mean cross-sectional fiber residue area, A, and by multiplying A with l, the mean fiber residue volume, V, is estimated as shown in Equation (5).

$$A = \pi \cdot (b/2)^2 \tag{4}$$

$$V = A \cdot l \tag{5}$$

From the mean fiber residue volume and by using an estimate for the density of the cellulose fibres (1.55 g/cm^3, [42]), the average weight of one fiber, $\overline{w_f}$ can be estimated, see Equation (6). In Equation (7), the apparent residual fiber content, R_f, is estimated, where w_s is the dry weight of the sample investigated [42].

$$\overline{w_f} = V \cdot 1.55 \tag{6}$$

$$R_f(\%) = \frac{\overline{w_f} n}{w_s} \cdot 100 \tag{7}$$

2.4.5 Atomic Force Microscopy

Atomic Force Microscopy (AFM) can be used to acquire high resolution images of material surfaces, down to nanometer scale. AFM can also be used for force measurements which can give information about e.g. the physio-chemical properties of a sample [43]. Force measurements using AFM will not be discussed in this report, as AFM only has been used as a microscopy technique in this thesis.

The core components of an AFM apparatus is illustrated in Figure 9 and includes the cantilever with a fine tip, focused laser beam and a quad photodiode [43]. During AFM imaging, either the cantilever tip moves across the sample or the sample moves underneath the cantilever tip. While the tip slides over the surface, the cantilever will be deflected upwards or downwards depending on the height of the surface investigated. As can be seen from Figure 9, a laser beam is reflected on top of the cantilever back to the quad photodiode. When the position of the cantilever changes, the position of the laser beam will change. By examining a sample in x and y direction, these changes in laser beam position can be used to create a 3D topographical image [43].

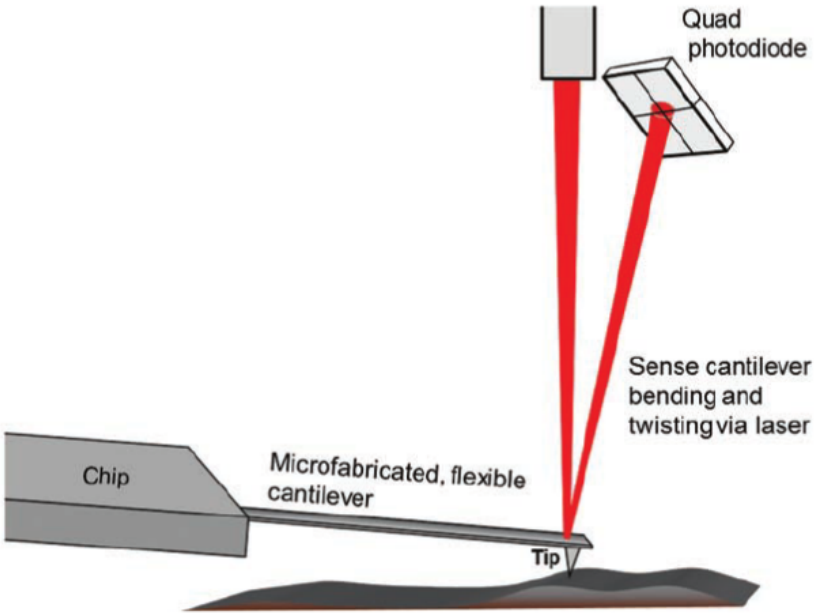

Figure 9: Schematic illustration of the main components of an AFM apparatus. The figure is collected from [43], as a part of a larger figure.

The topographical images acquired by AFM can further be used to assess the degree of fibrillation of a material, by measuring the average surface roughness, R_a. Less fibrillated materials will have a higher surface roughness [42]. Surface roughness is a measure of how much the height of points on a surface deviates from a set zero point. The equation for calculating the mean surface roughness can be seen in Equation (8) [44]. By using special softwares, the topographical images can be analysed and the roughness quantified.

$$R_a = \frac{1}{l} \int_0^l | Z(x) | \, dx \tag{8}$$

2.4.6 ζ-potential

ζ-potential, also known as electrokinetic potential, describes the surface charges of a material when it is suspended in a fluid [45]. Figure 10 shows a negatively charged particle suspended in a fluid. As the particle is negatively charged, positive charges from the fluid will be attracted and form what is called the stern layer which is considered an immobile layer. Surrounding

the stern layer is the diffusive layer which consists of both positively and negatively charged ions, with ability to diffuse into the bulk phase of the suspension and back again. The boundary between the diffusive layer and the bulk liquid is termed the slipping plane, or shear plane. The ζ-potential is defined as the potential at the slipping plane [45]. The ζ-potential is dependent on which solvent is used for the measurement, as well as the solvent pH [46].

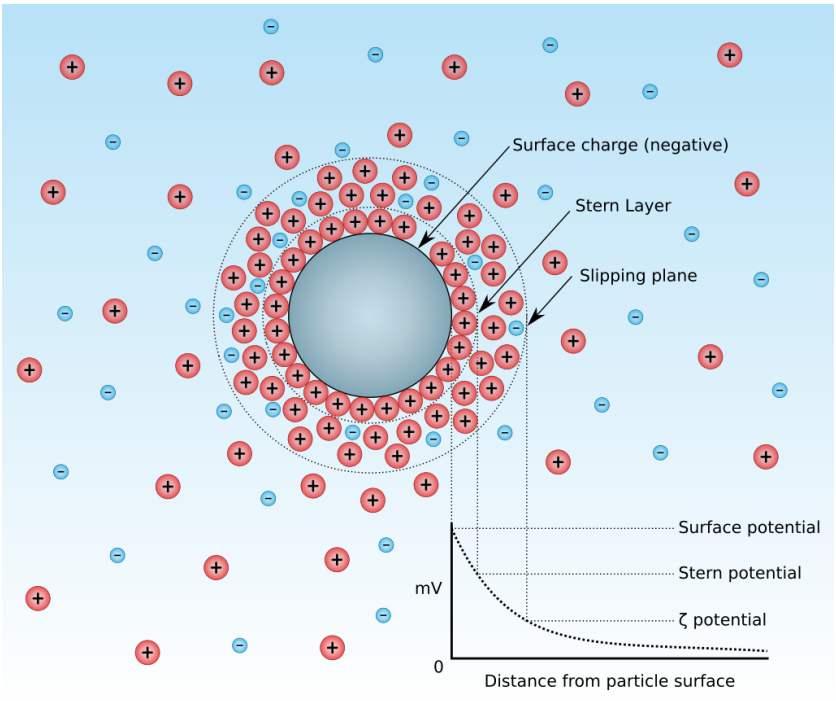

Figure 10: The zeta potential is defined as the potential at the slipping plane. The figure is collected from [47].

2.4.7 Contact angle

Water contact angle, θ, is a parameter used to evaluate the relationship between a solid surface and water with regard to hydrophobicity/hydrophilicity and water adsorption properties [48]. The contact angle is the angle between a water droplet deposited on a solid surface, as shown in Figure 11. Hydrophobic materials will have $\theta > 90°$, while hydrophilic materials have $\theta < 90°$. Different functional groups on a material surface can affect the hydrophobic/hydrophilic properties of the material [8], in addition, surface roughness can play an important role [12]. The contact angle of rough surfaces can be substantially increased due to heterogeneous wetting; there can be trapped air underneath parts of the water droplet preventing surface-water contact.

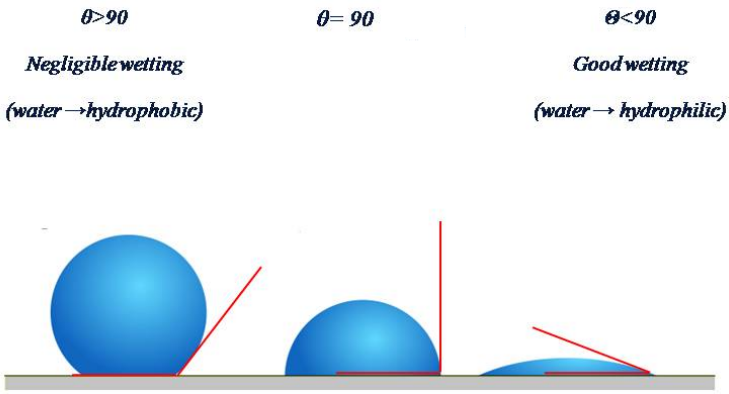

Figure 11: The water contact angle is the angle between a water droplet and the solid surface it is deposited on. The figure is collected from [49].

2.4.8 Protein adsorption

An important requirement for scaffold materials is that cells must be able to grow and proliferate normal on or inside the material. However, cells in contact with a scaffold materials or other biomedical implants will not bind to the material surface directly. From the moment an implant gets in contact with biological fluid such as human blood serum, blood serum proteins will adsorb to the material surface. The adhesion of cells is therefore depending on protein adsorption on or inside the material. Blood serum contains more than 150 proteins with different functions where cell adhesion is facilitated by adhesive ECM glycoproteins such as fibronectin, laminins and vitronectin [6]. Protein adsorption in itself is therefore not sufficient; the right proteins must attach in high enough concentrations. The proteins adsorbed to different materials are influenced by several parameters such as the chemical and physical properties of the serum proteins and the material, protein concentration and the composition of different proteins in the serum [50]. The complexity of these factors will be briefly discussed in this section.

As previously mentioned, human blood serum is a cocktail of proteins with different properties such as hydrophilicity/hydrophobicity, charge and size, which all can affect protein adsorption. In general, hydrophilic proteins will adsorb more easily on hydrophilic materials and similarly with hydrophobic proteins on hydrophobic surfaces. This is due to presence or absence of polar interactions respectively. An opposite effect is observed when it comes to charges on protein surfaces versus material surfaces; opposite charges attract. The size of proteins can also affect the diffusion rate of proteins to the material surface, where small proteins generally diffuse faster and thus reach the points of adsorption more rapidly than large proteins. However, large proteins can bind to a larger material surface area than small proteins and possibly achieve stronger adsorption. [50]

The hydrophilicity/hydrophobicity and charge of scaffold materials will, similarly as for proteins, affect the adsorption of proteins on the surface. In addition can surface chemistry, meaning the presence of different functional groups, and topography affect protein adsorption. When it comes to material surfaces, it is generally observed that hydrophobic materials adsorb more proteins than hydrophilic surfaces. This is because there will be a competition between the water molecules and proteins upon getting in contact with hydrophilic surfaces, while hydrophobic

material surfaces only attracts proteins. However, it is reported in literature that cell adhesion to polymeric materials is greatest for hydrophilic materials, indicating the important factor that more proteins adsorbed not necessarily increases cell adhesion [8]. Surface chemistry is another important factor affecting protein adsorption to materials. In literature, the following general observations have been reported and are summarized in Table 1. Topography of a material was also mentioned as a factor that can affect protein adsorption, where increased surface roughness generally provides more surface area and thus increases protein adsorption. [50]

Protein concentration and the presence of different proteins affects their adsorption. Higher protein concentration surrounding a material will only lead to higher concentration of adsorbed proteins up to a certain point due to the fact that serum proteins do not adhere to one another. Thus, the proteins will be adsorbed on a material surface as a monolayer and there will be a maximum total protein concentration possible to achieve on the surface. However, the protein concentration of different proteins can vary by increasing or decreasing a protein concentration relative to other proteins in the mixture, thus the presence of other proteins in the serum affects cell adhesion as not all proteins facilitated this. [50]

Table 1: The effect of surface functional groups on protein adsorption. Table adapted from [50]. In order to fit the entire table, 'fn' is used as an abbreviation for fibronectin.

Functional group	**Properties**	**Effect on proteins and cells**
-OH	Neutral; hydrophilic	Has decreased affinity for plasma proteins; induces exposure of cell adhesive domains on fn; increases differentiation of osteoblasts
-COOH	Negative; hydrophilic	Has increased affinity for fibronectin and albumin

2.5 Cytocompatibility of nanocellulose

Cellulose is the worlds most abundant biopolymer and major sources except wood includes grasses and corn [51]. Through the diet, many animals depend on cellulose as their primary source of energy and even though humans cannot digest native cellulose, it is safe to eat. Industrial use of cellulose or cellulose derivatives as e.g. thickening agents in food is more and more common and applications within the pharmaceutical industry are also increasing [52]. However, cellulose for the use in TE applications will not be aimed for the use inside the digestive system. Safety regarding cellulose and its derivatives have therefore been investigated and they are generally well tolerated by most tissues and cells [19]. Today, cellulose is used in several biomedical applications including as blood coagulant, artificial kidney membranes, wound care dressings and as implant material [19].

When nanoscaled cellulose products were introduced, new concerns about safety aspects arose. Even though native cellulose is generally regarded as safe, the same can not directly be said about nanocellulose. Nanomaterials can interact with the body in different ways than their large scale counterparts [5]. Investigation of the safety of nanocellulose must therefore be evaluated, for every nanocellulose quality. *In vitro* cytocompatibility investigation can provide useful information about cells response to the material and can be evaluated by assessing the

cell viability, morphology, proliferation and differentiation of cells, either in direct or indirect contact with the material.

Several of the assays used to evaluate the cytocompatibility of the nanocellulose qualities in this project have involved the use of optical microscope, both with and without fluorescence. A brief explanation of the working principle of these imaging techniques will therefore follow below. A brief explanation about the properties of bone marrow mesenchymal stem cells is also given, as this type of stem cells were used for the cytocompatibility studies.

2.5.1 Optical microscope

An optical microscope is a microscope that uses light to create magnified images of a sample. A schematic of the working principle of an optical microscope is shown in Figure 12 with ocular lens, objective lens, condenser lens, specimen stage and the illuminator (light source). In an optical microscope, light from the illuminator is sent through the condenser lens where the light beam is focused before hitting the sample on the sample stage. The light will further be transmitted through the sample and focused by the objective lens before finally being transmitted through the ocular lens where the sample can be viewed by the human eye. The image is magnified both through the objective and ocular lenses, the final magnification applied is the product of the two magnifications. [53]

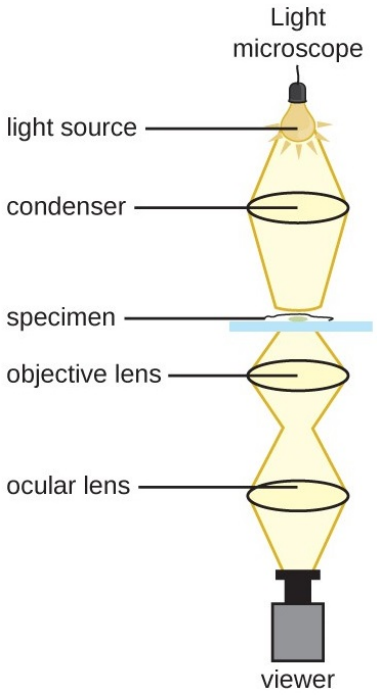

Figure 12: A schematic of the working principle of an optical light microscope. The figure is collected from [54].

2.5.2 Fluorescence microscope

A fluorescence microscope is a type of optical microscope used to image fluorescent objects, either autofluorescent or dyed with fluorescent stain. Fluorescent object, so-called fluorophores or fluorochromes, are objects that can adsorb light at certain wavelengths and re-emit light of longer wavelengths, thus lower energy [55]. Figure 13 show a schematic of the working principle of a fluorescence microscope. As can be seen from the figure, a fluorescence microscope have both excitation and emission filters to produce a fluorescent image of the specimen. The excitation filter ensures that only certain wavelengths of light is directed onto the sample, while the emission filter only allows wavelengths of the emitted light from the fluorescent object to be transmitted [53]. Before using a fluorescent microscope it is therefore necessary to know both the excitation and emission wavelength of the fluorescent object of interest.

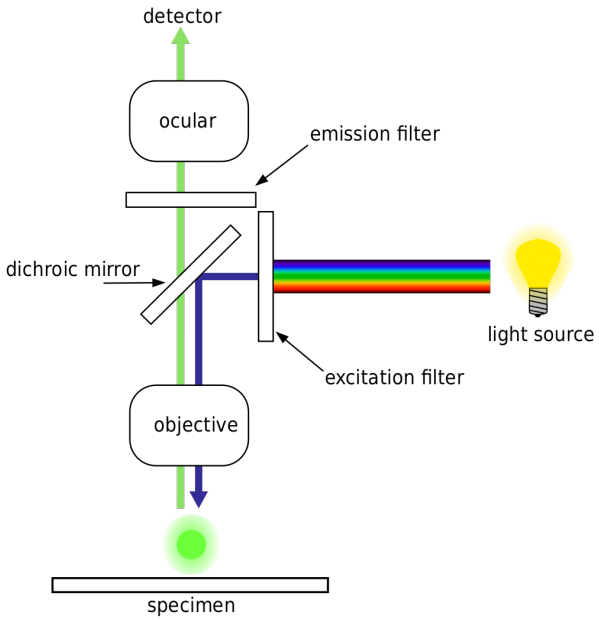

Figure 13: A schematic of the working principle of a fluorescence microscope. The figure is collected from [56].

2.5.3 Bone marrow mesenchymal stem cells

Bone marrow mesenchymal stem cells, BMSCs, are stem cells initially discovered by their ability to attach to cell culture plastics [57]. BMSCs have the ability to differentiate into cells of the connective tissue such as adipocytes, osteoblasts and chondrocytes [58]. The cells are easily cultured in cell culture dishes and by changing the growth medium, the cells can selectively be differentiated. In addition, the cells can be harvested from the same patient that needs them, autologous transplantation, and the stem cells do not carry the same ethical burden as embryonic stem cells [59]. Due to these properties, the cells are attractive to use within bone and cartilage tissue engineering [57].

2.5.4 Cell viability

Viable cells are cells with intact plasma membranes and intracellular activity [60]. There are several ways to evaluate the indirect cytotoxicity (using material extract) and direct cytotoxicity (direct contact between the material and the cells) of a material. Among these assays are alamarBlue, live/dead staining and measurement of lactate dehygrogenase (LDH) levels common.

Indirect cytotoxicity
Cell viability in response to a material can be evaluated using indirect contact between the material and the cells. This can provide information about potential toxic components released from the material, thus not the material itself [3]. Such toxic components can arise from e.g. the production method. One way of evaluating this is by soaking the material of interest in culture medium to release possible toxic compounds. The cells can further be cultured in this extract medium instead of normal culture medium. The cellular response compared to growth in normal culture medium can be evaluated and the difference is a measure of cell viability.

One way of measuring cell viability is through alamarBlue staining. alamarBlue reagent contains resazurin, a cell permeable compound with blue color and it is virtually non-fluorescent [61]. In viable cells, resazurin will be reduced to resorufin which is a pink and highly fluorescent compound. The cell viability can thus be determined by the amount of fluorescence detected from a cell culture.

Live/dead staining
Cell viability can be evaluated through the use of a live/dead staining assay. In such assays, live and dead cells will be differently labelled using fluorescent dyes. Examples of such dyes are calcein-AM which stains live cells green and ethidium homodimer-1 which stains dead cells red. The live cell dye is plasma-membrane permeant and becomes fluorescent upon reaction with intracellular esterases [60]. The dead cell dye is not plasma-membrane permeant, therefore it will only permeate into cells with compromised plasma membranes. The dye binds DNA with high affinity which increases the fluorescence of the molecule [60].

Lactate dehydrogenase assay
LDH is an intracellular and stable enzyme which catalyses the conversion of pyruvate to lactate. When cells are compromised or damaged, LDH can leak out from the cell plasma. Measuring the LDH level in the medium when culturing cells can thus be used as a way of assessing the cell viability. LDH levels can be measured using a colorimetric assay such as Abcam's Lactate Dehydrogenase (LDH) Assay Kit. In this kit, LDH reduces NAD^+ to NADH which further interacts with a compound to form a colorful substance with OD_{max}= 450 nm [62]. The amount of the colorful substance formed can be related to LDH levels in the evaluated sample.

2.5.5 Morphology

The morphology of cells involves their shape, size and general appearance. The morphology will vary between different cell types in order to support cell function. Cell morphology can also vary within the same cell line depending on factors such as cell health [63].

Stem cells are cells that can self-renew and differentiate into other types of cells. According to literature, two major sub-populations based on morphology exist for mesenchymal stem cells: a spindle shape or a flattened, polygonal shape (Figure 14) [59]. By studying the morphology of cells cultured in different environments, information about cell health can be obtained by evaluating that the observed cell morphology is within what is expected as normal [8].

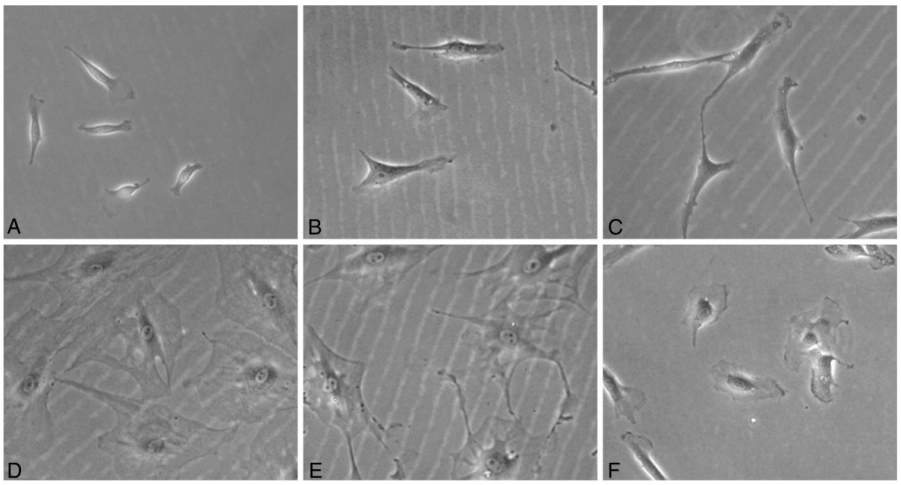

Figure 14: The morphology of mesenchymal stem cells. Image A-C show cells with spindle shapes, while D-F show flattened, polygonal shaped cells. The images are collected from [59].

2.5.6 Proliferation

Cell proliferation describes the increase in cell number. Cultured cells will generally follow a standard growth pattern, as shown in Figure 15. After seeding the cells, they will proceed from lag phase to log phase. Within the log phase, the cells grow exponentially. When the availability of either nutrients or space becomes limited, the growth will cease [64].

Cell proliferation is an important marker for cell health. It is therefore important to evaluate that cells can proliferate normally on or inside a possible scaffold material to ensure that the material is not inhibitory for normal cell function. The proliferation characteristics of a cell culture can be evaluated by the use of e.g. Quant-iT^{TM} PicoGreen^{TM} dsDNA Assay Kit (Invitrogen). In this kit, Quant-iT^{TM} PicoGreen® dsDNA reagent binds to dsDNA and forms a fluorescent compound which can be detected using e.g. microplate readers [65].

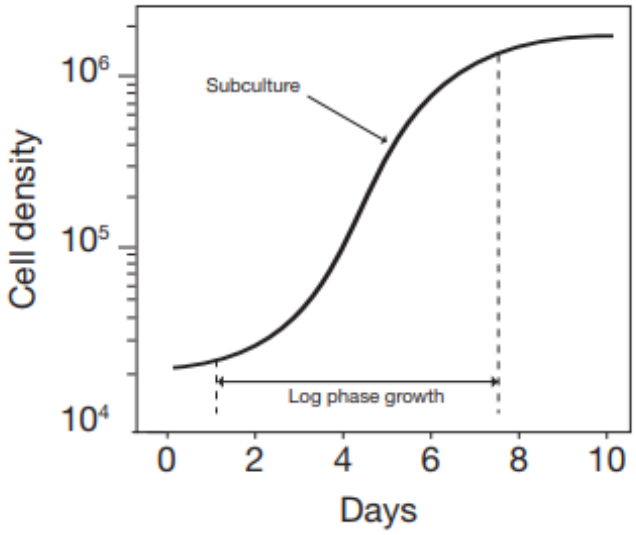

Figure 15: Characteristic growth pattern of cultured cells. Figure collected from [64].

2.5.7 Differentiation

Stem cells are undifferentiated cells which have the potential to either divide and make more stem cells, or differentiate to other cell types [57]. The differentiation of stem cells is crucial for tissue regeneration, in order to get cells with the right function. The differentiation of stem cells is generally a response to chemical or physical stimuli. A way to differentiate stem cells to the osteogenic lineage, bone cell lineage, is by supplementing serum-containing medium with ascorbic acid, B-glycerophosphate and dexamethasone [66]. After growing cells in osteogenic medium, there can be several ways to assess that the osteogenic differentiation actually has occurred. A known early osteogenic marker is alkaline phosphatase (ALP). ALP is an enzyme which catalyses the hydrolysis of phosphomonoesters, R-O-PO_3, where the chemical formula of the R group can vary [67]. ALP is expressed early in mineralization processes where the role of ALP is complex. Readers are referred to literature for elaborate information [67]. Mineralization, calcium deposition, is a late marker for osteogenic differentiation [68]. Bone cells accumulate calcium salts in order to form hydroxyapatite, the main inorganic component of bone structures [69], [70]. The formation and deposition of inorganic components is referred to as mineralization [70].

ALP levels can be measured using e.g the 'Alkaline Phosphatase Assay Kit (Colorimetric)' (Abcam). This kit uses p-Nitrophenyl phosphate as a phosphatase substrate which turns yellow (OD_{max}=405 nm) when it is dephosphorylated by ALP [71]. The mineralization of osteogenic cells can be evaluated by e.g. alizarin red S (ARS) staining [68]. ARS binds to calcium minerals and as ARS is red colored, mineralization can be evaluated by the presence of red color after ARS staining [69].

2.6 Functionalization of nanocellulose

Tissue engineering combines stem cells, growth factors and scaffolds. Ensuring growth factor availability for the stem cells during tissue regeneration is crucial, and one challenge with regard to growth factor delivery is that many growth factors interact with other materials through hydrophobic interactions [72]. Nanocellulose is a hydrophilic material due to the many hydroxyl groups, as a result, direct attachment of growth factors to the scaffold material can be inefficient.

One way of ensuring growth factor availability at the site of tissue regeneration, is by storing growth factors in the scaffold material. For nanocellulose scaffolds, this can be achieved by grafting the scaffold with β-Cyclodextrin (βCD) and further use the βCD to encapsulate other growth factors. For clarification, grafting is used as a word to describe either covalent or non-covalent binding of βCD to the CNFs.

βCD is a chemical with the formula $C_{42}H_{70}O_{35}$ [73]. The molecular structure consist of 7 β-glucose units bound through (1,4)-glycosidic bonds as shown in Figure 16. There exist other cyclodextrin (CD) modalities, where the most common ones are known as αCD and γCD. These have 6 and 8 glucose units, respectively [74].

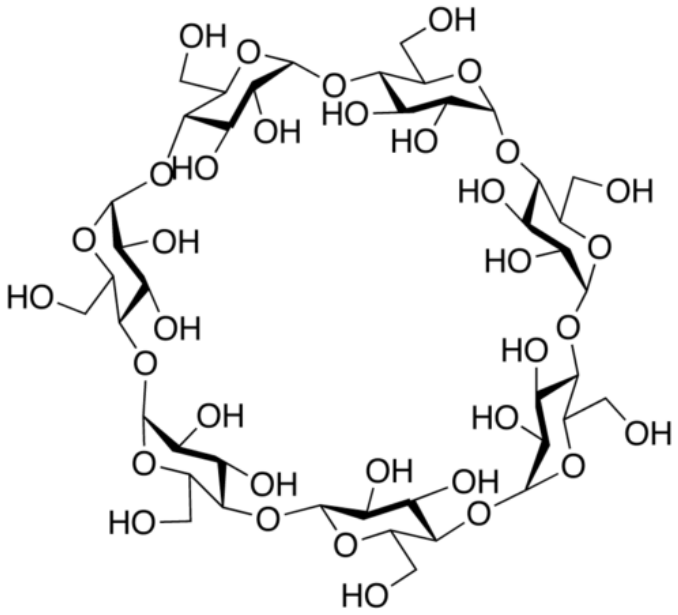

Figure 16: βCD structure. Figure collected from [75].

The structure of βCD gives the molecule highly attractive properties as a delivery agent for e.g. small drugs or growth factors. The core of βCD is hydrophobic, while the exterior is hydrophilic. Different hydrophobic molecules can thus be entrapped in the CD core, as shown in Figure 17 [74].

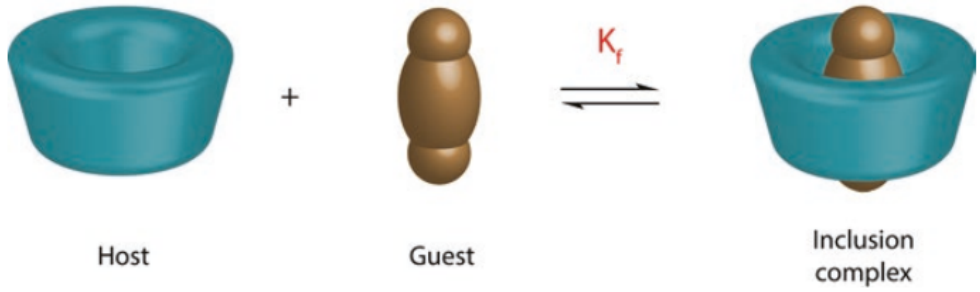

Figure 17: βCD, shown as the "Host" in the figure, can entrap hydrophobic guest molecules in their hydrophobic core and form an inclusion complex. The figure is collected from [74].

2.6.1 Methods for grafting

Several methods can be used to obtain βCD grafted to nanocellulose materials, such as direct covalent grafting and grafting through the use of a crosslinker, both of these methods are explained below. Other methods are also described in literature, such as preparing TEMPO-oxidized nanocellulose with primary amines bound to the carboxylic group, and reacting the amines with activated carboxymethyl βCD [76].

Direct covalent grafting of βCD
TEMPO-oxidized nanocellulose contain carboxylic groups which can be utilized in various chemical modifications, such as esterification reactions [77]. As βCD contains OH groups, a covalent ester bond between the carboxylic group and OH groups can be formed as illustrated in Figure 18, through thermal treatment. As shown in Figure 19, the reaction is catalysed by acid.

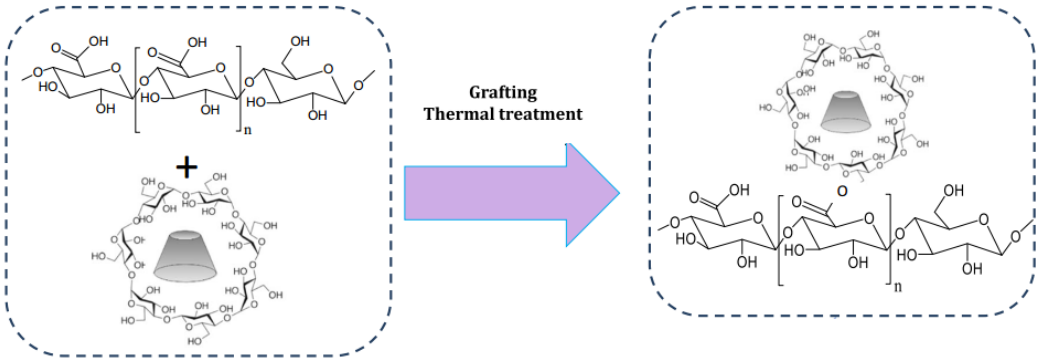

Figure 18: Schematic illustration of the grafting of βCD to TEMPO-oxidized nanocellulose, through the formation of an ester bond. The illustration is collected from the paper by Saini et al, as a part of a bigger figure [77].

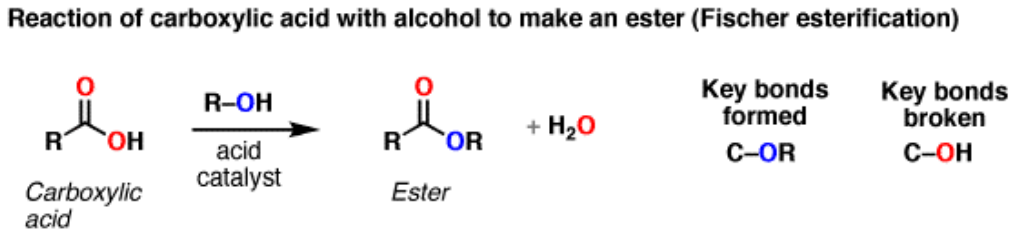

Figure 19: Formation of an ester through reaction of a carboxylic acid with an alcohol. The figure is collected from [78].

Crosslinker

Instead of directly binding βCD to the carboxylic groups on the TEMPO-oxidized nanocellulose, a crosslinker molecule can be used, as shown in Figure 20, where both fumaric acid and succinic acid are possible crosslinking agents. For this reaction, the carboxylic group on the crosslinker reacts with OH groups on both the CNF and the βCD molecule, thus it is not necessary to use a TEMPO-oxidized CNF for the process. A limitation to βCD grafting through this process is that the crosslinker can bind only to either the nanocellulose or the βCD molecules. This must be taken into account when choosing method for assessing if the βCD grafting has been successful.

The use of crosslinker can be performed in different ways. One way is to mix the fumaric acid and βCD with the nanocellulose at the same time, while another method is to introduce the nanocellulose to fumaric acid prior to the βCD.

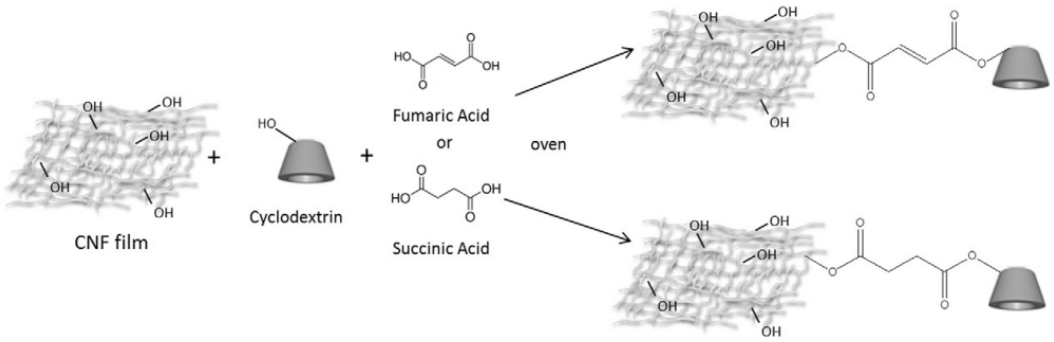

Figure 20: Illustration of the grafting of βCD through cross-linking, using either succinic acid or fumaric acid as crosslinking agent. The illustration is collected from [79].

2.6.2 Confirming the βCD grafting

After βCD grafting, the βCDs can both be covalently bound and absorbed on the nanocellulose material. To distinguish between covalently bound or absorbed βCD, Fourier Transform Infrared Spectroscopy (FTIR) can be used to detect ester bonds, as a proof of covalently bound βCD. However, as long as the βCD is attached to the nanocellulose material for a sufficiently long time to ensure guest molecule delivery, the attachment-mechanism is not important.

Fourier Transform Infrared Spectroscopy
FTIR is an analytical tool that can be used to obtain information about the chemical properties of a sample. An FTIR apparatus consist generally of an IR source, the interferometer, detector, laser and computer [80]. The IR source creates a beam of infrared light which is passed through the sample of interest and the molecules of the sample will absorb or transmit the infrared light. By passing IR radiation at different frequencies through the sample, and detecting the absorbed radiation at each frequency, the molecular nature of the sample can be evaluated as molecules have specific IR fingerprints [80].

One major sampling technique in FTIR is Attenuated Total Reflection (ATR) [80]. ATR is an FTIR accessory that can be used to examine the surface structure in stead of measuring the chemical structure of the bulk. In ATR, the infrared beam hit a crystal and from the crystal, evanescent waves hits the sample as shown in Figure 21. It is therefore necessary to have sufficient contact between the sample and the crystal surface.

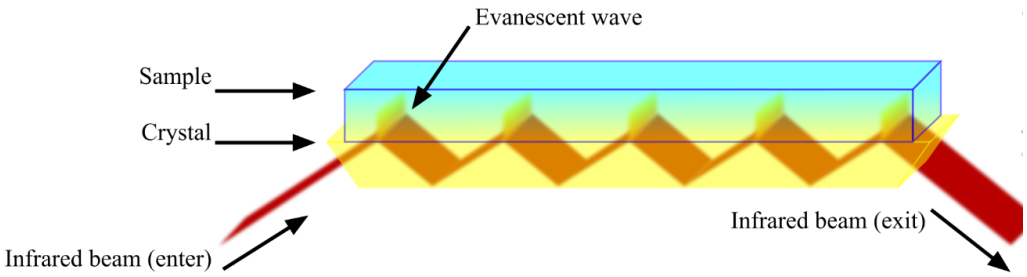

Figure 21: Principle of an FTIR-ATR apparatus. An infrared beam hits the crystal and evanescent waves hit the sample. A detector creates an IR-specter based on the amount of IR radiation absorbed by the sample and the molecular content of the sample can be evaluated. The figure is collected from [81].

In order to evaluate FTIR spectra, the position of functional groups given by the reference chart shown in Figure 22 can be used. As can be seen from the reference chart, the infrared bond peak of an ester bond (at 1740 cm^{-1}) is close to the infrared bond peak from carboxylic acids (at 1720 cm^{-1}). As carboxylate groups have infrared bond peak position at 1600 cm^{-1} [77], increasing the pH of the material before running an FTIR analysis where ester bonds are of interest, can be smart to convert carboxylic acids into carboxylate groups.

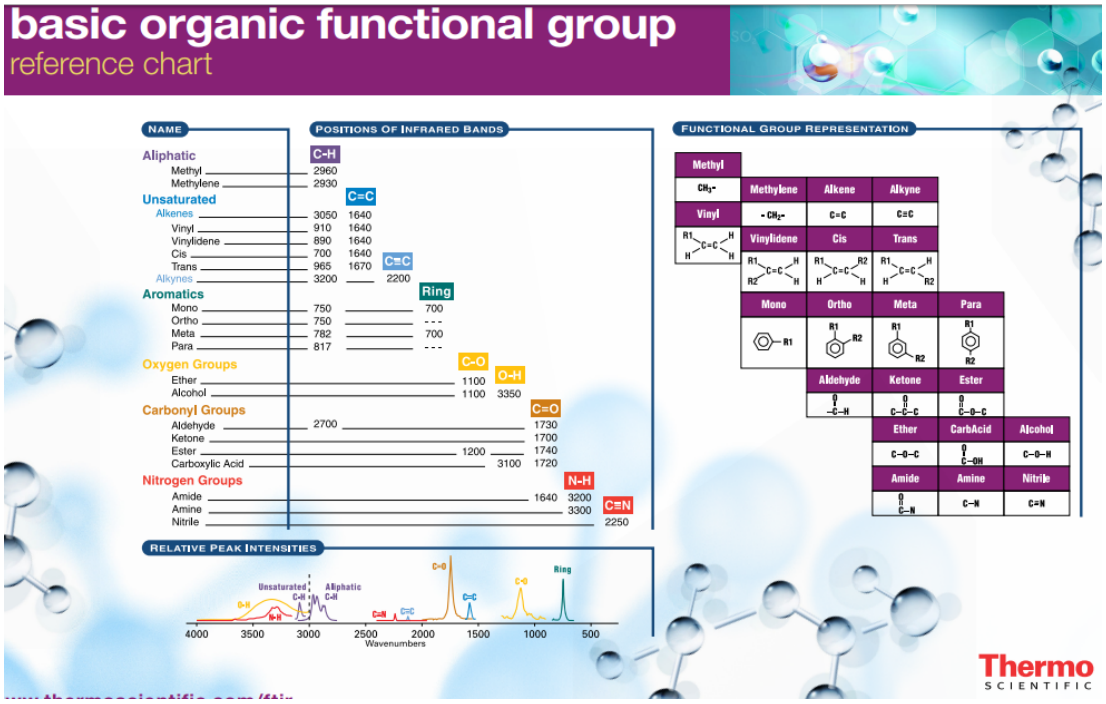

Figure 22: Reference chart of infrared band positions for basic organic functional groups. The figure is collected from [82].

3 Experimental

All percentage concentrations listed in this thesis refers to weight/weight % (wt/wt %) and they are calculated as the fraction of the weight of the solute/suspended material (usually dry CNFs/BNC) related to the total weight of the suspension. For all nanocellulose suspensions, water has been used as a solvent unless otherwise stated.

3.1 Chemicals and samples

The different chemicals used in this project are listed in Table 2, including manufacturer. The sample names and treatment methods used for each sample are listed in Table 3.

The pulp used as cellulose material in this project was a bleached, never-dried mixture of spruce (picea abies, about 75%, and some picea sichensis) and pine (pinus sylvetris, about 25%) extracted through the kraft-process. The mass was delivered by Södra.

Table 2: List of chemicals used including manufacturer.

Chemical	**Manufacturer**
TEMPO	Sigma-Aldrich
NaClO	Roth
CH_3OH	Romil
CH_3COOH	Roth
NaBr	Sigma-Aldrich
$NaClO_2$	Sigma-Aldrich
NaOH	Reagecon
HCl	Sigma-Aldrich
KI	Merck
H_2SO_4	Roth
$Na_2S_2O_3$	Romil
NaCl	Merck
Fumaric acid	Sigma-Aldrich
β-Cyclodextrin	Sigma-Aldrich
TTC	Sigma-Aldrich
Crystal Violet	Merck
$NaC_{12}H_{25}SO_4$	Sigma-Aldrich
PBS	Gibco
α-MEM Medium	Gibco
BSA	Sigma-Aldrich
FBS	Sigma-Aldrich
SDS	Sigma-Aldrich
Penicillin - Streptomycin solution	GE Healthcare
Trypsin-Versene mixture	Lonza
Calcein-AM	Invitrogen
Ethidium homodimer-1	Invitrogen
DAPI	Sigma-Aldrich
Dexamethasone	Sigma-Aldrich

L-Ascorbic acid	Sigma-Aldrich
β-glycerophosphate disodium salt hydrate	Sigma-Aldrich
Phalloidin	Sigma-Aldrich
Pierce BCA Protein Assay Kit	Thermo Scientific
LDH Assay Kit	Abcam
DMSO	Sigma-Aldrich
Tryphan blue stain 0.4%	Invitrogen
Formaldehyde	Merck
Triton X	Sigma-Aldrich
Alizarin red S	Sigma-Aldrich
Cetylpyridinium chloride	Sigma-Aldrich
AlamarBlue	Invitrogen
Quant-iT^{TM} PicoGreen^{TM} dsDNA Assay Kit	Invitrogen
KOH	J.T.Baker
D-(+)-Glucose	Sigma-Aldrich
Alkaline Phosphatase Detection Kit	Sigma
Cetylpyridium chloride	Sigma-Aldrich

Table 3: List of sample names including treatment methods used for each sample in this project.

Sample	**Treatment**
TO-CNF	TEMPO-oxidized wood based CNFs
TO-O-CNF	TEMPO-oxidized and further oxidised wood based CNFs
TO-R-CNF	TEMPO-oxidized and further reduced wood based CNFs
BNC	Bacterial nanocellulose from JeNaCell

3.2 Apparatus

The different apparatus used in this project are listed in Table 4 along with model and manufacturer.

Table 4: List of apparatus used including model and manufacturer.

Apparatus	**Model**	**Manufacturer**
pH measurer	inoLab pH	WTW
pH measurer	HI2002-02 Edge	HANNA
Conductivity measurer	inoLab Cond	WTW
Automatic titrator	902 Titrando	Metrohm
Conductivity module	856 Conductivity Module	Metrohm
Homogenizer	Rannie 15 type 12.56X	APV, SPX Flow Technology
Fiber Tester	912 Plus	ABB AB / Lorentzen & Wettre
Viscometer	DV2TLV	Brookfield
Ultra Turrax	T25	IKA
FT-IR spectrometer	Spectrum 65	Perkin Elmer

UV spectrophotometer	UV-1800	Shimadzu
AFM	Dimension ICON	Bruker
Dynamic absorption tester	DAT 1100	FIBRO system ab
Autoclave	3150EL	Tuttnauer
Shaker	-	Edmund Bühler GmbH
Vortex mixer	SA8	Stuart
Microplate reader	Varioskan LUX	Thermo Scientific
Automated cell counter	Countess	Invitrogen
Zeta potential analyzer	Zeta-sizer NANO ZSP	Malvern
Stereo microscope	M205C	Leica
Fluorescence microscope	Eclipse Ti	Nikon
Fluorescence microscope	Eclipse 80i	Nikon
Optical microscope	Eclipse TS100	Nikon
Thermoshaker	SW22	Julabo
Incubator	FORMA STERI-CYCLE CO_2 Incubator	Thermo Scientific
Centrifuge	5810 R	Eppendorf

3.3 Production of the TO-O-CNF sample

Three different nanocellulose qualities were produced as a part of the specialization project; the TO-CNF and TO-R-CNF material used in this master thesis, as well as a TEMPO-oxidized and further oxidized sample, now referred to as TO-O-CNF*. The TO-O-CNF* material produced last fall was not the same TEMPO-oxidized and further oxidized material used in this master thesis, called TO-O-CNF. The TO-O-CNF batch was produced this spring due to concerns regarding the production of TO-O-CNF*. However, the production methods used to produce the TO-O-CNF sample are the same as the methods used for the TO-O-CNF* sample this fall. The methods described in this section were therefore written as a part of the specialization project and included here as they still are relevant.

3.3.1 Determine the concentration of NaClO

The amount of NaClO affects the numbers of carboxylate groups introduced by the TEMPO-mediated oxidation [30]. To achieve the desired carboxylate content, precise amounts of NaClO must be added, and the concentration must be evaluated before use.

The NaClO concentration was measured by adding 5 % KI solution (10 mL) and 20 % H_2SO_4 solution (5 mL) to a beaker containing water (around 35 mL). The solution was mixed using a magnetic stirrer and NaClO (0.5 mL) was added. The solution was stirred for three minutes before $Na_2S_2O_3$ was added until the solution became colourless. The concentration of the NaClO solution was calculated by equation (9). In equation (9), $C_{Na_2S_2O_3}$ is the concentration of $Na_2S_2O_3$, b is the volume of $Na_2S_2O_3$, a is the volume of NaClO and MW_{NaClO} is the molecular weight of NaClO equal to 74.44 g/mol. The concentration was measured in three parallels.

$$C_{NaClO} = \frac{C_{Na_2S_2O_3} \cdot b \cdot MW_{NaClO}}{2a} \tag{9}$$

3.3.2 TEMPO-mediated oxidation

The TEMPO-mediated oxidation was performed similarly as described in [33]. Pulp from Södra (110 g dry) was suspended in water (8.25 L) containing TEMPO (1.375 g) and NaBr (13.750 g). The slurry was kept around pH 10.5, using inoLab pH measurer (WTW), by adding 0.5 M NaOH, before and while the reaction proceeded. The reaction began by adding 2.5 mmol NaClO/g dry cellulose slowly to the slurry. When all NaClO was added and the pH had stabilised, usually after $\sim$ 50 minutes, the pH was adjusted to 7 using 0.5 M HCl. Metanol (100 mL) was added to remove TEMPO left in the slurry. The cellulose was washed thoroughly using a filter paper in a Büchner funnel until the conductance of the filtrate was below 5 μS/cm, measured with a Inolab Cond conducitivity measurer (WTW).

3.3.3 Oxidation with $NaClO_2$

The oxidation of the already TEMPO-oxidized cellulose fibers was performed as described in literature [34]. TEMPO-oxidized cellulose (100 g dry) was suspended in water (final volume of 5.0 L) and mixed with $NaClO_2$ (90.5 g) and 5 M acetic acid (1.0 L). The slurry was stirred for 48 hours, and then washed in the same way as the TEMPO-oxidized cellulose.

3.3.4 Homogenization

The pretreated cellulose fibers, diluted to solid content 1.2 % in water, was homogenized using a Rannie 15 type 12.56X homogenizer (APV, SPX Flow Technology). The homogenization was performed in two passes, first at 600 bar, then at 1000 bar pressure, by Per Olav Johnsen and Johnny Kvakland Melbø from RISE PFI.

3.4 Characterization of the nanocellulose qualities

When referring to the nanocellulose qualities, this include the three CNF qualities produced during the specialization and master project, and the BNC sample bought from JeNaCell. When referring to the CNF samples, the BNC sample is excluded. Due to the nature of the nanocellulose qualities, not all characterization methods are as applicable to the BNC sample as to the CNFs. The BNC sample has therefore not been characterized in the same way as the CNFs.

The CNF qualities produced during the specialization project were characterized by, amongst others, determining the carboxylate content, viscosity and degree if fibrillation (by the use of a fiber analyzer). These characterization methods have been used to characterize the TO-O-CNF sample during the master thesis. The description of these methods have therefore been included here. New characterizations have also been conducted for all the nanocellulose qualities, such as multiscale imaging, determining aldehyde contents, ζ-potentials, contact angle, surface roughness using AFM and protein adsorption properties.

3.4.1 Carboxylate content

The carboxylate content of the CNF qualities was determined by the electric conductivity titration method [33]. CNFs (0.2 g dry) were suspended in MQ water (about 450 mL). 0.1 M NaCl (5 mL) was added and the pH was adjusted to 2.5-3.0 using 0.1 M HCl. MQ water was added to a final volume of 500 mL. The solution was stirred for 30 minutes before 0.05 M NaOH was added and the stirring continued throughout the titration. NaOH was added at a rate of 0.2 mL/min, using the 902 Titrando automatic titrator (Metrohm). During the titration, the conductivity of the solution was measured using the 856 Conductivity Module (Metrohm). The data was recorded with the Tiamo Titration Software, and further transferred to MATLAB where the calculations of the carboxylate contents of the samples were completed. Example calculation is shown in Appendix A.1 and it was performed two measurements per CNF quality. The BNC sample was not evaluated, as bacterial synthesis of BNC does not include incorporation of carboxylate groups [20].

To be able to calculate the carboxyl contents, the concentration of the NaOH solution used as a titrant had to be known. The NaOH concentration was determined by adding 0.1 M HCl (1 mL) and 0.1 M NaCl (2 mL) to a 200 mL beaker with MQ water (around 180 mL). The total volume was adjusted to 200 mL and stirred for a couple of minutes using a magnetic stirrer. NaOH, with concentration around 0.05 M, was added using a 902 Titrando automatic titrator (Metrohm). During the titration, the conductivity of the solution was measured using 856 Conductivity Module (Metrohm). The data was recorded with the Tiamo Titration Software, and further transferred to MATLAB where the exact NaOH concentration was calculated. Example calculation is shown in Appendix A.1.1.

3.4.2 Aldehyde content

The aldehyde contents of the nanocellulose qualities were determined by a spectrophotometric method, described in literature [38]. 0.4 % nanocellulose suspension (4 g) was added to a 15 mL test tube followed by the addition of 0.3 M KOH (0.5 mL) and 0.01 M TTC (0.5 mL). The tube was constantly shaken for 8 minutes in water bath at 80°C. 9 mL methanol was added to extract TTF and the amount of TTF was recorded spectrophotometrically at 482 nm using the UV-1800 spectrophotometer (Shimadzu). The amount of aldehyde groups was calculated from a calibration curve prepared with D-glucose as a substrate. Example calculation is shown in Appendix A.2. D-glucose was added as 4 g of different glucose-suspensions, ranging in concentration from 0 % to 0.05 % in water. Two parallels per nanocellulose quality were measured and the absorbance of each parallel was measured in duplicates. A blank sample with water instead of TTC was also prepared for each nanocellulose quality to correct the measured absorbances.

3.4.3 Viscosity

For the viscosity measurements, 0.4 % CNF suspension (600g) was added to a 600 mL beaker, and a DV2TLV viscometer (Brookfield) was used along with the Rheocalc software. Each CNF sample was evaluated in three parallels, and the viscosity of each parallel was measured from 0.1 RPM to 100 RPM. Sample TO-CNF and TO-R-CNF was measured with spindle V-72,

while sample TO-O-CNF was measured using spindle V-71 because the torque measured using spindle V-72 for sample TO-O-CNF was outside the accuracy range.

3.4.4 Fiber analysis

For the quantification of residual fiber content, the fiber analyzer Fiber Tester 912 Plus (ABB AB/Lorentzen Wettre) was used. As BNC do not contain larger residual fiber structures [20], it was not analyzed. 0.25 % CNF solution (40 g) was added to a 400 mL beaker and water (around 300 mL) was added. In the fiber analyzer, the CNF suspension was pumped through a flow cell [83], where the fiber residues were photographed with a resolution of 4 μm. The photographs were further used to analyze fiber properties such as the mean length and mean width of the fibers detected, by the Fiber Tester Plus software. From these data, the residual fiber content of the samples was calculated, see example calculation in Appendix A.5. Each sample was run in three parallels.

3.4.5 AFM

0.01 % nanocellulose suspensions were prepared and 25 μL of each sample was added to freshly cleaved mica and left to dry in air. When dry, the samples were analyzed on a Dimension ICON AFM (Bruker) using NanoScope 9.4 Software and Scan Asyst in Air (SA-air AFM probes from Bruker, material: silicon tip on nitride lever, f0=70kHz, k=0.4N/m).

One image was acquired for the samples with image size 10x10μm^2. The scan rate was 0.988 Hz with 1024 samples per line, aspect ratio equal to one. Surface roughness and image export was done using NanoScope Analysis software (version 1.9) after plane fit (2nd order) and Flatten (2nd order) commands. The AFM imaging and surface roughness analysis was conducted by Birgitte Hjelmeland McDonagh from RISE PFI.

3.4.6 Multiscale imaging of the nanocellulose fibers

0.26 % nanocellulose suspension (40 μL) was added to an object glass and dried at 37°C. 100 μL crystal violet (1:1 diluted with water) was added to stain the fibers and the stain was let soak for 2 minutes. The object glass was washed with water to remove excess dye and the fibers where visualized using an Eclipse 80i microscope (Nikon). The images without crystal violet were also imaged using the same microscope.

3.4.7 ζ-potential

The ζ-potential of the nanocellulose qualities was determined using the Zeta-sizer NANO ZSP (Malvern) apparatus connected to the Zetasizer software (version 7.11). The nanocellulose qualities were prepared at a concentration of 0.08 g/L in both distilled water (pH 5.3) and α-MEM medium containing 10 % FBS (pH 7.3). A folded capillary zeta cell was used for the measurements. Each nanocellulose quality was measured in three parallels, and each parallel was run 5 times. The ζ-potential of pure water and pure medium was also measured.

3.4.8 Film preparation

Circular films with grammage 20 g/m^2 were prepared to measure the contact angle of the nanocellulose qualities. The films were made by adding 40 g 0.275 % nanocellulose suspension to petridishes with a diameter of 5.6 cm. The water evaporated by storing the petridishes at room temperature (RT) for about two weeks.

3.4.9 Contact angle

To study the effect of surface modifications on the wettability of the materials, the contact angle was measured with a DAT 1100 dynamic absorption tester (FIBRO system ab) at 23°C and 50 % relative humidity (RH). A droplet of water (4 μL) was deposited on the specimen surface. Series of images were captured and analyzed by the DAT3 software. The dynamic wetting (contact angle) was measured as a function of time between 0 and 175 s. A minimum of ten readings were taken for each sample.

3.4.10 Protein adsorption

The extent of adsorbed proteins on nanocellulose coated surfaces, relative to each other, was evaluated using three different protein solutions: 10 % FBS in α-MEM medium, 100 % FBS and 5 % BSA in α-MEM medium. 500 μL of the protein suspensions were added to nanocellulose coated TCPs, in 24-well plates, and incubated for 4 hours at 37°C with 5 % CO_2 humidified atmosphere. The TCPs had previously been coated using 0.26 % nanocellulose suspensions (400 μL/well) and the water was evaporated by incubating the plates at 37°C. The wells were washed with PBS to remove weakly adsorbed proteins and incubated with 2 % sodium dodecyl sulfate (SDS, 500 μL/well) for 24 hours to dissolve the adsorbed proteins.

The amount of protein adsorbed to the different qualities was measured by a commercial protein assay kit (Pierce BCA Protein Assay). 25 μL of the protein-SDS solutions from each sample was added to 96-well plate wells and 200μL BCA working reagent was added. Four blank samples were made by adding 25 μL 2 % SDS instead of the protein-SDS mixture to 96-well plate wells. The BCA working reagent consisted of 50:1, BCA reagent A:B. The plate was covered with aluminum foil and incubated at 37°C for 30 minutes before the absorbance at 562 nm was read using the Varioskan LUX microplate reader (Thermo Scientific). The absorbance of the samples was corrected by subtracting the mean absorbance of the blank samples. The amount of proteins adsorbed to each nanocellulose quality was measured in 5 parallels and each parallel were measured in duplicates.

3.5 Cytocompatibility of the nanocellulose qualities

The in vitro cytocompatibility of the nanocellulose qualities was evaluated at the Department of Clinical Dentistry, University of Bergen using rBMSC. The nanocellulose materials used in these procedures had been sterilized using the 3150EL autoclave (Tuttnauer), at 120°C for 20 minutes. The cells were cultured in α-MEM medium supplemented with 10 % FBS and 1 % antibiotics (10 000 units/mL penicillin and 10 000 ug/mL streptomycin), referred to as 'regular medium', unless otherwise stated. Fresh medium was supplied twice a week. Incubation was performed in the FORMA STERI-CYCLE CO_2 incubator (Thermo Scientific) at 37°C with 5

% CO_2 humidified atmosphere.

3.5.1 Cell culturing

Before any of the cytocompatibility analyses could be performed, the rBMSCs had to be woken up and cultured to reach the desired amount of cells. A vial containing DMSO (1 mL) and rBMSCs (around $4x10^6$) was stored in liquid nitrogen and the cells were woken up by placing the vial in water bath at 37.5°C for 60 seconds. The DMSO and rBMSC mixture was transferred to a tube with culture medium (4 mL) to dilute the DMSO. The cell mixture was divided and added to two flasks with culture medium (10 mL) and incubated for 24 hours. The flasks had a growth surface area of 75 cm^2.

After the first 24 hours of incubation, dead cells plus old medium were removed from the cell culturing flasks. Medium (10 mL) was added and the cells were incubated. Medium was replaced in the culturing flasks every third-fourth day. After six days of culturing, the cells in the small flask had reached 85-90 % confluence and the cells were split to bigger flasks with growth area of 175 cm^2. The culture medium was removed and PBS (10 mL) was added to wash. Trypsin (3 mL) was added to detach the cells from the flask surface and the cells were incubated with the trypsin for 5 minutes. The detachment of the cells was confirmed by looking at the flask in a microscope for free-floating cells. If many cells still were attached to the flask surface, gentle knocking on the flask was performed. Medium (3 mL) was added within 10 minutes after the trypsin addition, as trypsin is toxic for the cells. The cell-trypsin-medium mixture was transferred to a tube and centrifuged at 1200 rpm for 5 minutes using the 5810 R centrigufe (Eppendorf). The supernatant was discarded and the cell pellet was disrupted before medium (1-2 mL/million cells expected) was added.

The number of cells that was in the cell pellet had to be known before adding the cells to new flasks, as the 175 cm^2 flasks should be incubated with around 1 million cells to ensure good growth conditions. Cell suspension (10 μL) was mixed with tryphan blue (10 μL) and the mixture was added to two cell counting chambers before counting was done using the Countess automated cell counter (Invitrogen). Around 1 million cells were added to three 175 cm^2 flasks with culture medium (total volume around 20 mL).

3.5.2 Cell seeding

The following paragraph applies to all cytocompatibility assays except the indirect cytotoxicity assay which will be explained below. To evaluate the cytocompatibility of the four nanocellulose qualities (TO-CNF, TO-O-CNF, TO-R-CNF and BNC) in regards to cell viability, morphology, proliferation and osteogenic differentiation, rBMSCs were grown on nanocellulose-coated 24-well tissue culture plates (TCPs). The wells were covered by adding 0.26 % nanocellulose suspension (400 μL) before drying over night at 37°C to evaporate the water. Uncoated TCP wells were used as controls. The plates were sterilized by placing the plates under UV for one hour. The cell density used was 5000 cells/well and the cells were cultured with 500 μL medium in each well.

3.5.3 Cell viability

Indirect cytotoxicity
To evaluate that the production methods are safe and that the washing of the nanocellulose materials is sufficient to remove any harmful chemicals, an indirect cytotoxicity assay was conducted. For this assay, cells were cultured directly on TCP surfaces, in 24-well plate wells, in regular medium for 24 hours to allow the cells to attach. After this, the medium was changed to extract medium and the cell viability was evaluated after one and three days. The extract medium was made by incubating 10 g of each nanocellulose quality suspended in α-MEM medium without FBS (0.26 %) at 37°C with constant shaking (60 rpm) for 24 hours before filtration (0.2 μm pore size). Cells cultured with regular medium instead of extract medium were used as control groups.

After one and three days of culturing the cells in extract medium, alamarBlue reagent (50 μL) was added to each well and incubated for 4 hours. 50 μL alamarBlue reagent was also added to two cell-free wells with 500 μL regular medium, to produce blank samples. 100μL of stained medium was collected from each well and transferred to a 96 well-plate in duplicates to analyze the fluorescence using the Varioskan LUX microplate reader (Thermo Scientific). The absorbance of the samples was corrected by subtracting the mean absorbance of the blank samples. The excitation wavelength used was 560 nm while the emission wavelength was 590 nm. The rest of the stained medium in the 24-well plate was removed and the wells were washed with PBS. 10 % formaldehyde (250 μL) was added to each well for about 10 minutes before again washing with PBS. The fixed cells were imaged using an Eclipse TS100 optical microscope (Nikon). There were prepared four wells per nanocellulose sample, at each time point, for the indirect cytotoxicity analysis. The alamar blue staining was performed while protecting the plate from light.

Live/dead staining
The viability of the cells cultured on nanocellulose coated TCPs after one day was analyzed by live/dead staining. The culture medium was removed and the wells were washed with PBS (500 μL). The cells were incubated in the dark for 45 minutes with a working solution (300 μL/well) containing Calcein-AM (1.5 μL, stains living cells green) and ethidium homodimer-1 (1.5 μL, stains dead cells red) dissolved in 5 mL PBS. After incubation, the working solution was replaced with PBS and the plate was covered in aluminium foil before imaged using an Eclipse 80i fluorescent microscope (Nikon). Three wells were prepared and imaged per nanocellulose sample, however only one representative picture per sample is included in the report.

Lactate dehydrogenase assay
The medium from the wells used for the proliferation analysis was collected after day one and day three to evaluate the immediate toxicity of the nanocellulose qualities relative to each other and to the control group. The medium from the proliferation analysis plates after one day could be used as the proliferation plates intended for one day of culturing had reached the assigned time point. The medium from the other proliferation analysis plates could be used after three days as it could be combined with the supply of fresh medium. The medium was stored in the freezer at -80°C until the analysis was conducted. The levels of LDH were measured using the colometric LDH assay kit (Abcam).

25 μL of medium from each sample was added to 96-well plate wells and 25 μL assay buffer (from the assay kit) was added. Four blank samples were prepared by adding clean, regular medium to 96-well plate wells instead of the medium from the sample wells. 50 μL reaction mixture was also added to each well. To prepare 50 μL reaction mixture, 48 μL assay buffer and 2 μL substrate mix solution were mixed. The substrate mix was made by dissolving the substrate reagent in the kit, in 1.1 mL MilliQ water. The absorbance was measured at 450 nm after 30 minutes of incubation at 37°C, protected from light, using the Varioskan LUX microplate reader (Thermo Scientific). The absorbance of the samples was corrected by subtracting the mean absorbance of the blank samples. The medium was collected from four wells for each sample after both one and three days, and measured in duplicates.

3.5.4 Morphology

The morphology of the rBMSCs cultured on nanocellulose coated TCPs was evaluated after 3 and 24 hours. The medium was removed and the wells were washed using PBS (500 μL). The cells were incubated at RT with 4 % formaldehyde (400 μL/well) for 10 minutes to fix the cells, before washing two times using PBS and adding 0.1 % Triton X (500 μL) to each well. After another 10 minutes at RT, the plates were washed and stored with PBS in the fridge until staining.

To observe the morphology of the rBMSCs, the cells were stained in the dark using phalloidin (dilution 1:50 with PBS) and DAPI (dilution 1:2000 with PBS). Phalloidin stains the cytoskeleton of the cells green while DAPI stains the nuclei blue. DAPI can also stain cellulose fibers blue. The PBS which the cells were stored in was removed and phalloidin (150 μL/well) was added. The plates were incubated for 45 minutes at RT before washing twice with PBS. DAPI (150 μL/well) was added and the plates were incubated for 5 minutes at RT before washing with PBS. The cells were imaged using an Eclipse Ti fluorescence microscope (Nikon). It was prepared three wells for each of the five groups, for both time points.

ImageJ was used to analyze the surface area and maximal cell length of the cells imaged. It was taken three images per well, as there were three wells for each group, this resulted in a total of nine images per sample, at each time point. Of the nine images, three were chosen for the image analysis, all from different wells, and a minimum of 20 cells were analyzed. The average value as well as the standard deviation of the surface area and max cell length was calculated from the measurements of the $\geq$20 cells.

3.5.5 Proliferation

The proliferation properties of rBMSCs were evaluated after culturing the cells on nanocellulose coated TCPs for 1, 7 and 14 days. Four wells in 24-well plates were used for each sample, at each time point, and non-coated TCPs were used as controls. The proliferation properties were investigated with cells grown both with regular medium and with osteogenic medium. The osteogenic medium was made by mixing regular medium (α-MEM, FBS and antibiotics), dexamethasone (20 μL/100 mL medium), L-Ascorbic acid (35 μL/200 mL medium) and β-glycerophosphate disodium salt hydrate (500 μL/100 mL medium). When the cells had grown

for the decided time period, the medium was removed and the wells were washed with PBS. 0.1 % Triton X (500 μL) was added to each well and the plates were stored in a freezer at -80°C until analysis.

For the proliferation analysis, the well plates were subjected to two freeze-thaw cycles, freezing at -80°C and thawing at RT. This was done in order to complete cell breakage to release double-stranded DNA (dsDNA) in the wells. Scratching the bottom of the wells using pipette tips was also conducted to release all dsDNA-material in the liquid. The mixture was transferred to eppendorph tubes, centrifuged (2 minutes, 8000 rpm, 4°C) before 50 μL of the supernatant from each sample was collected in 96-well plate wells. 50 μL 0.1 % Triton X was used instead of the supernatant for the four blank samples prepared. Analysis of the proliferation properties of the cells were evaluated using Quant-iT^{TM} PicoGreen^{TM} dsDNA Assay Kit (Invitrogen), and 50 μL of the working solution from the kit was also added to the 96-well plate wells. The working solution in the kit consisted of 1 part of A (Quant-iT^{TM} PicoGreen$^{®}$ dsDNA reagent) and 200 parts of B. The B reagent was 20x concentrated and had to be diluted in distilled, DNase-free water, prior to mixing with A. After the working solution had been added to the 96-well plate wells, the fluorescence at 485/535 nm was measured with a Varioskan LUX microplate reader (Thermo Scientific). The fluorescence of the samples was corrected by subtracting the mean fluorescence of the blank samples. As there were prepared four wells per sample, at each time point, and each sample was analyzed in duplicates, eight measurements were performed for each group.

3.5.6 Differentiation

ALP activity, an early marker of osteogenic differentiation, was analyzed after 1, 7 and 14 days to assess the osteogenic potential of the nanocellulose coated surfaces, using the colorimetric Alkaline Phosphatase Detection Kit (Sigma). The ALP analysis was conducted with cells cultured in both regular and osteogenic medium. 50 μL of the same centrifuged liquid collected for the proliferation analysis was collected in duplicates for the ALP analysis and added to 96-well plate wells. Four blank samples were made using 50 μL 0.1 % Triton X solution instead of the supernatant from the centrifuged samples. 50 μL alkaline buffer solution (from the kit) was added to each well and the absorbance was recorded at 405 nm after 60 minutes of incubation at 37°C. The measured absorbances were corrected by subtracting the mean absorbance for the blank samples.

ARS staining was also conducted to assess the osteogenic potential of the rBMSCs grown on nanocellulose coated surfaces for 21 days, in both regular and osteogenic medium. The growth medium was removed and the wells were washed with PBS. 4 % formalin (500 μL) was added to each well for fixation. The formalin was removed after one hour and 2 % ARS (300 μL/well) was added and the plates were incubated for 15 minutes at RT. After washing and air-drying, images were taken with a camera and an Eclipse TS100 optical microscope (Nikon). For quantification, the color was extracted with 100 mM cetylpyridium chloride solution (1 mL/well) for 2 hours under shaking (150 rpm). 100 μL of the extracted color in cetylpyridium chloride solution from each well was transferred to 96-well plate wells in duplicates. Two cell-free TCP wells were stained to act as blank samples and 100 μL of the solution from these wells were also transferred in duplicates to 96-well plate wells. The absorbance was measured

at 540 nm using the Varioskan LUX microplate reader (Thermo Scientific) and the absorbance measured for each sample was corrected by subtracting the mean absorbance for the blank samples. For both the ALP and ARS analysis, four wells with rBMSCs were cultured for each nanocellulose/TCP group at each time point and for both types of medium.

3.6 Statistical analysis

Statistical analysis was performed using Oneway ANOVA with a Tukey's posthoc comparison of the mean using SPSS software (IBM, Armonk, NY, U.S.A.). Differences were considered statistically significant at $p \leq 0.05$, and generally, '*' will be placed in figures between results that are significantly different from one another. Results from the characterization and cyto-compatibility assays are expressed as the mean $\pm$ standard deviation (SD), unless otherwise stated. The equation used to calculate the SD is shown in Appendix A.3.

3.7 Normalization

Some data have been normalized relative to the control group to facilitate comparison. This has only been done for unit-less data, which involves data measured in absorbance/fluorescence. The normalization has been done by regarding the mean result for the control group at the first time point in each measurement, as 100 %. The results (all results, not just the means) of the other groups have been divided on this 100 % result, before again calculating the mean for these other groups and standard deviation. Example of the normalization procedure is shown in Appendix A.4.

3.8 Functionalization of the TO-CNF material

Different methods were used to produce films where the goal was to achieve βCD grafted to the TO-CNF material. Two films without βCD were made as controls. The production method for each type of film is summarized in Table 5, where the different films have been given explanatory names. The control films have been named 0%βCD and 0%βCD/100°C/V. These names imply that neither films contain βCD and the latter have been esterified at 100°C in vacuum oven (V-oven).

0.5 % TO-CNF suspension (50 g) was added to a 100 mL beaker and stirred for 3 minutes using the T25 Ultra Turrax (IKA). 0.1 M HCl (2 mL) was added to adjust the pH to around 2.7. From here, films were either produced through the direct covalent grafting method or by the use of fumaric acid as a crosslinker. For the direct covalent grafting method, both bulk and surface grafting of βCD were tested. When using fumaric acid as a crosslinker, only surface grafting was tested, in one or two steps. All of these methods are further explained below.

For the direct covalent bulk grafting method, 10 % βCD was added before the suspension was stirred for around 1 hour using a magnetic stirrer. After stirring, the suspension was casted in a 9.5 cm diameter petri dish, which after drying at 40°C over night (ON) in regular oven (R-oven), resulted in thin films. All the films made using the direct covalent bulk grafting method are named 10%βCD, followed by information regarding the esterification process.

For the three different surface grafting methods (direct covalent, by the use of fumaric acid in one step or by the use of fumaric acid in two steps) the suspensions were stirred for around 1 hour using a magnetic stirrer. After stirring, the suspensions were casted in 9.5 cm diameter petri dishes, which after drying at 40°C ON in R-oven resulted in thin films. Pieces (around 2x2 cm) of the films were dipped for 15 seconds in different solutions, depending on which surface grafting method the films were made for. The direct covalent surface grafting film (named βCD-surface/100°C/V) was dipped in a 1.8 g/L βCD solution and the film where fumaric acid was used as a crosslinker in one step (named onestep-surface/100°C/V) was dipped in a solution containing both βCD (1.8 g/L) and fumaric acid (1.5 g/L). After the dipping, both films were dried over night in RT. Finally, the film where fumaric acid was used as a crosslinker in two steps (named twosteps-surface/100°C/V) was dipped in a solution containing fumaric acid (1.5 g/L) before drying over night in RT. This was followed by dipping in a solution containing βCD (1.8 g/L) before again drying over night in RT.

After drying, the films were heated in order to initiate the esterification reaction for βCD covalent grafting. Different heating techniques were tested to evaluate their effect on degree of esterification. The different heating techniques tested were esterification at 70°C and 100°C, using either a V-oven or R-oven. Which esterification process used for the different films is indicated in the film name by the temperature followed by either V or R, specifying the oven type.

The films were analyzed using FTIR both before and after dipping in 0.05 M NaOH for 5 seconds. NaOH dipping was conducted to ensure that all carboxylic acid groups (introduced by the TEMPO-mediated oxidation to the cellulose material) were present as carboxylate groups, to avoid overlapping peaks in the FTIR spectra. FTIR-ATR spectroscopy of the films was carried out using a Spectrum 65 FTIR Spectrophotometer (Perkin Elmer) with an ATR attachment, connected to the Spectrum software. The spectra were recorded over a range from 600 to 4000 cm^{-1} with a resolution of 4 cm^{-1} and 16 scans per sample, followed by baseline correction and smoothing.

Table 5: Overview of the film names and the different methods used to produce these CNF films grafted with βCD.

Film name	**Addition of βCD**	**Esterification process**
0%βCD	No	No
0%βCD/100C/V	No	100°C V-oven
10%βCD	10 % directly	No
10%βCD/70C/R	10 % directly	70°C R-oven
10%βCD/70C/V	10 % directly	70°C V-oven
10%βCD/100C/R	10 % directly	100°C R-oven
10%βCD/100C/V	10 % directly	100°C V-oven
βCD-surface/100C/V	Dipped in βCD-sol.	100°C V-oven
Onestep-surface/100C/V	Dipped in one step	100°C V-oven
Twosteps-surface/100C/V	Dipped in two steps	100°C V-oven

4 Results

Due to the large size of raw data, these are included in an external zip-file.

4.1 Characterization of the nanocellulose qualities

The results presented here regarding carboxylate content, viscosity and degree of fibrillation for the TO-CNF and TO-R-CNF sample were acquired during the specialization project, while the results for the TO-O-CNF and BNC sample have been produced as a part of the master thesis. All other results presented in this section have been produced as a part of the master thesis for all nanocellulose qualities.

4.1.1 Carboxyl and aldehyde contents

The three pretreatment methods resulted in CNF qualities which differed in carboxyl and aldehyde contents. The carboxyl content was determined using conductometric titration and it was performed two measurements per sample. In Table 6, the mean carboxylate content for the CNF qualities are shown including SD between the two parallels. Example calculation is shown in Appendix A.1. All carboxyl values are significantly different from each other. The carboxyl content of the BNC sample was not evaluated as the bacterial synthesis of BNC do not include incorporation of carboxyl groups [23].

Table 6: The carboxyl contents of the CNF qualities.

Sample	**Carboxyl [μmol/g]**
TO-CNF	804 ± 3
TO-O-CNF	992 ± 24
TO-R-CNF	675 ± 14

The aldehyde content of the nanocellulose qualities was determined by a spectrophotometric method, where oxidation of aldehydes leads to the reduction of TTC to the red compound TTF [38]. The amount of aldehyde groups was calculated from a calibration curve prepared with D-glucose as a substrate. The calibration curve is related to glucose concentration (wt/wt % in water) for simplicity reasons, as glucose at different concentrations was used to make the calibration curve.

Figure 23 shows how the red color of TTF increases with increasing glucose concentration, while Figure 24 shows how the absorbance measured at 482 nm changes as the glucose concentration changes. The linear area of the curve shown in Figure 24 was extracted and a trend line was fitted to the points. This linear part was used as a calibration curve to relate absorbance to aldehyde concentration. The equation of the calibration curve was y=81.631x-0.5727, with R^2-value equal to 0.9393. The calibration curve is included in Appendix A.2.

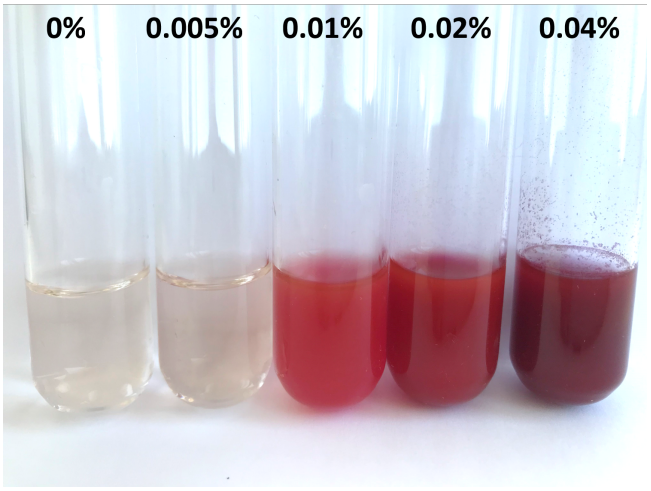

Figure 23: The red color increases as the glucose-, and thus the aldehyde-concentration, increases in reaction with TTC.

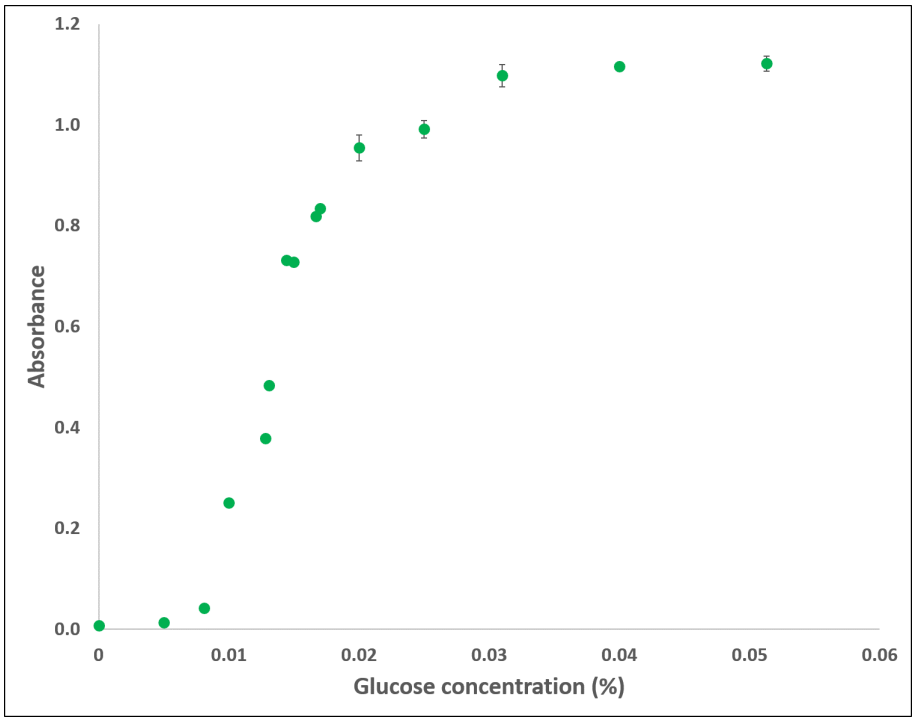

Figure 24: The absorbance measured as a function of glucose concentration in reaction with TTC.

The color of the nanocellulose qualities after reaction with TTC is shown in Figure 25. Two reaction mixtures were prepared for each nanocellulose quality and four absorbance measurements were conducted for each of these two parallels. The absorbance was also measured on a blank sample, a sample with water instead of TTC, for each nanocellulose quality. The blank samples were prepared in order to correct the absorbance of the samples, by subtracting the absorbance of the blank. For all the nanocellulose qualities except TO-CNF, the absorbance measured was too low to lie within the linear range of the standard curve (see Table 1 in Ap-

pendix A.2). The aldehyde content of these samples have thus not been determined. However, it is clear that the aldehyde content of sample TO-O-CNF, TO-R-CNF and BNC are lower than sample TO-CNF and close to zero. The aldehyde content of sample TO-CNF was determined as 280 $\pm$ 14 μmol/g dry cellulose. How to calculate the aldehyde content from the calibration curve is shown in Appendix A.2.

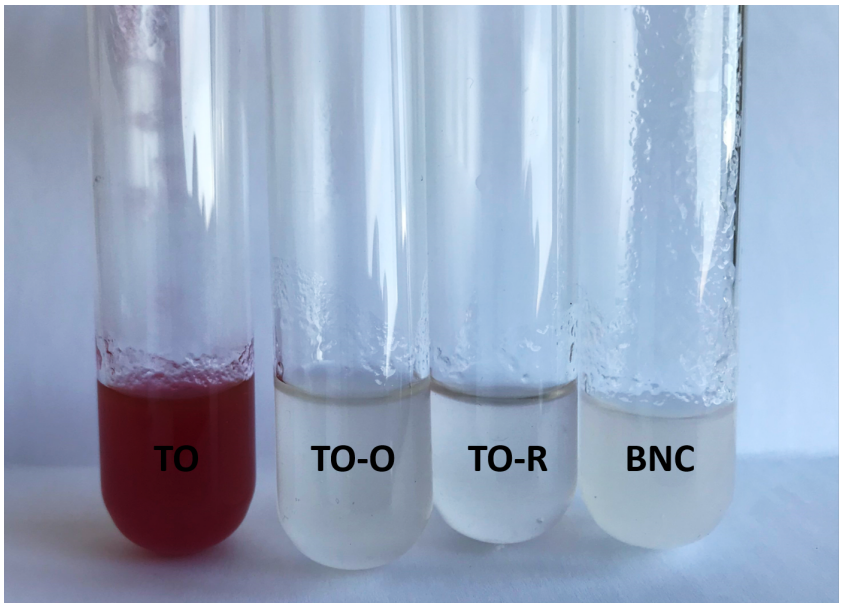

Figure 25: The color of the nanocellulose qualities after reaction with TTC.

4.1.2 Viscosity

The viscosity of the CNF samples was measured in three parallels per sample using a rotational viscometer. The viscosity was measured four times at different rotational speeds ranging from 0.1 RPM to 100 RPM. The mean of these twelve viscosity-measurements as a function of rotational speed is shown in Figure 26, for each sample.

In order to evaluate the significance of the difference in viscosity for the three groups, statistical analysis was performed at four different rotational speeds (6 RPM, 20 RPM, 60 RPM and 100 RPM). The mean viscosity including SD at these rotational speeds is shown in Figure 27 and significant differences are indicated by the '*' symbols.

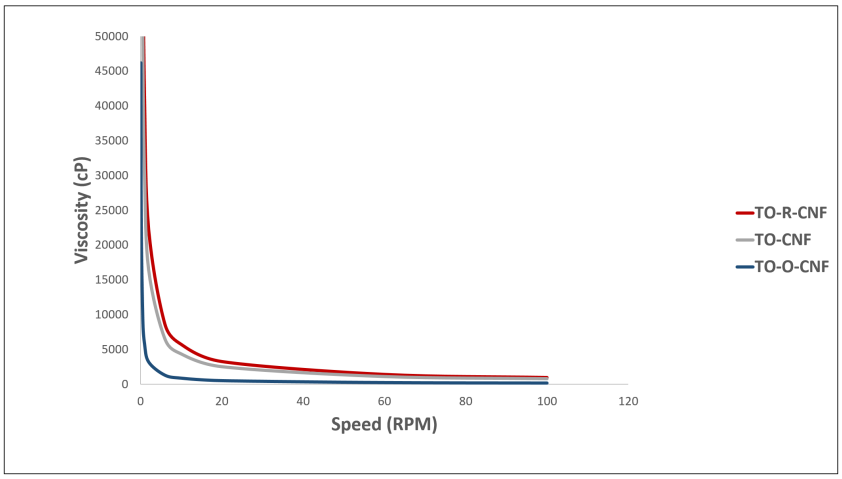

Figure 26: The mean viscosity as a function of rotational speed for the different CNF qualities suspended in water.

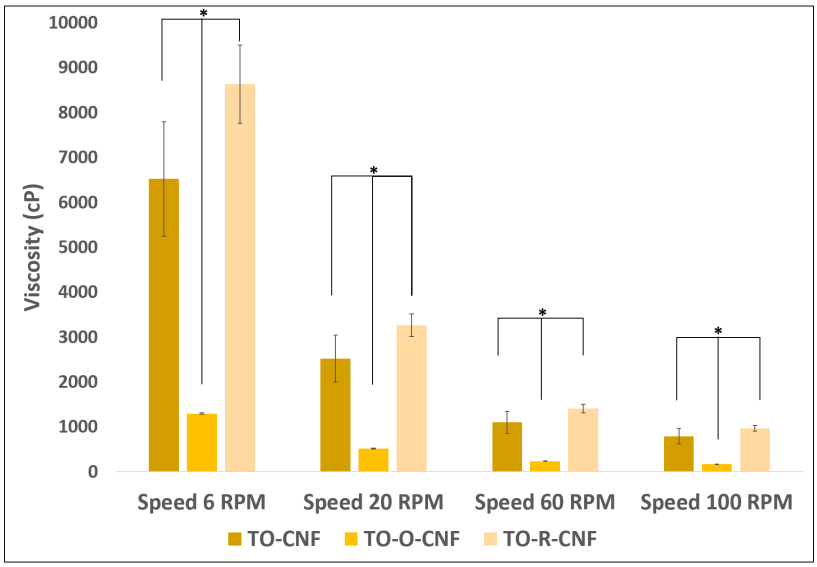

Figure 27: The mean viscosity $\pm$ SD for the different CNF qualities suspended in water at selected rotational spindle speeds.

4.1.3 Fiber analyzer

Fibrillation of cellulose through processes such as homogenization will lead to a mixture of fibers, residual fibers and nanofibrils. A better fibrillated material will contain a higher fraction of nanofibrils. Sample TO-CNF, TO-O-CNF and TO-R-CNF have been produced using different pretreatment methods, before fibrillation. Pretreatment methods can affect the degree of fibrillation, thus it is an interesting characteristic to evaluate for the materials produced in this project.

The results from the fiber analysis have been used to estimate the apparent residual fiber fraction (example calculation in Appendix A.5) and the average value from three parallels for each CNF

is shown in Table 7. The SD between the parallels is also included. The significance of the differences observed have been evaluated and there are significant difference of the residual fiber fraction measured for sample TO-O-CNF compared to the two other CNF qualities.

Table 7: The table shows the mean apparent residual fiber fraction and SD measured with the Fiber Tester plus apparatus. Significant difference was detected between the TO-O-CNF sample and the other two CNF qualities.

Sample	**Mean apparent residual fiber fraction ± SD (%)**
TO-CNF	4.3±0.6
TO-O-CNF	10.6±0.3
TO-R-CNF	4.0±0.1

4.1.4 Atomic Force Microscopy

AFM was used to image the nanocellulose qualities (Figure 28) and to measure the average surface roughness across an area of 100 μm^2 (Figure 29). Only one image at 100 μm^2 could be taken due to time limitation, therefore there it is not listed any SD for the surface roughness values, in addition, statistical analysis could not be performed.

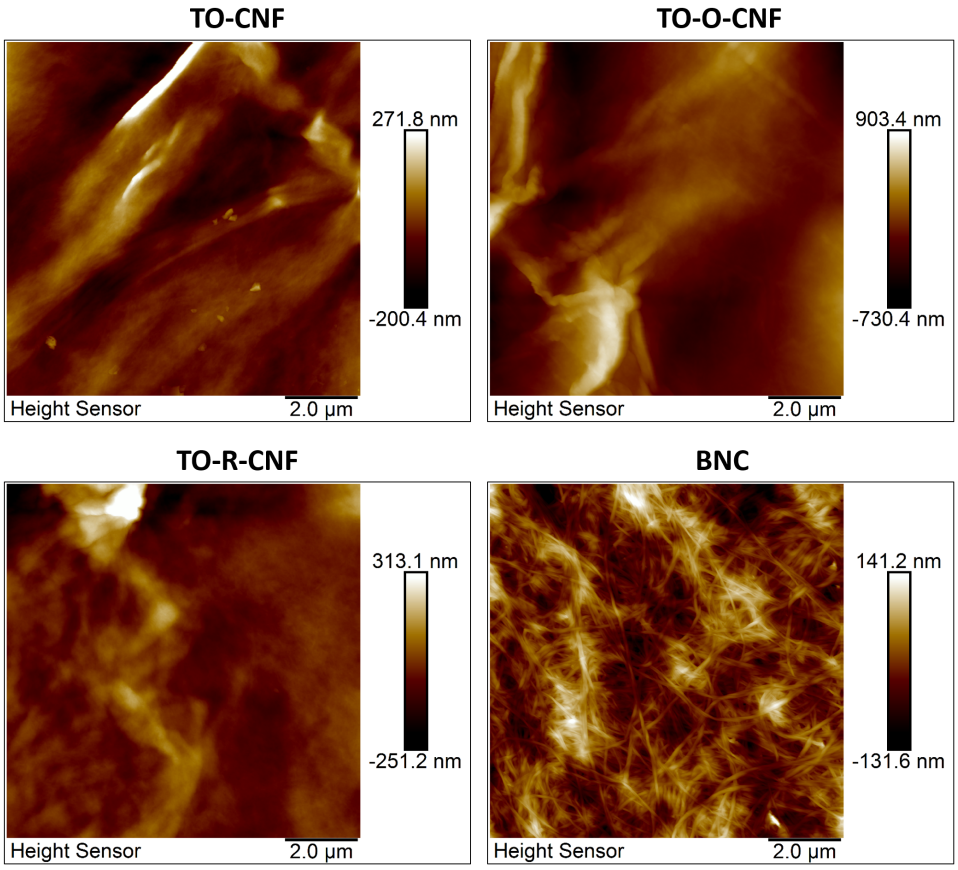

Figure 28: AFM images of the nanocellulose samples.

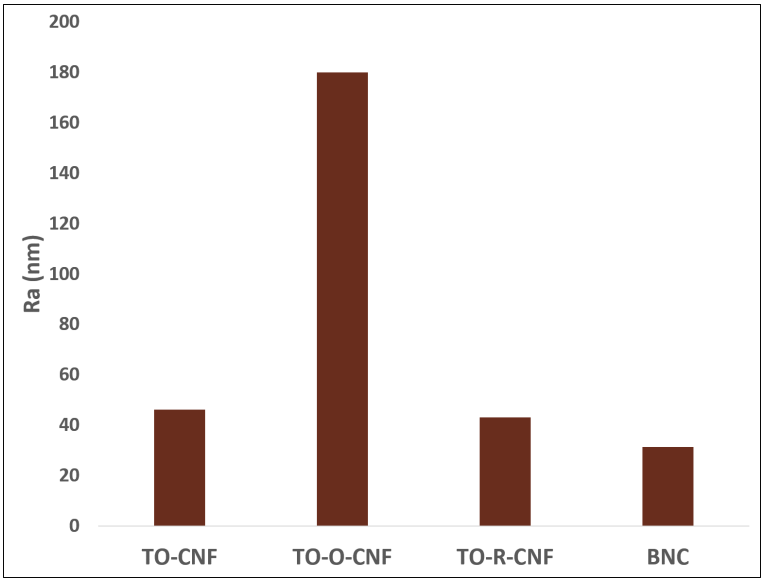

Figure 29: Average surface roughness of the nanocellulose qualities measured using AFM. The surface roughness data is referred to as the average surface roughness as the surface roughness value obtained is the average between all the points evaluated within the 100 μm^2 area.

4.1.5 Multiscale imaging of the nanocellulose fibers

The nanocellulose qualities have been imaged as suspensions with 1 % solid content (Figure 30) in addition to capturing multiscale pictures of the nanocellulose fibers (Figure 31). The multiscale pictures were taken to evaluate the fiber structure of the samples. Crystal violet was used to stain the fibers.

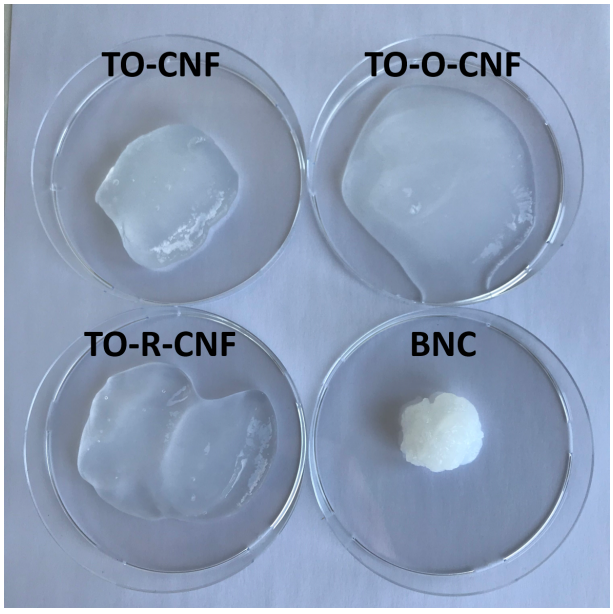

Figure 30: Image of all the nanocellulose qualities at 1 % solid content in water.

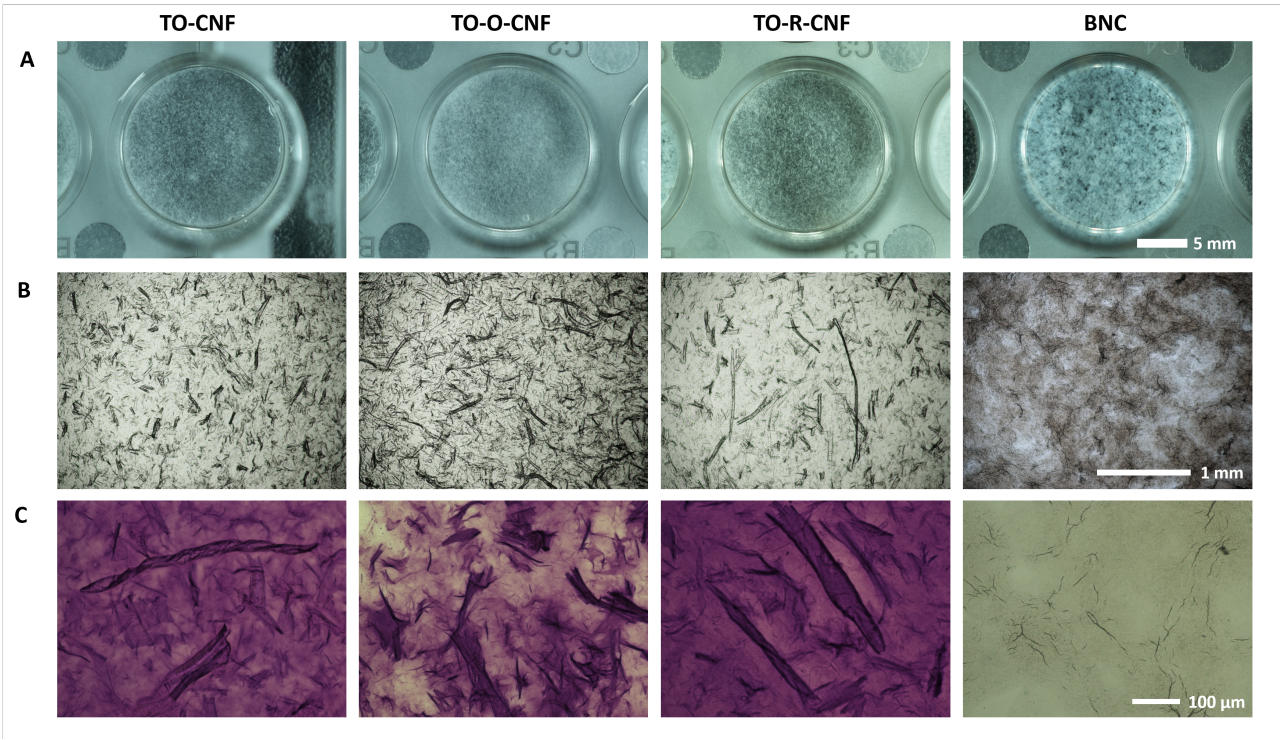

Figure 31: Multiscale pictures of the fiber structures of the nanocellulose qualities. **A** show pictures of the samples in 24-well plate wells, **B** show optical microscope images without staining and **C** show optical microscope images with crystal violet staining. The images within a row have the same scale.

4.1.6 ζ-potential

The ζ-potential analysis was performed to evaluate the surface charge properties of the nanocellulose qualities relative to each other. The nanocellulose qualities were suspended in both distilled water and α-MEM medium containing 10 % FBS. The mean ζ-potentials for the samples in medium are shown in Figure 32 while Figure 33 shows the mean ζ-potentials for the samples in water. The SDs between the 15 measurements performed for each sample, in each type of diluent, are also included in the figures.

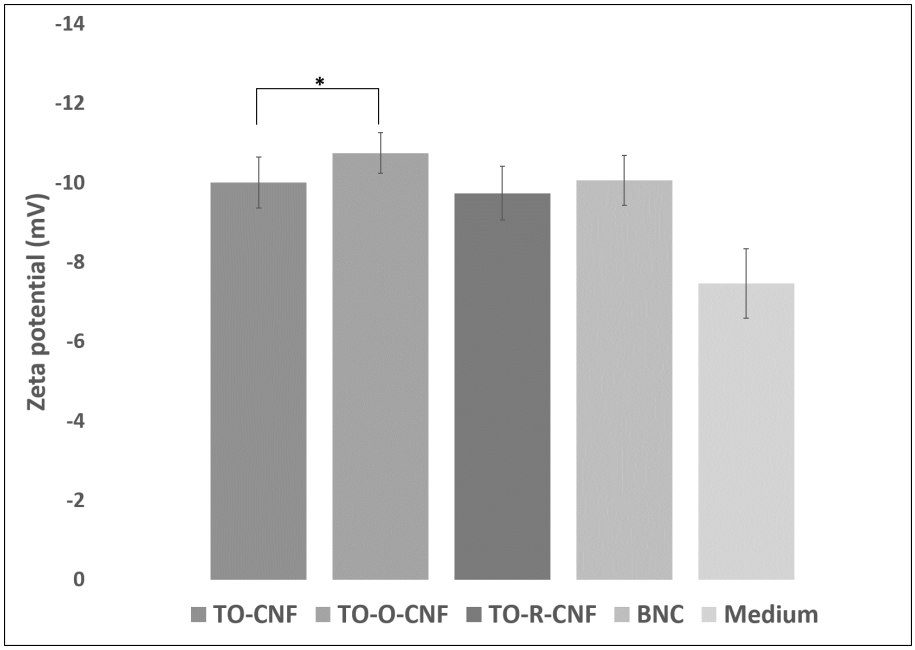

Figure 32: The mean ζ-potentials for the different nanocellulose qualities suspended in α-MEM medium containing 10% FBS $\pm$ SD.

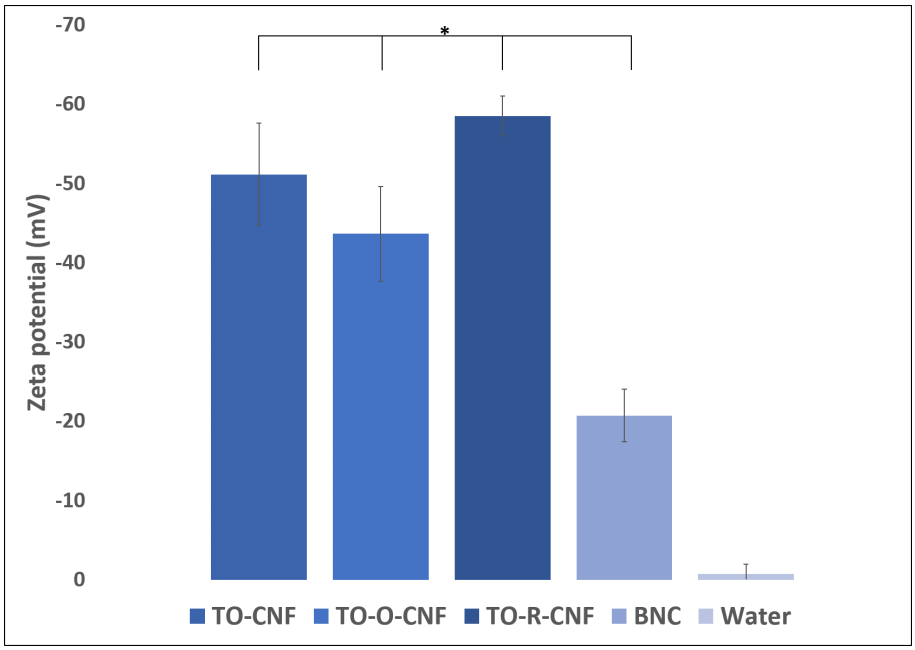

Figure 33: The mean ζ-potentials for the different nanocellulose qualities suspended in water $\pm$ SD.

4.1.7 Contact angle

Contact angle measurements were conducted to estimate the hydrophobicity/hydrophilicity of the different nanocellulose qualities. After water droplets had been deposited on the material surfaces, the water can adsorb into the material or evaporate. This can lead to a decrease in the contact angle over time, as observed for the different samples in Figure 34. To avoid these effects, the mean water contact angle after 10 seconds was determined and presented in Figure 35, including SD between the minimum 10 measurements contributing to the mean value.

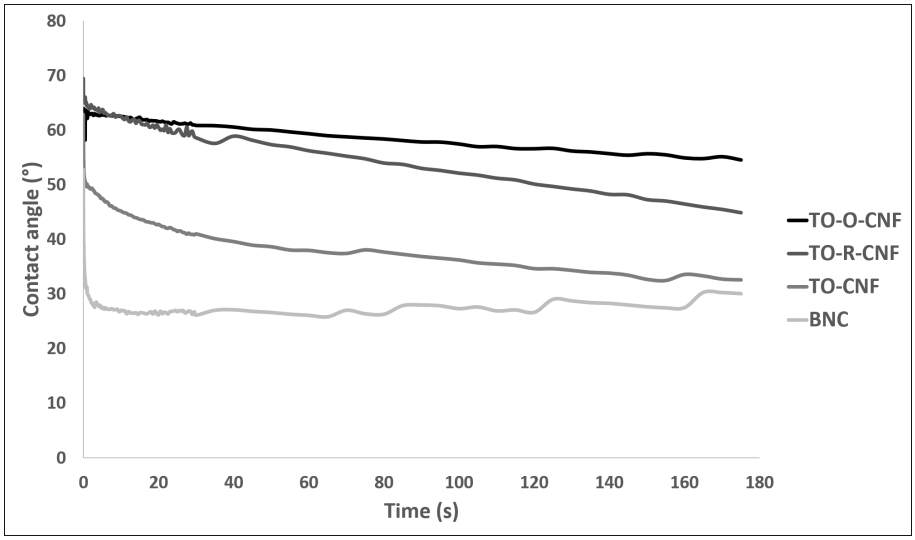

Figure 34: Mean contact angle from minimum 10 measurements as a function of time.

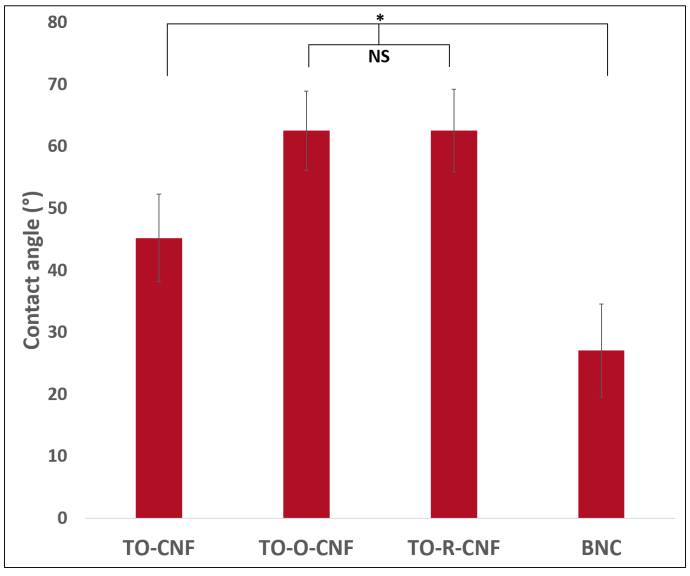

Figure 35: Mean contact angle results after 10 seconds including SDs. NS = not significant.

4.1.8 Protein adsorption

Protein adsorption onto materials is a highly complex process influenced by many factors such as protein and material properties (hydrophobicity/hydrophilicity, charges, surface area etc.) in addition to protein concentration and protein content. To observe how the nanocellulose qualities adsorbed serum proteins relative to each other using different protein concentrations and compositions, three protein solutions were used. These were 10 % FBS in α-MEM medium, 100 % FBS solution and 5 % BSA in α-MEM medium. The amount of protein adsorbed to the materials was determined and the behavior of the different groups relative to each other is shown in Figure 36, 37 and 38. The figures show the average value and SD based on 10 measurements for each sample.

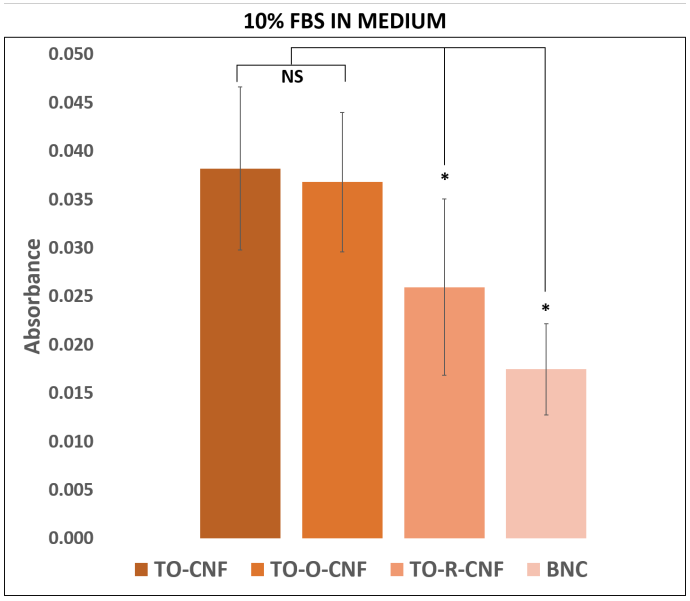

Figure 36: The mean amount of proteins adsorbed to the different nanocellulose qualities with 10 % FBS in medium as protein solution $\pm$ SD.

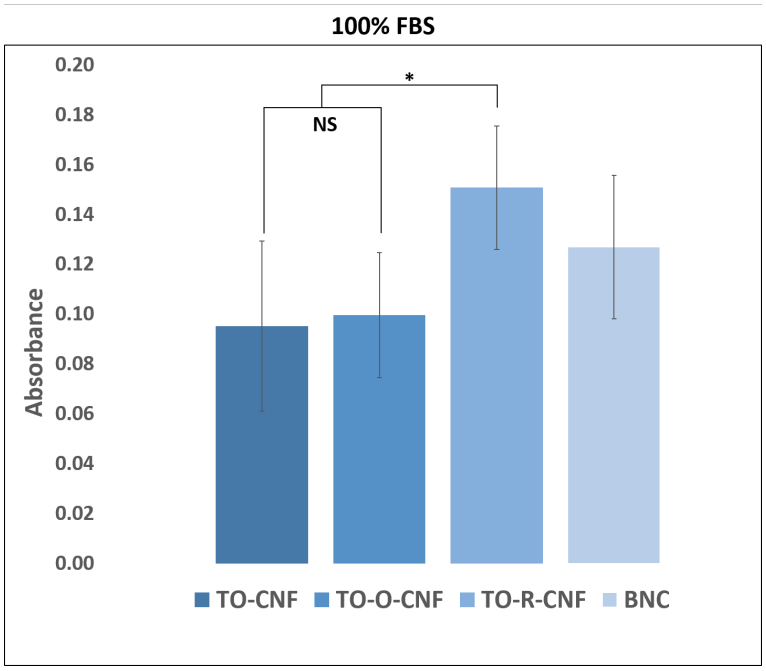

Figure 37: The mean amount of proteins adsorbed to the different nanocellulose qualities with 100 % FBS as protein solution ± SD.

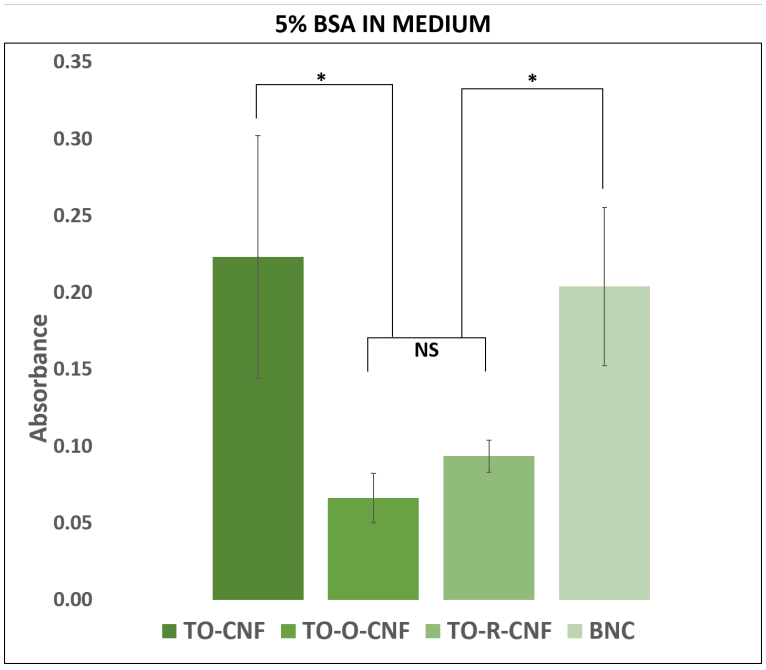

Figure 38: The mean amount of proteins adsorbed to the different nanocellulose qualities with 5 % BSA in medium as protein solution ± SD.

4.1.9 Summary of the characterization analyses

In order to evaluate all the material properties at once, a summary has been made in Table 8. The letters L (low), M (medium) and H (high) have been used to present how the different samples have behaved in the specific analyses compared to each other. The results presented in the 'Deg. of fib.' column are based on the viscosity and fiber analyzer measurements, while the results presented in the 'Surf. rough' column are based on the surface roughness analysis using AFM. It was chosen to only include the protein adsorption results using 10 % FBS in α-MEM medium as protein solution, in the table, as this was the protein concentration used further in the cell culturing work.

Table 8: Summary of the characterization analyses. Some abbreviations are used to fit the entire table; 'deg. of fib' = degree of fibrillation, 'surf. rough.' = surface roughness, 'ζ-pot. = ζ-potential in water, CA=contact angle and 10 % FBS are the results from the protein adsorption analysis with 10 % FBS in α-MEM medium as protein solution. The units for the carboxyl and aldehyde columns are μmol/g.

Sample	**Carboxyl**	**Aldehyde**	**Deg. of fib.**	**Surf. rough.**	**ζ-pot.**	**CA**	**10 % FBS**
TO-CNF	804 ± 3	280 ± 14	M	M	M	M	H
TO-O-CNF	992 ± 24	-	L	H	M	H	H
TO-R-CNF	675 ± 14	-	M	M	M	H	M
BNC	-	-	-	M	L	L	L

4.2 Cytocompatibility of the nanocellulose qualities

The results presented in Figure 41, 43, 47, 48, 49, 50, 55 and 56 have been normalized relative to the value of the control group at the first time point in the measurement. This has been done to ease the comparison between the nanocellulose groups to the control group in each of the analyses.

4.2.1 Cell culturing

Prior to seeding rBMSCs on the surface of the nanocellulose qualities, the cells had to reach a certain cell number. This was achieved by growing the cells in culture flasks. When the appropriate cell number was reached, after 14 days, the rBMSCs were seeded in the nanocellulose coated tissue culture plates to evaluate their cytotoxicity, proliferation, morphology and osteogenic differentiation. The growth of the rBMSCs was documented and pictures from different time points are shown in Figure 39.

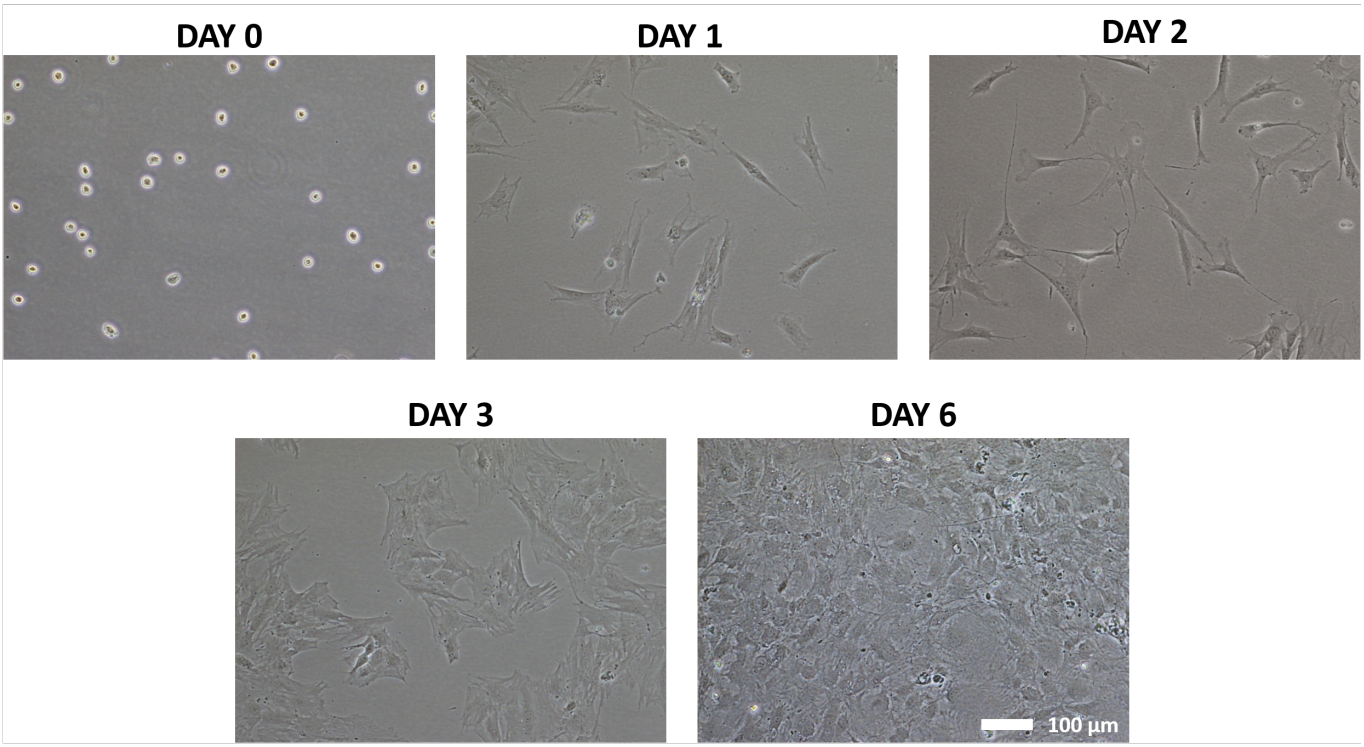

Figure 39: Pictures of the cell growth in culture flasks from day 0 to day 6. The scale is equal for all images.

4.2.2 Cell viability

Indirect cytotoxicity

The indirect cytotoxicity was evaluated after one and three days by both examining the morphology of the cells (Figure 40) and measuring the cell viability using alamarBlue assay. The results relative to the control group (regular culture medium) from the alamarBlue assay are shown in Figure 41.

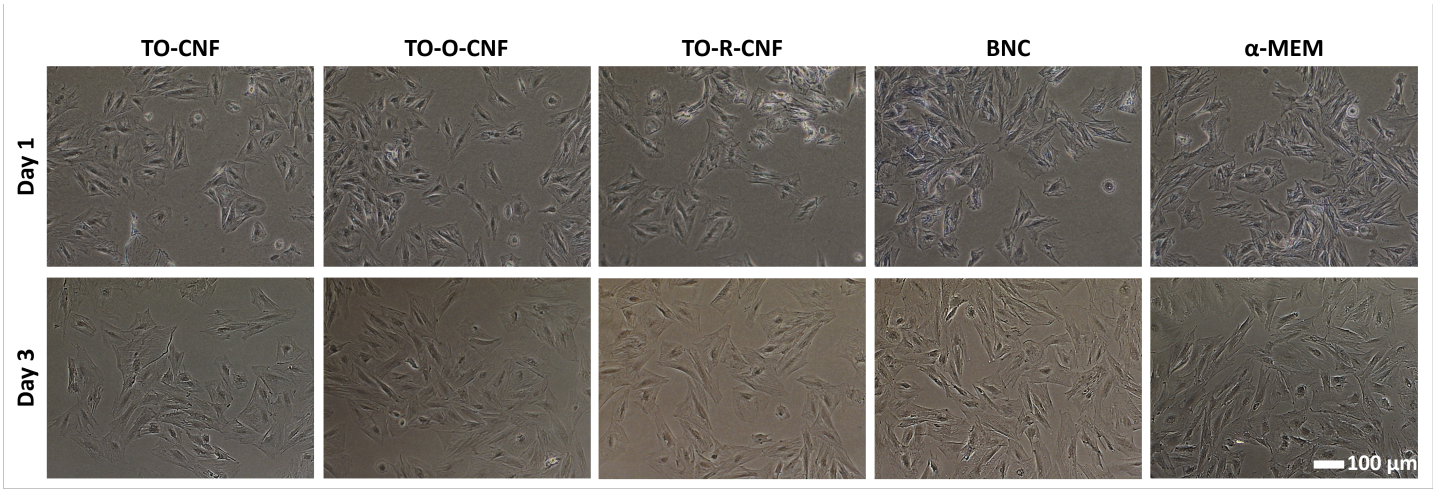

Figure 40: Morphology of rBMSCs cultured on TCPs with extract medium after one and three days. The scale is equal for all images.

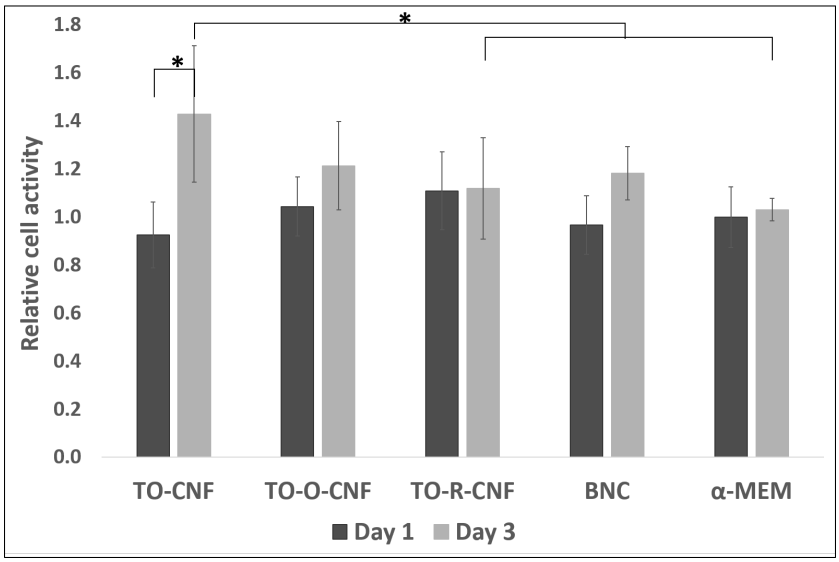

Figure 41: Results from the indirect cytotoxicity assay after one and three days. Results are presented as relative means ± SD.

Live/dead staining

To evaluate the amount of live compared to dead rBMSCs when cultured on the different nanocellulose surfaces, live/dead (L/D) staining was performed after one day. Figure 42 shows representative fluorescent images where the green cells are alive and the dead cells are red. The arrows in the figure point towards dead cells.

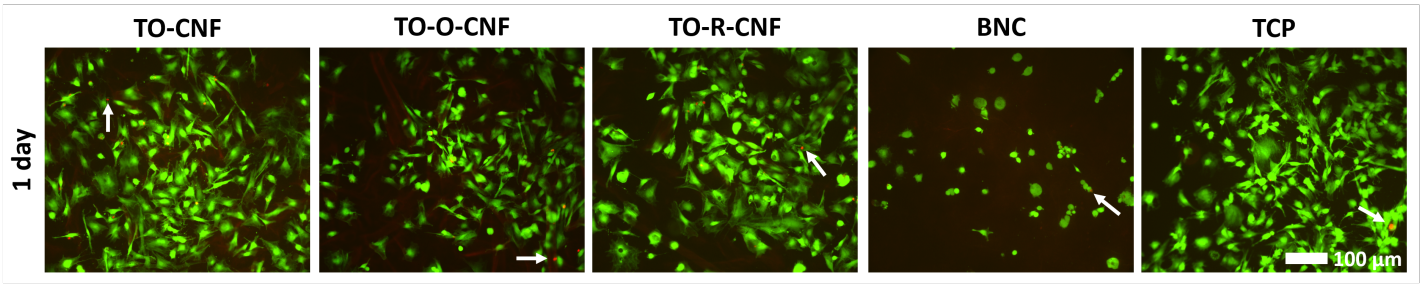

Figure 42: Fluorescent images of live/dead stained rBMSCs cultured on different nanocellulose qualities or directly on TCPs.

Lactate dehydrogenase assay

LDH is released from cells in response to stress. The levels of LDH released from the cells were measured after one and three days and the mean results including SD relative to the control group are shown in Figure 43.

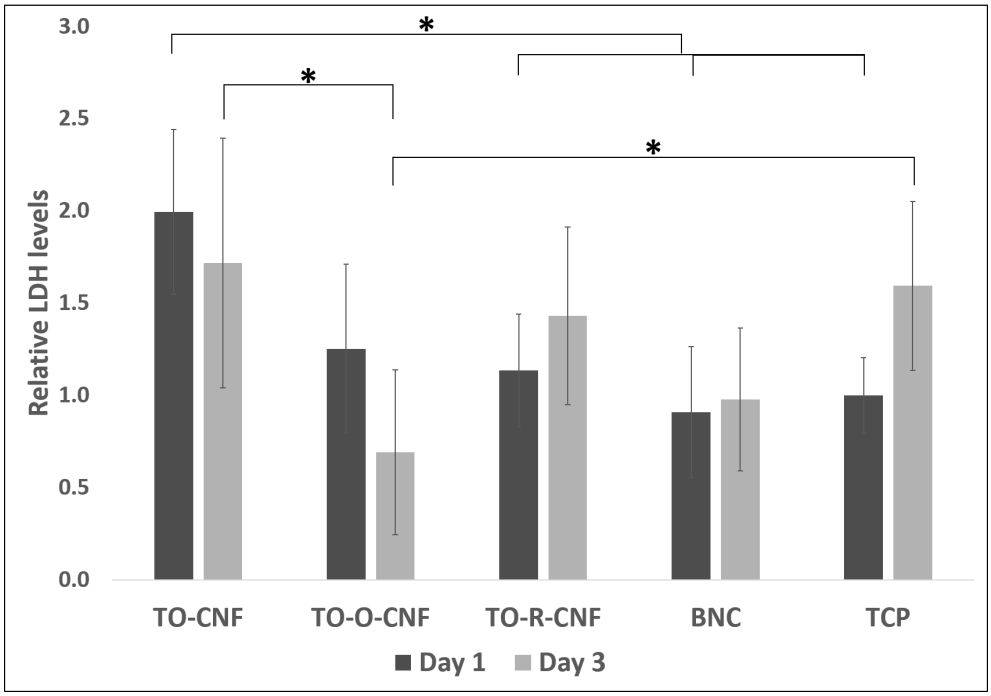

Figure 43: Levels of LDH released from the rBMSCs after one and three days of culturing on the different surfaces. Results are presented as relative means ± SD.

4.2.3 Morphology

The morphology of rBMSCs grown on nanocellulose coated TCPs was compared to the morphology of rBMSCs grown directly on TCPs. This was investigated after 3 and 24 hours by taking fluorescent images (Figure 44) of the cells stained with phalloidin (stains the cytoskeleton of the cells green) and DAPI (stains the nuclei and cellulose fibers blue). In addition, the surface area and maximal cell length were analyzed using ImageJ. The average surface area and average maximal cell length including standard deviation for each sample are shown in Figure 45 and 46, respectively. The average and standard deviation values have been calculated based on the image-analysis performed on $\geq$20 cells for each sample, as clarified in Section 3.5.4.

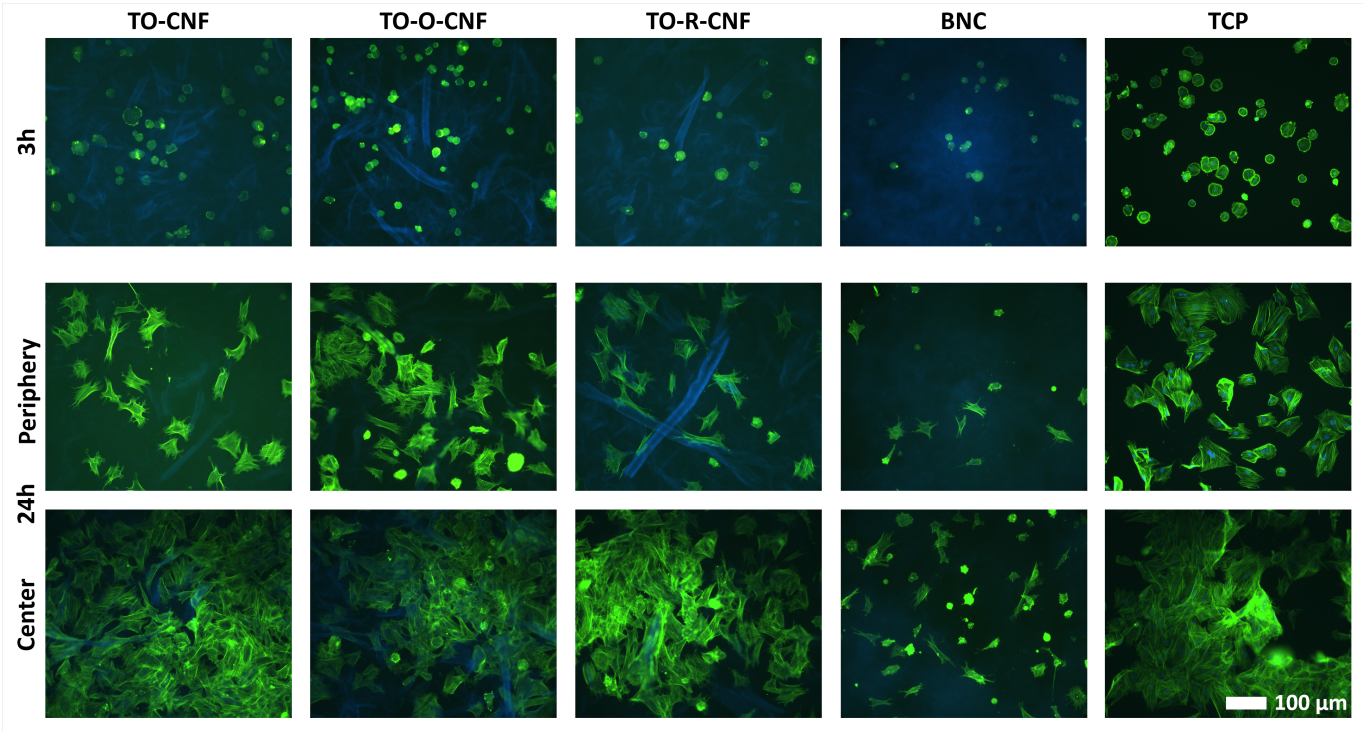

Figure 44: Fluorescent images of rBMSCs cultured on different nanocellulose qualities or directly on TCPs. After 24 hours, both images from the center of the wells and the periphery are included to show differences in cell concentration. The scale is equal for all images.

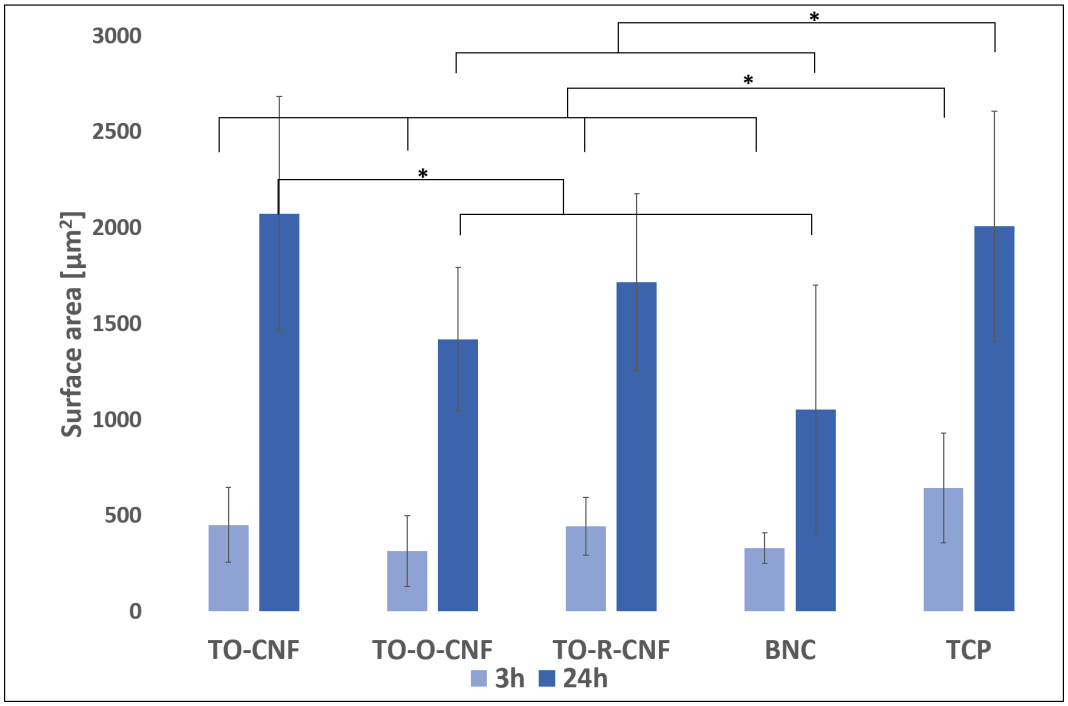

Figure 45: Surface area of rBMSCs cultured on different surfaces. Results are presented as means ± SD.

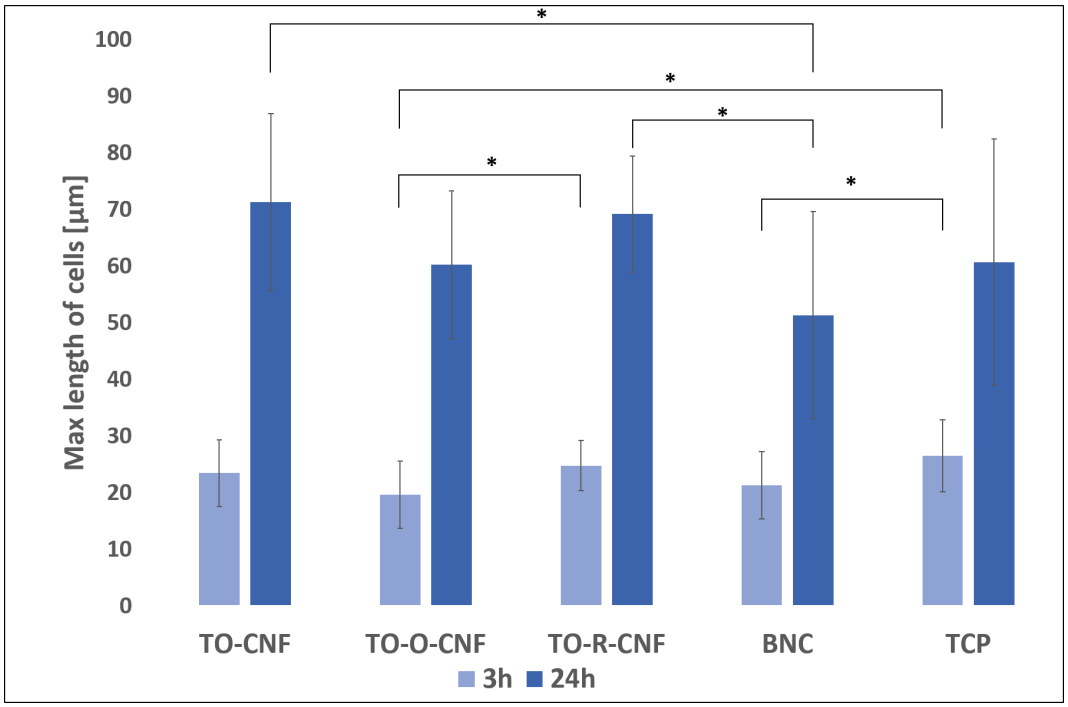

Figure 46: Max length of rBMSCs cultured on different surfaces. Results are presented as means ± SD.

4.2.4 Proliferation

In tissue engineering, one of the primary roles of the scaffold is to direct cell proliferation to support tissue formation. The proliferation of rBMSCs grown on the nanocellulose coated TCP was compared to cells grown on uncoated TCPs, by a dsDNA based assay. The assay was conducted using both regular medium (Figure 47) and osteogenic medium (Figure 48).

Statistical analysis have been performed and the bars indicating significant differences are included in the figures. However, to avoid too many bars in the figures which can make the figures difficult to read, not all are included here. Figures including all results from the statistical analysis are shown in Appendix A.6.1.

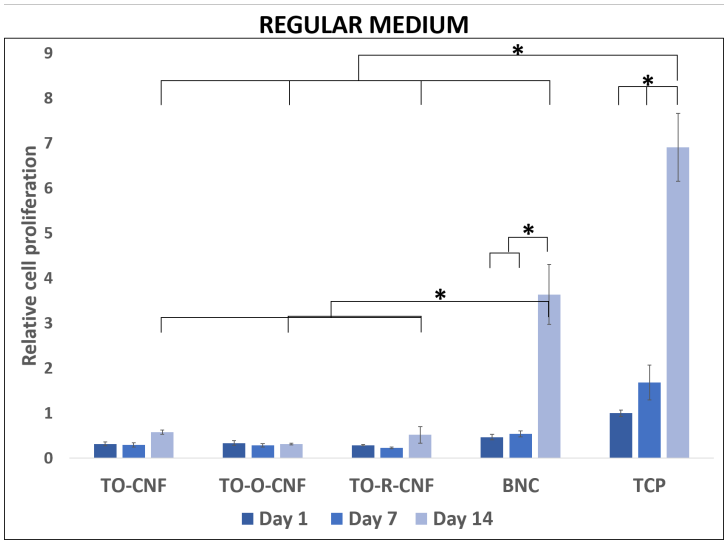

Figure 47: The proliferation of rBMSCs cultured on different surfaces with regular medium. Results are presented as relative means ± SD.

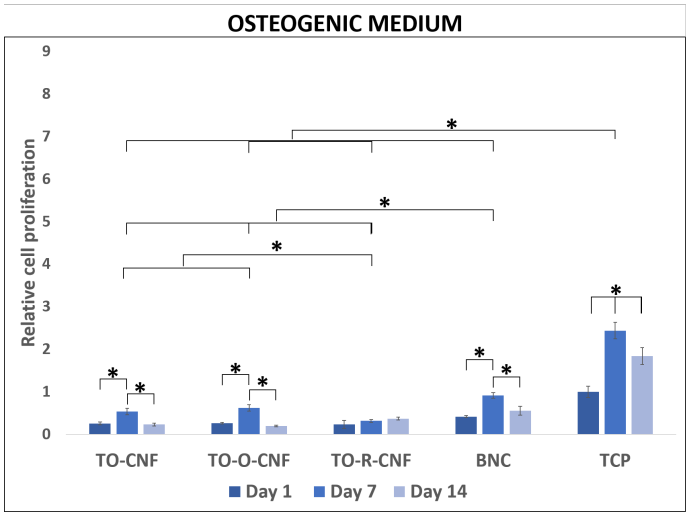

Figure 48: The proliferation of rBMSCs cultured on different surfaces with osteogenic medium. Results are presented as relative means ± SD.

4.2.5 Differentiation

Stem cells are undifferentiated cells which can differentiate into other cell types. The differentiation of stem cells are crucial for tissue regeneration. Osteogenic differentiation of rBMSCs was evaluated by both investigating the ALP and mineralization activity of the cells. ALP activity is an early marker for osteogenic differentiation and the ALP levels were measured after 1, 7 and 14 days, in regular medium (Figure 49) and osteogenic medium (Figure 50). Statistical analysis have been performed and the bars indicating significant differences are included in the figures. However, to avoid too many bars in the figures which can make the figures difficult to read, not all are included here. Figures including all results from the statistical analysis are shown in Appendix A.6.2.

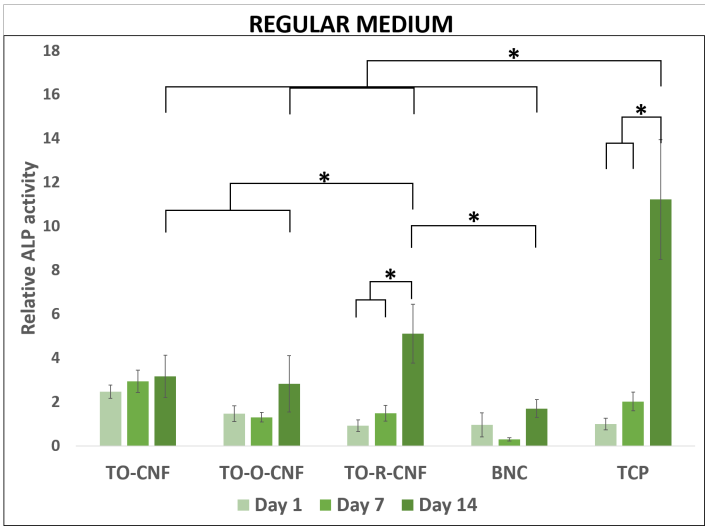

Figure 49: ALP activity after 1, 7 and 14 days for rBMSCs cultured on different surfaces with regular medium. Results are presented as relative means ± SD.

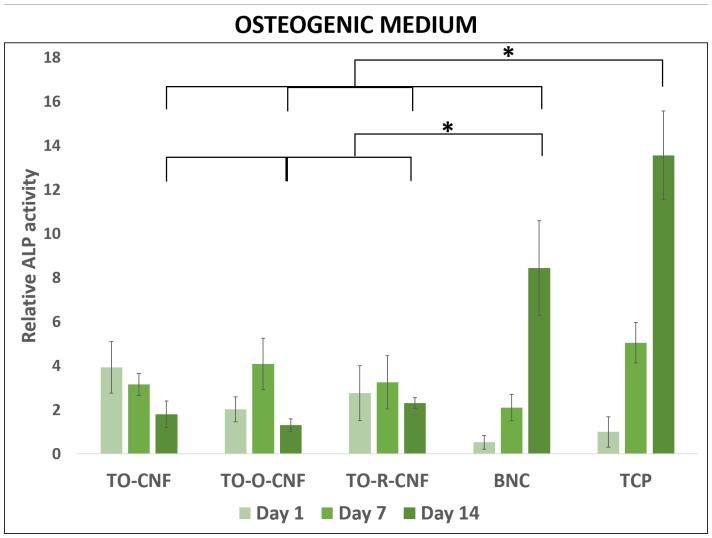

Figure 50: ALP activity after 1, 7 and 14 days for rBMSCs cultured on different surfaces with osteogenic medium. Results are presented as relative means ± SD.

To study the late stages of osteogenic differentiation, mineralization after 21 days was evaluated by ARS staining. The rBMSCs for late stage differentiation were cultured both with regular medium and osteogenic medium. Images of the staining for each group are shown in Figure 51 (regular medium) and 52 (osteogenic medium). For some of the nanocellulose groups there were big differences in the amount of ARS stain adsorbed in the wells. Images showing all of the wells for each group have therefore been included in Figure 53 (regular medium) and 54 (osteogenic medium).

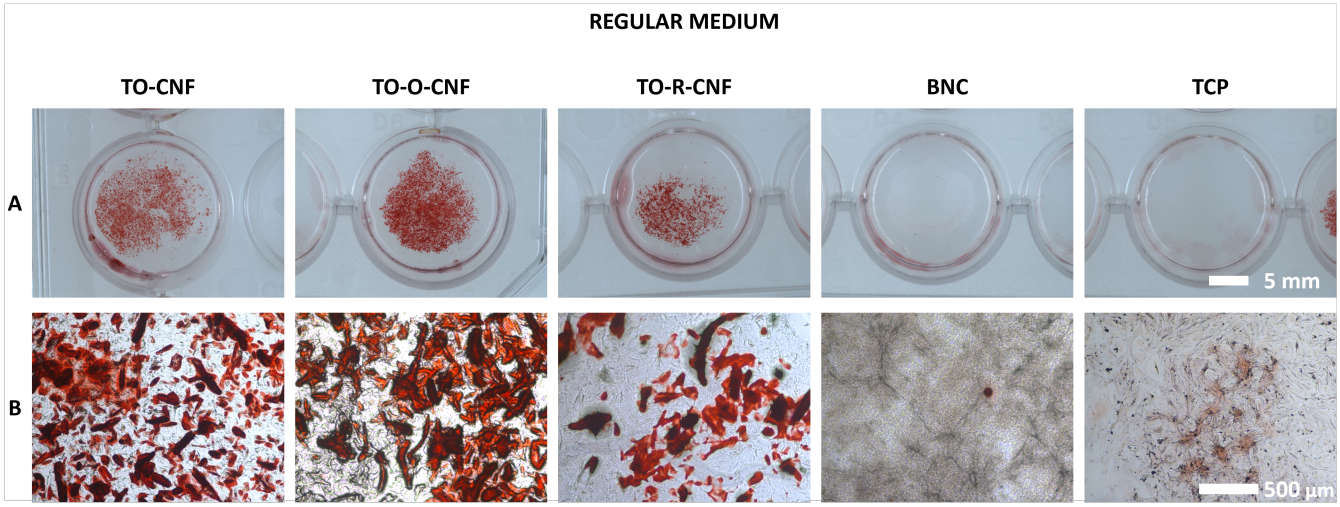

Figure 51: Images of wells stained with ARS after rBMSCs had been cultured with regular medium for 21 days on different surfaces. **A** show images of the samples in 24-well plate wells and **B** show optical microscopy images. The images within the same row have the same scale.

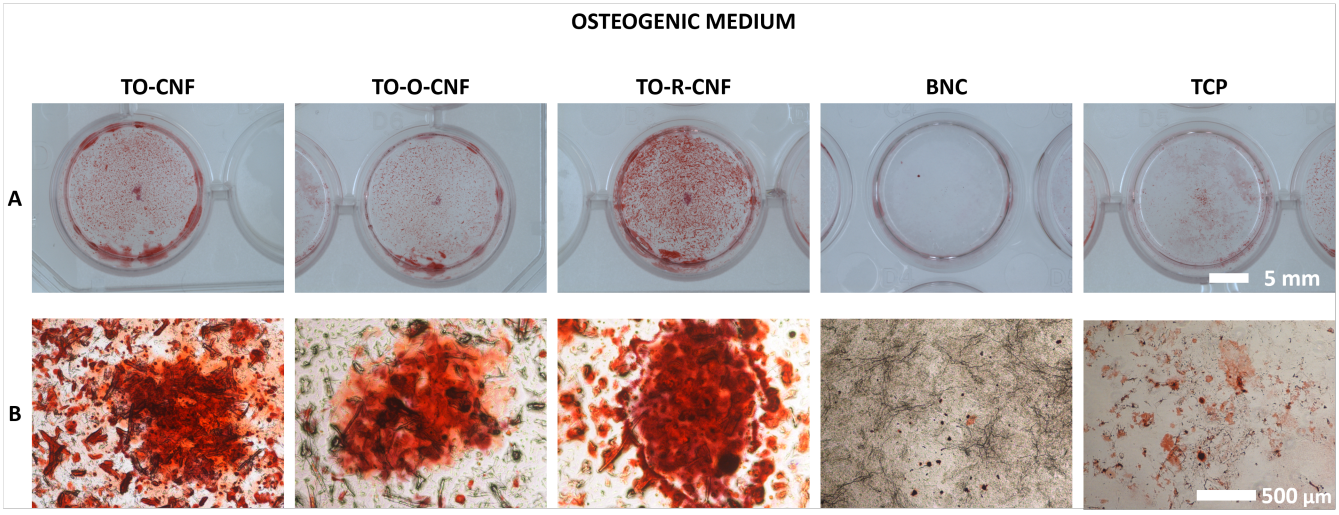

Figure 52: Images of wells stained with ARS after rBMSCs had been cultured with osteogenic medium for 21 days on different surfaces. **A** show images of the samples in 24-well plate wells and **B** show optical microscopy images. The images within the same row have the same scale.

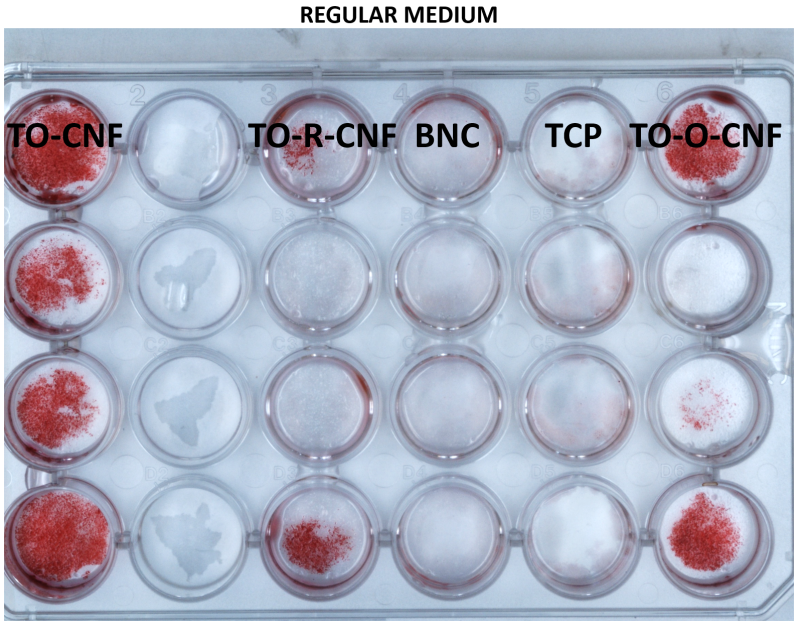

Figure 53: ARS stained plate with rBMSCs grown on different surfaces in regular medium.

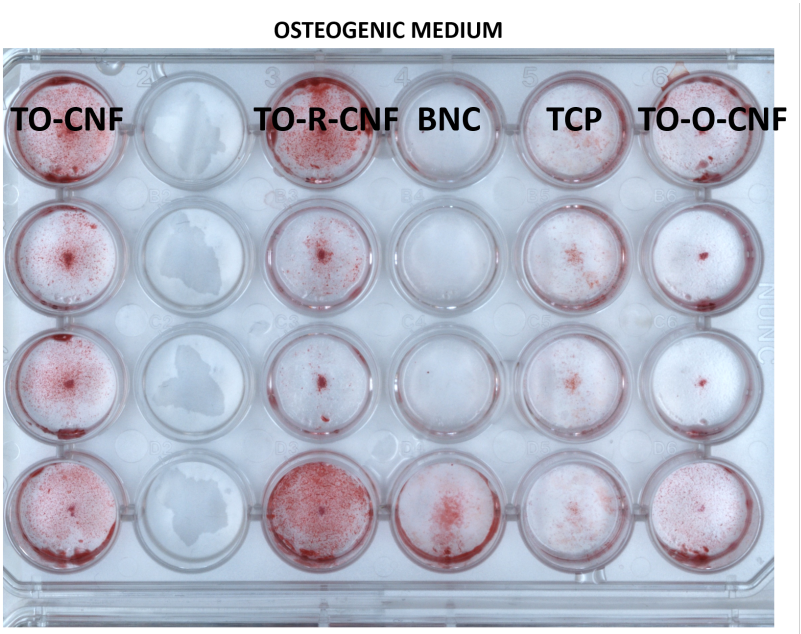

Figure 54: ARS stained plate with rBMSCs grown on different surfaces in osteogenic medium.

After imaging, the ARS stain was dissolved in cetylpyridium chloride solution and the amount of stain was measured using a microplate reader. The mean levels of ARS stain for each group cultured with regular medium are shown in Figure 55 while the results for each group cultured with osteogenic medium are shown in Figure 56. The extracted ARS from all wells shown in Figure 53 and 54 have been included to calculate the mean ARS from each group, despite the large variations observed within each group.

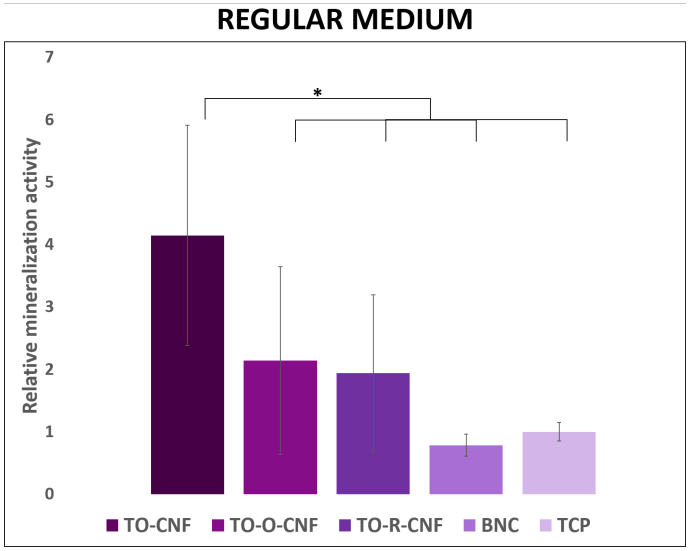

Figure 55: The levels of ARS after rBMSCs have been cultured on different surfaces with regular medium. Results are presented as relative means ± SD.

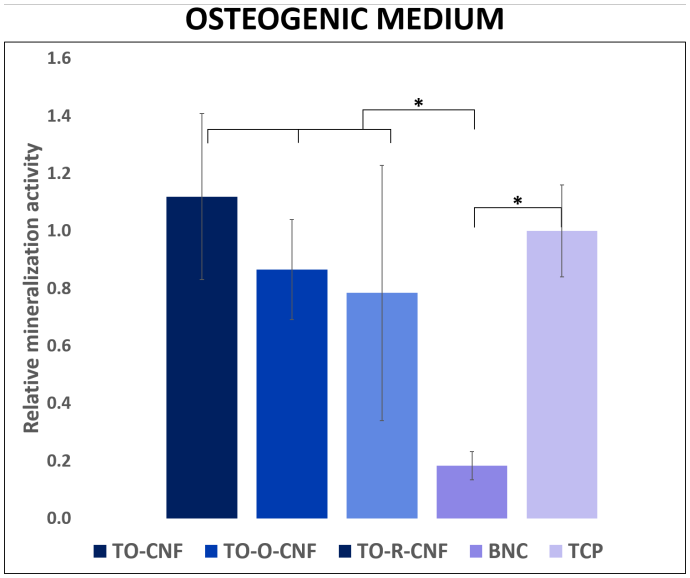

Figure 56: The levels of ARS after rBMSCs have been cultured on different surfaces with osteogenic medium. Results are presented as relative means ± SD.

4.2.6 Summary

In order to evaluate all the results from the cytocompatibility study, a summary is given in Table 9. The behaviour of the control group is always assigned as '0'. The control group have usually been cells grown directly on TCPs instead of on nanocellulose coated surfaces. However, in the indirect cytotoxicity assay, all cells were cultured on TCPs and the type of medium differed between the groups.

If the cells grown on a nanocellulose coated surface or in nanocellulose extract medium have shown significantly better or worse behaviour compared to the control in the analysis evaluated, the group have been assigned '+1' or '-1', respectively. For the proliferation, ALP and ARS analysis, two values are given. The first value is for the result in regular medium, while the second value represents the behavior in osteogenic medium. For the alamarBlue indirect cytotoxicity and LDH analysis, the results after day 3 are included for all groups. For the morphology, proliferation and ALP analysis, all time points have contributed to the overall result presented in Table 9.

For clarification, the cells grown on the BNC surfaces in the L/D staining analysis behaved similarly as the control group, when disregarding the size of the cells. Evaluating the cell size was conducted in the morphology assay. Similarly as the control group, there were an access of viable cells present on the BNC surface, and very few dead cells. Therefore, the BNC quality got the '0' result from this analysis.

Table 9: Summary of the cytocompatibility studies. Some abbreviations have been used to fit the entire table: 'morph' = morphology results and 'pro.' = proliferation results.

Sample	**Indirect**	**L/D**	**LDH**	**Morph.**	**Pro.**	**ALP**	**ARS**
TO-CNF	+1	0	0	0	-1 and -1	-1 and -1	+1 and 0
TO-O-CNF	0	0	+1	-1	-1 and -1	-1 and -1	0 and 0
TO-R-CNF	0	0	0	0	-1 and -1	-1 and -1	0 and 0
BNC	0	0	0	-1	-1 and -1	-1 and -1	0 and -1
Control	0	0	0	0	0 and 0	0 and 0	0 and 0

4.3 Functionalization of the TO-CNF material

Functionalization of TEMPO-oxidized nanocellulose scaffolds by βCD grafting can be a way to facilitate growth factor availability at the site of tissue regeneration. Films with βCD, added either through bulk or surface methods, were produced to test different methods for grafting βCD to the TO-CNF material produced during the specialization project. The effect of the different production methods, as well as the effect of heating method in order to initiate the esterification reaction, have been assessed using FTIR. The reader is referred to Table 5 to see an overview of the film names and the different methods used to produce these films.

In order to compare the TO-CNF material to other materials used in Grenoble, some material characterization was conducted with the standard methods used at LGP2. The methods used as well as the results obtained are included in Appendix A.7. It was chosen not to present the results in this thesis as only one of the CNF materials were functionalized. The material characterizations previously presented are more relevant for this report as all materials have been evaluated equally, which facilitates comparison of the results obtained.

4.3.1 Effect of dipping films in NaOH

All films that were analyzed using FTIR were analyzed both before and after dipping in 0.05 M NaOH. NaOH dipping was conducted to ensure that all carboxylic acid groups were present as carboxylate groups, to avoid overlapping peaks in the FTIR spectra. Figure 57 shows the difference in the spectra for film 0%βCD/100C/V and 10%βCD/100C/V before and after dipping in NaOH. Figures showing the same trend for film onestep-surface/100C/V and twosteps-surface/100C/V are included in Appendix A.8.

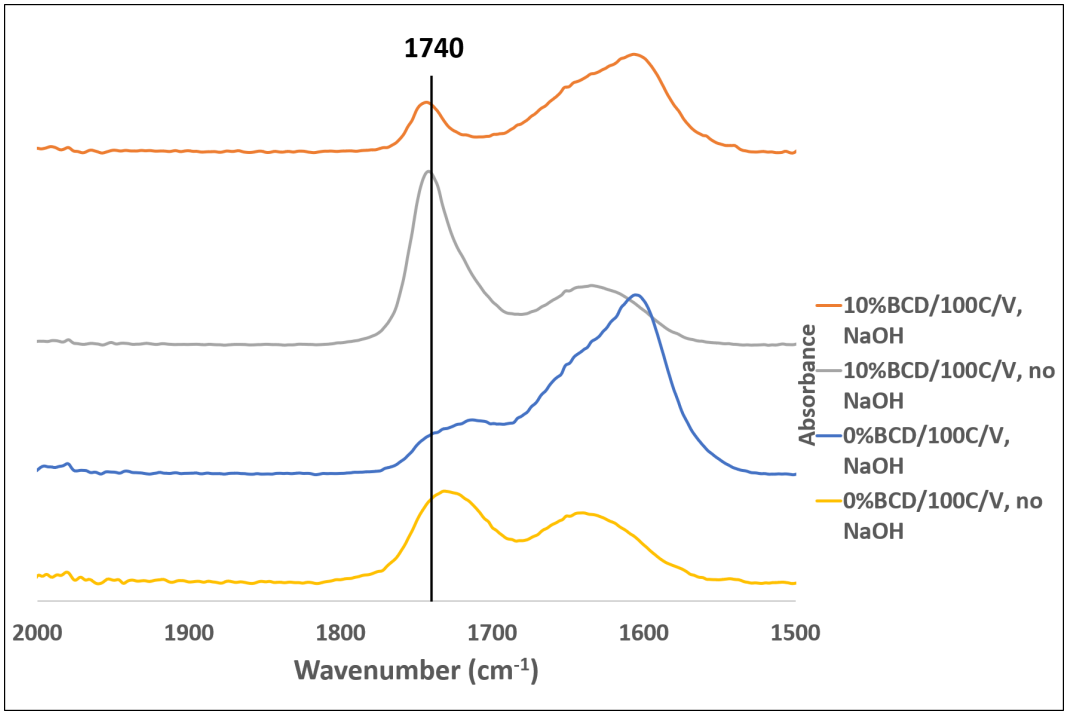

Figure 57: FTIR spectra of film 0%βCD/100C/V and 10%βCD/100C/V before and after dipping in NaOH.

4.3.2 Comparison of films with and without βCD

In Figure 58, film 0%βCD and 10%βCD are compared. Neither of the films have been through any esterification process, however film 10%βCD contains βCD. In Figure 59, film 0%βCD/100C/V and 10%βCD/100C/V are compared. Both films have been through an esterification process at 100°C in V-oven over night, while only the latter film contains βCD.

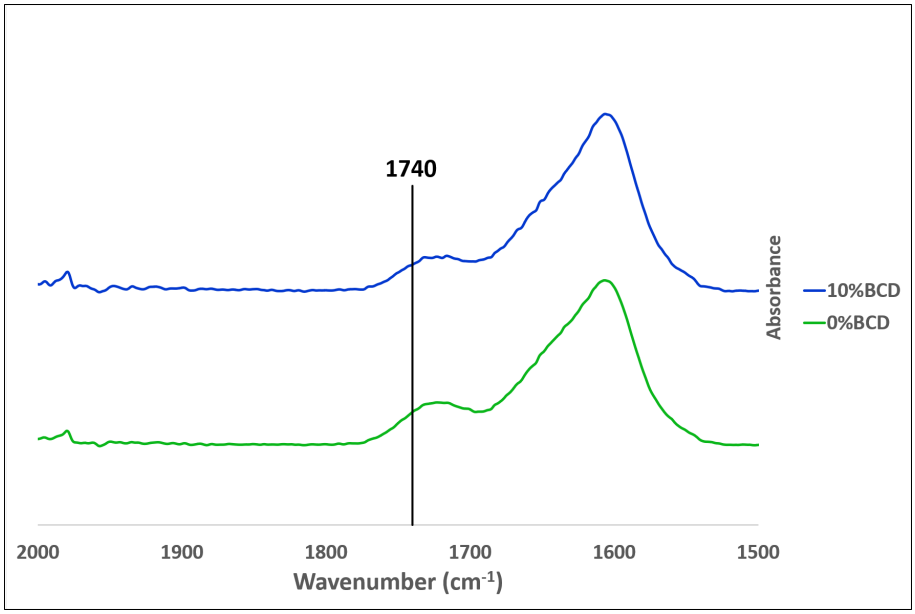

Figure 58: FTIR spectra of film 0%βCD and 10%βCD, both after dipping in NaOH. Only the latter film contains βCD.

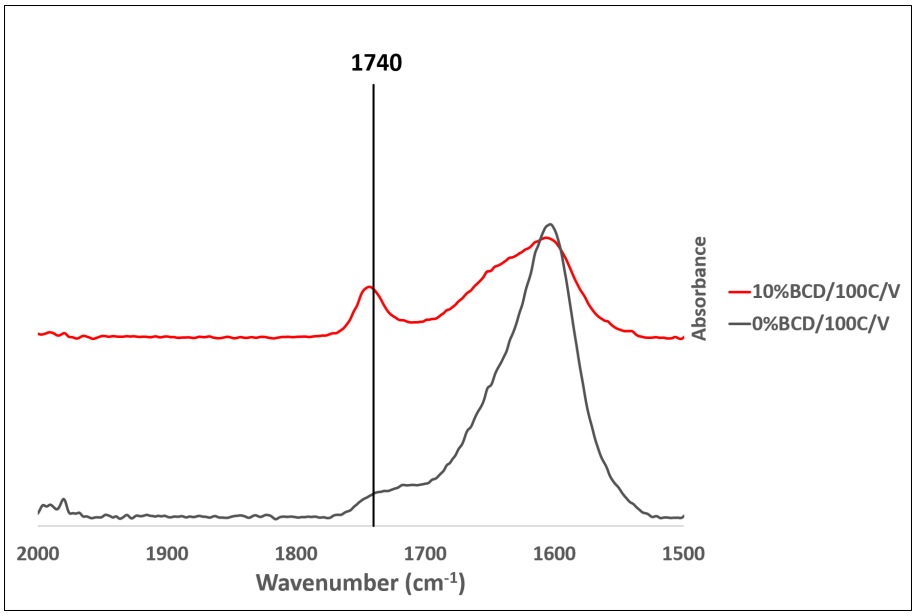

Figure 59: FTIR spectra of film 0%βCD/100C/V and 10%βCD/100C/V, both after dipping in NaOH. Only the latter film contains βCD.

4.3.3 Effect of esterification conditions

Due to previous reported results [77], esterification at 70°C over night was expected to be sufficient to initiate esterification of βCD to the TO-CNF material. However, as can be seen from Figure 60 with the FTIR spectra of film 10%βCD/70C/R and 10%βCD/70C/V, no significant peak around 1740 cm^{-1} can be seen after heating at 70°C over night in R- or V-oven, respectively. Esterification at 100°C over night in either R-oven or V-oven was also tested with film 10%βCD/100C/R and 10%βCD/100C/V, respectively. The FTIR spectra for these films can also be seen in Figure 60.

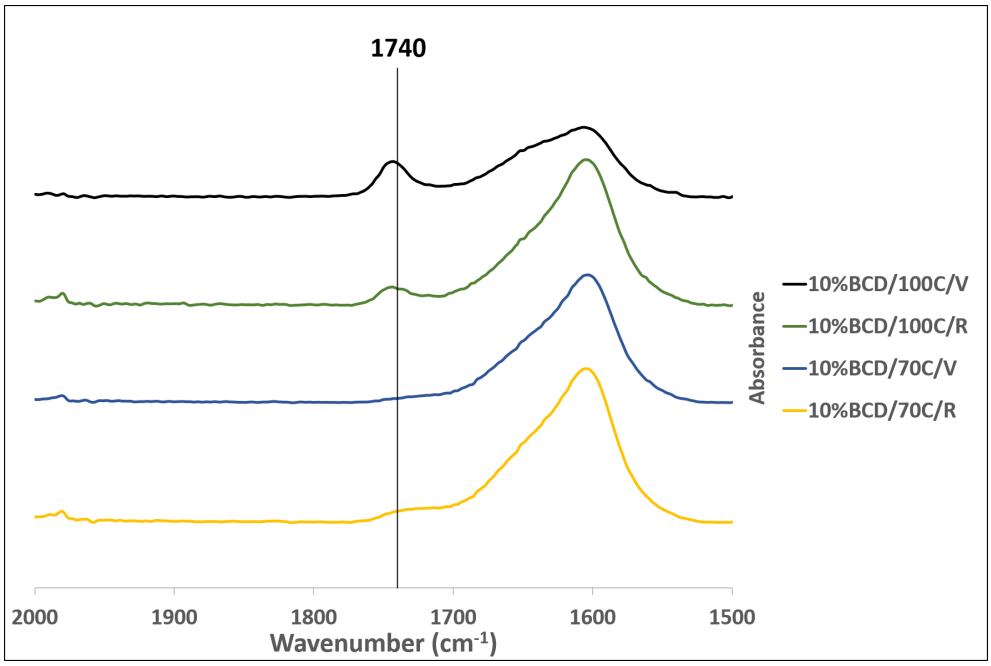

Figure 60: FTIR spectra for film 10%βCD/70C/R, 10%βCD/70C/V, 10%βCD/100C/R and 10%βCD/100C/V. All films have been made through the direct covalent bulk grafting method, however, the films vary by esterification conditions. All films have been dipped in NaOH.

4.3.4 Effect of grafting method

The different grafting methods tested were direct covalent bulk (10%BCD/100C/V) or surface grafting (βCD-surface/100C/V) in addition to surface grafting by the use of fumaric acid in one (onestep-surface/100C/V) or two (twosteps-surface/100C/V) steps. FTIR spectra of these films are shown in Figure 61. These films vary by grafting method while all of them have been heated at 100°C in V-oven over night.

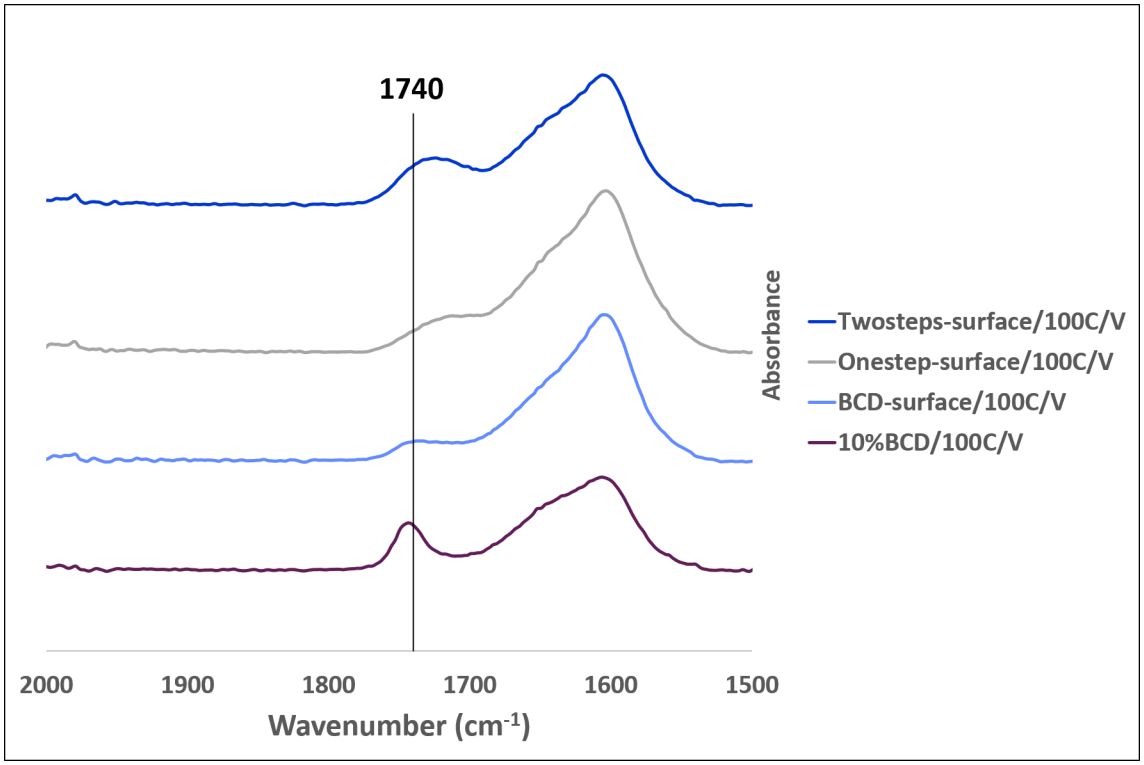

Figure 61: FTIR spectra for film 10%BCD/100C/V, βCD-surface/100C/V, onestep-surface/100C/V and twosteps-surface/100C/V. The films have been produced through different grafting methods, while the esterification process are the same for all of them. All films have been dipped in NaOH.

5 Discussion

There were three main goals in this master thesis. First, characterizing the nanocellulose qualities used. Second, evaluating the effect of the aldehyde groups introduced on CNFs by TEMPO-mediated oxidation, on the cytocompatibility of CNFs in regards to *in vitro* cell viability, morphology, proliferation and osteogenic differentiation. The cellular response towards a BNC sample was also investigated in the cytocompatibility studies. The BNC sample was included because BNC is a material that has been studied extensively, both *in vivo* and *in vitro*, and showed acceptable performance for different tissue engineering applications [84, 85], and it would be interesting to compare the CNF qualities towards such a material. The final goal was to investigate the functionalization of a TEMPO-oxidized CNF quality by βCD grafting.

5.1 Characterization of the nanocellulose qualities

TEMPO-oxidized wood based CNFs have shown promising properties regarding the cytocompatibility as a possible scaffold material [3]. However, TEMPO-mediated oxidation introduces both carboxylate and aldehyde groups to C6 in the glucose units of the cellulose chains. Previous studies have shown that cell response to aldehyde groups can be negative [4], therefore it is relevant to test if the cytocompatibility of TEMPO-oxidized wood based CNFs can be even better with the aldehyde groups removed. This resulted in the production of three different CNF qualities: one TEMPO-oxidized quality (TO-CNF), one TEMPO-oxidized and further oxidized quality (TO-O-CNF) and one TEMPO-oxidized and further reduced quality (TO-R-CNF). The two latter qualities had respectively an oxidation or a reduction treatment following the TEMPO-mediated oxidation, in order to remove the aldehyde groups to either carboxylate groups or alcohols. Figure 25 confirms the low aldehyde content of sample TO-O-CNF and TO-R-CNF compared to sample TO-CNF, as no red color were observed for these samples after reaction with TTC. The pretreatment methods were thus successful in removing the aldehyde groups introduced by the TEMPO-mediated oxidation. The BNC sample showed similar aldehyde content as TO-O-CNF and TO-R-CNF.

The carboxyl contents of the different CNF qualities are summerized in Table 6. It was expected that sample TO-CNF and sample TO-R-CNF would have similar carboxyl contents as they came from the same TEMPO-oxidized material. The measured carboxylate content of sample TO-R-CNF decreased after reduction, compared to the carboxylate content of the TO-CNF sample, even though $NaBH_4$ is a selective reducing agent, not strong enough to reduce the carboxylate groups [35]. A possible explanation to the decrease in carboxylate content can be that after the reaction with $NaBH_4$, there were several washing steps of the material. The parts of the cellulose material with the highest content of carboxylate groups will have the least dense structure [20]. Through the washing, it is therefore easier to wash away the highly carboxylated parts of the cellulose material, which can lead to an overall decrease in carboxylate content.

The carboxylate content of sample TO-O-CNF was, as expected, higher than the other two CNF qualities. The $NaClO_2$-oxidation converts the aldehyde groups to carboxylate groups, increasing the carboxylate content. For the BNC sample, there was no point in measuring the

carboxylate content, as bacterial synthesis of BNC does not include incorporation of carboxylate groups [20].

The size of wood cellulose fibers is at macro-scale, with lengths typically ranging from 1-3 mm and widths of about 10-50 μm [40]. During fibrillation processes such as homogenization, many of the fibers will be fibrillated to nanofibrils, however, the mixture will be inhomogenous and contain fibers and residual fibers [41]. The pretreatment method used can affect the efficiency of the fibrillation process [20]. As the CNF qualities had different pretreatment methods, it was interesting to see how that affected their degree of fibrillation.

Viscosity, fiber analysis and surface roughness measurement using AFM can all give information about the fibrillation degree of CNF samples. It was interesting that sample TO-O-CNF contained the largest apparent residual fiber fraction (Table 7) in addition to the lowest viscosity as a function of rotation spindle speed (Figure 26) and the highest surface roughness (Figure 29). It was expected that sample TO-O-CNF would be the most fibrillated material due to the highest carboxylate content. A higher carboxylate content increases ionic repulsion between fibers, which can ease the fibrillation process [20, 86]. However, that was not the case here, which can be due to the extra washing steps conducted after the $NaClO_2$-oxidation. The most oxidized parts of the TO-O-CNF sample will have higher water-solubility and can be removed to the filtrates during the washing process [33]. The loss of such disordered regions will lead to an increase in the amount of crystalline regions left which are more difficult to fibrillate during the homogenization process [20]. The BNC sample had the lowest surface roughness based on the results presented in Figure 28 and 29.

The nanocellulose samples are shown in Figure 30, and as observed the BNC sample had a completely different structure compared to the CNF samples. Also, the TO-O-CNF sample was less viscous compared to the other two CNF samples. The nanocellulose qualities can also be compared from the multiscale images shown in Figure 31. The TO-O-CNF sample and BNC sample stand out compared to the other two qualities. From row **B** in Figure 31, more fibers can be detected for the TO-O-CNF sample compared to the other CNF qualities, which can confirm the increased surface roughness. In addition, the different fiber structure of the BNC sample was confirmed, compared to the CNF samples. Row **C** also present interesting results; crystal violet staining of TO-CNF and TO-R-CNF looks similar, however the stain adsorbs less to the TO-O-CNF material and not at all to the BNC sample.

The ζ-potentials of the nanocelluloses were measured both with water and medium with FBS, as diluent. When the nanocelluloses were suspended in medium with FBS, not much difference could be observed between the groups (Figure 32). FBS is a complex mixture of growth factors, proteins, vitamins, trace elements, hormones and so on [87]. As shown in Figure 32, the ζ-potential of medium and FBS alone is approximately the same as the ζ-potentials measured with medium, FBS and the nanocelluloses together. As FBS contain several charged molecules, their surface charge will cover up the surface charge of the nanocelluloses and the ζ-potentials will be less affected by which nanocellulose quality that is suspended in the solute.

When the nanocelluloses were suspended in water, each materials surface charge properties became more apparent as water does not contribute to the ζ-potential (Figure 33). It was ex-

pected that TO-O-CNF would have the most negative ζ-potential due to the highest amount of carboxylate groups. Instead, TO-R-CNF with the lowest amount of carboxylate groups (of the CNF samples) had the most negative ζ-potential, followed by TO-CNF, TO-O-CNF and finally BNC. It has been speculated if the degree of fibrillation can have affected the ζ-potentials. With bigger fiber residues in the TO-O-CNF sample, there can be increased tendency of aggregation of the fibers. This can lower the over all surface charge of the fiber residues [38]. The ζ-potential of the BNC sample with water as a diluent was lower than the CNF qualities, as a result of no carboxylate groups present. Negatively charged functional groups lower the zeta potential [88].

The water contact angle (WCA) of the different nanocellulose surfaces are presented in Figure 34 as a function of time. Over time, the WCA decreased for the samples due to water absorption into the materials, or water evaporation. To avoid these effects, the WCAs measured 10 seconds after the water droplets were deposited, are shown in Figure 35. As can be seen from the figure, sample TO-O-CNF and TO-R-CNF had similar WCAs after 10 seconds, while both had significantly higher WCAs compared to TO-CNF and BNC.

There are several factors that can affect the WCA of a material, such as the functional groups present on the surface and the surface roughness of the material [8, 12]. Increased carboxylate content have shown to lead to an increase in WCA [12], which can explain why the three CNF samples all had higher WCA than BNC. The WCA of rough surfaces can be substantially increased due to heterogeneous wetting; there can be trapped air underneath parts of the water droplet preventing surface-water contact [12]. The high carboxylate content in combination with a rough surface can explain the high WCA of sample TO-O-CNF.

By first glance it can be surprising that sample TO-R-CNF had similar WCA as TO-O-CNF. Based on carboxylate contents and surface roughness, the TO-R-CNF sample should have had WCA closer to TO-CNF compared to TO-O-CNF. However, hydroxyl groups can also affect the WCA of material surfaces. Hydroxyl groups can contribute to even higher WCAs than carboxylate groups [8], and as the TO-R-CNF sample had more OH groups (as the COH groups had been reduced to OH-groups) than the TO-CNF sample, this can explain the higher WCA for sample TO-R-CNF.

Protein adsorption onto material surfaces is a highly complex process influenced by many factors. By changing the concentration of FBS in α-MEM medium or by using a mono-protein solution, BSA instead of FBS, this complexity was confirmed as the amount of proteins adsorbed on the nanocellulose qualities relative to each other changed (Figure 36-38). As the results from the protein adsorption experiments differed when changing the conditions, it has been difficult to relate the results observed to the material's differences in surface chemistry.

The conditions most similar to the cell culturing work performed in this project were the test performed with 10 % FBS in α-MEM medium. From Figure 36, this implies that the TO-CNF material adsorbed most serum proteins and the BNC material least. However, this does not mean that cells more readily can adhere to a TO-CNF surface compared to a BNC surface, as it is important that the proteins adsorbed are adhesive proteins which were not evaluated in these protein adsorption tests.

Another interesting result, observed from Figure 38, is that both the TO-CNF and BNC samples adsorbed significantly greater amounts of the BSA protein compared to TO-O-CNF and TO-R-CNF. If BSA has a high affinity for these materials it can be unfavourable as BSA do not have cell adhesion properties [50]. High concentrations of BSA on material surfaces can instead block adsorption of adhesion proteins and reduce cell attachment.

It was desired to compare materials which only differed in surface chemistry. However, the changes in surface chemistry lead to several changes as observed with the degree of fibrillation, ζ-potential, contact angle and protein adsorption properties. A summary of the nanocellulose samples properties' are shown in Table 8. The sum of all of these differences must be taken into account when evaluating the cytocompatibility of the different materials compared to each other. Another aspect not taken into account is that the nanocellulose qualities were sterilized before use in the cytocompatibility assays and sterilization can affect the content of surface groups [89].

5.2 Cytocompatibility of the nanocellulose qualities

Nanocellulose surfaces can possess a large degree of heteregenecity due to difference in fibril size, surface roughness, uneven distribution of functional groups etc. All of these parameters, and more, can affect the cellular response to the materials. Before testing the materials *in vivo* as possible scaffold materials, it was desirable to test how the material surface can support viability, morphology, proliferation and osteogenic differentiation of cells *in vitro*. To test the cytocompatibility of four different nanocellulose qualities, rBMSCs were grown on nanocellulose coated TCPs.

Prior to seeding the rBMSCs on nanocellulose coated surfaces, the cells had to reach a certain cell number. This was achieved by growing the cells in culture flasks. The growth of the rBMSCs were documented and pictures from different time points are shown in Figure 39. As can be seen from the figure, no images were captured after day 6. When the cells in the flasks reached high confluence, as seen in the picture from day 6, the cells were split to new flasks. When splitting cells, the passage number increases (number of times a cell culture has been sub-cultured), while the growth in days is re-set to zero.

Figure 39 shows the different cell morphologies expected for mesenchymal stem cells, with the the spindle shaped cells (day 1 and 2) and flattened, polygonal shaped cells (day 3 and 6) [59]. Day 0 shows the cells as rounded because the cells had not attached to the bottom of the culture flask.

5.2.1 Cell viability

Viable cells are cells with intact plasma membranes and intracellular activity [60]. The cell viability was evaluated through an indirect cytotoxicity assay, live/dead staining and a LDH assay.

The cytotoxicity assay was used to evaluate the potential release of toxic compounds from the nanocelluloses. The cellular response to the nanocellulose extracts was visually examined af-

ter fixation (Figure 40) and the cells treated with extract medium showed no changes in cell morphology compared to the control group. The results from the alamarBlue assay (Figure 41) show that the rBMSCs cultured with extract medium had similar or better viability than the rBMSCs cultured with regular α-MEM medium. The results thus imply that there were no harmful quantities of toxic compounds in the nanocelluloses after production.

After three days, the metabolic activity of cells cultured in TO-CNF extract medium was significantly better compared to the cells grown in TO-R-CNF extract medium and regular α-MEM medium. Rashad et al. also reported higher metabolic activity for cells exposed to TO-CNF extract compared to regular medium [3] and suggested that this might be due to hydrolysis of cellulose. Hydrolysis of cellulose can release glucose, which can give the cells increased substrates for metabolic activity. This behaviour was not observed for the other nanocellulose extracts.

Cell viability was also evaluated after one day of culturing utilizing live/dead staining. Fluorescent images showing rBMSCs cultured on the different nanocellulose coated surfaces are shown in Figure 42. For all groups, cells maintained good viability with a large majority of live cells compared to dead. However, a difference in cell morphology and proliferation was observed for the cells grown on BNC coated TCPs. The cells were smaller and fewer in number, which indicates an abnormal cell attachment and spreading.

The above-mentioned difference of the rBMSCs grown on BNC coated TCPs was not confirmed with higher LDH levels released after one or three days (Figure 43). The cells grown on TO-CNF surfaces on the other hand showed significantly higher LDH levels after one day, compared to the control group, TO-R-CNF and BNC. However, after three days, no groups showed significantly higher LDH levels compared to the control, indicating good viability for rBMSCs on the different surfaces.

5.2.2 Morphology

The morphology of rBMSCs grown on nanocellulose coated TCPs was evaluated after 3 and 24 hours by imaging stained cells (Figure 44). The morphology, size, and growth judged by visual inspection, showed that the BNC sample differed from the cells grown on the other surfaces. They differed by having a smaller cell size and higher presence of rounded cells compared to the flattened, polygonal shaped cells observed on the other surfaces. In addition, the BNC cells were much less crowded in the center of the wells compared to the other groups.

The rounded cell structure observed for some of the cells grown on BNC surfaces can imply that the cells not had attached to the surface properly. The same rounded structure for unattached cells can be observed in Figure 39 at day 0, just after culturing the cells. The average surface area and average maximum length of $\geq$20 cells (Figure 45 and 46 respectively) from each group were also analyzed and the results after 24 hours confirmed the observed decrease in cellular size for the cells grown on a BNC surface. The same phenomena was observed with the live/dead staining.

There are some differences between the other groups as well, which were more apparent from the surface area analysis (Figure 45) compared to the maximum length of cells analysis. After 3 hours, the cells grown on either of the nanocellulose coated surfaces were smaller than those grown on the TCPs. After 24 hours there were no significant difference in the surface area of the cells grown on TO-CNF, TO-R-CNF and TCP. The cells grown on TO-O-CNF and BNC surfaces were significantly smaller than the cells grown on both TO-CNF and TCP. Thus, judging by the morphology analysis, the BNC and TO-O-CNF materials provided surfaces that reduced cell size. The BNC sample also provided a less favourable surface for rBMSCs' early attachment and cell clustering, as observed in Figure 44.

5.2.3 Proliferation

The ability of rBMSCs to proliferate when cultured on nanocellulose coated surfaces was investigated using a dsDNA based proliferation assay. The assay was conducted with cells grown in both regular medium (Figure 47) and osteogenic medium (Figure 48). For the cells grown in regular medium, it was expected to see elevations in cell number from each time point to the next. That is because the cells were continuously fed with fresh medium and it was ensured during the entire experiment-period that the cells had enough space to proliferate. However, this trend was only observed for the cells grown on the BNC and TCP surfaces.

For the cells cultured in osteogenic medium, it was expected to see an increase from day 1 to day 7 and a decrease from day 7 to day 14. The decrease from day 7 to day 14 was expected due to previous reported results [3, 90, 91], and is possibly due to less growth while the cells differentiate, in addition, some cells can detach or die during differentiation which can give a decrease in cell number. It was not expected to see this effect before day 7, because it can take some time for the cells to go from growing and self-renewing to start differentiating [92]. For all groups except TO-R-CNF, the proliferation had the expected increase and decrease between the time points. By further examining Figure 48 it became clear that TO-R-CNF was not as different from the other two CNF qualities, even though it did not have the same 'increase and decrease' shape. It was only the cell number after day 7 on the TO-R-CNF surface that significantly differed from the cell number after day 7 on the other CNF surfaces. As the cell numbers in two of the three time points were in coherence with the two other CNF samples, it seems likely that something has gone wrong with the measurement at day 7, for the TO-R-CNF sample. What instead was noticed was that both the TCP and BNC samples had significantly higher cell numbers after day 7 compared to the CNF samples, which also was observed after day 14, in regular medium.

Increased surface roughness can induce a physical barrier to cell contact, migration and proliferation [93]. This can explain why the cell proliferation on the TCP surfaces were highest, followed by BNC and finally the CNF samples, in both regular and osteogenic medium. However, another possible explanation to the observed results can be that the seeding density used was too low. With a low seeding density, the cells will stay in the lag phase of a general growth curve for a long time and the increase in cell number will be slow, and possibly not detectable, as observed in Figure 47 for the cells grown on the CNF surfaces. A low seeding density could have affected the cells grown on the CNF surfaces more than the cells grown on the BNC and TCP surfaces, as the CNF surfaces in general were rougher (Figure 29). Rougher surfaces have

larger surface area which results in lower seeding densities. Due to this possible hypothesis, it is desirable to re-perform the proliferation experiment with a higher cell density, to ensure that the results observed were in fact a result of the materials' characteristics, not the seeding density.

5.2.4 Differentiation

Chemical or physical stimuli from the environment is usually needed for stem cells to develop into functional tissue [57]. The use of stem cells within tissue engineering requires that the cells can differentiate into the specific cell type of interest. Culturing cells in osteogenic medium can be a way of inducing osteogenic differentiation of stem cells [92]. Osteogenic medium generally consists of L-ascorbic acid, β-glycerophosphate and dexamethasone [94]. The role of the three components are explained in literature [92]. Osteogenic differentiation of rBMSCs was evaluated by the presence of both early and late osteogenic markers; ALP and calcium deposits.

The levels of ALP produced by rBMSCs were evaluated after 1, 7 and 14 days with growth both in regular medium (Figure 49) and osteogenic medium (Figure 50). As can be seen from Figure 49, the ALP levels increased from time point to time point for all groups except the cells cultured on the TO-O-CNF and BNC surfaces. However, only the increases observed for sample TO-R-CNF and TCP were significant, where the cells cultured on TCP and TO-R-CNF surfaces had produced significantly higher amounts of ALP after 14 days, compared to the cells cultured on the other samples. Highest ALP expression was observed for the cells cultured on the TCP surface. For the cells cultured in osteogenic medium, ALP expression was significantly higher for cells cultured on TCP and BNC surfaces compared to on the CNF qualities, after 14 days. Again, the cells cultured on TCP surfaces showed overall highest ALP expression.

For the cells cultured in regular medium, it was initially not expected to see high levels of ALP in any of the cell cultures. However, the differentiation of human bone marrow stem cells (hBMSCs) without osteogenic supplements have been confirmed when cultured on nanofibrous and rough surfaces [95, 96]. Rashad and colleagues have also shown that CNF coated surfaces can differentiate hBMSCs towards the osteogenic lineage, to a greater extent than un-coated TCPs [68]. The results observed in Figure 49 were thus in conflict with previous research. With osteogenic medium present (Figure 50), it was expected to see similar or higher ALP expression for the CNF samples compared to the control group, due to previous reported results [68]. However, it is wondered if a low seeding density can have affected the results from the ALP assay too.

The cell density used by Rashad and colleagues was 15 000 hBMSCs/well (around 6600 cells/cm^2), while 5000 rBMSCs/well (around 2200 cells/cm^2) were applied in this project. hBMSCs and rBMSCs do not have the same expansion rate and literature suggests that low plating densities of rBMSCs, around 2-8 cells/cm^2 (thus much lower than the plating density used here) is sufficient to achieve rapidly expanding cultures which can reach confluence [97]. Other literature suggests that a seeding density around 200 cells/cm^2 can be optimal for rBMSCs, for fast growth and expansion [59]. Therefore, it was chosen to decrease the cell density from 15 000 cells/well, and 5000 cells/well were used instead. The research referred to by

Javazon and colleages [97] and Neuhuber and colleagues [59] was conducted in TCPs, it can not necessarily be directly translated to culturing on nanocellulose coated surfaces. It is therefore needed to perform a new ALP analysis, with a higher seeding density.

As discussed earlier, a low seeding density will affect the cells grown on the nanocellulose coated surfaces more than the cells grown on the TCPs. When the cell expansion rate is decreased, there will be less cells present to differentiate and produce ALP, which leads to low ALP levels. For now, it is thus not concluded that culturing cells on CNF surfaces will limit cell differentiation compared to a TCP surface. However, it is suggested that more research must be done.

The cells grown on the BNC sample had significantly lower ALP production than the other groups, in regular medium. BNC surfaces have previously shown to induce osteogenic differentiation by evaluating collagen I levels, another osteogenic marker, without any osteogenic medium [98]. However, a comparison between the induced osteogenic differentiation of BNCs vs CNFs have not been found. It was thus an interesting result discovered, however it should be re-confirmed as the rest of the ALP-results.

The mineralization properties of rBMSCs cultured for 21 days on different surfaces were evaluated by ARS staining. Images of stained wells for each surface group are shown in Figure 51, for the cells grown in regular medium, and Figure 52, for the cells grown in osteogenic medium. For some of the nanocellulose groups there were big differences in the amount of ARS stain adsorbed in the wells. Images showing all of the wells for each quality are therefore included in Figure 53 (regular medium) and 54 (osteogenic medium). The mean levels of ARS extracted from the wells for each group are shown in Figure 55 and 56, for cells cultured in regular and osteogenic medium, respectively.

The proliferation of cells will, similarly as for ALP-levels, affect the amount of ARS extracted from the wells; if there have been a greater cell proliferation within one group compared to another, there will be more cells present to differentiate and produce minerals. From the proliferation analysis both in regular and osteogenic medium, the cells cultured on TCP and BNC surfaces showed most growth. Cells cultured in regular medium on these qualities showed the lowest ARS levels. This suggests that if the ARS levels measured for each quality had been presented as the amount of ARS produced per cell, the differences between the CNF, TCP and BNC surfaces would have been even greater. Nevertheless, the CNF surfaces and the TO-CNF surface especially, showed increased ability to induce osteogenic differentiation without osteogenic medium, in accordance with other literature [68]. It was also noted that the ARS levels extracted from the TO-CNF surface were significantly higher than the ARS levels from the TO-O-CNF and TO-R-CNF surfaces.

The mineral formation from the cells cultured on TCPs and the CNF surfaces in osteogenic medium, were similar. Even though osteogenic medium was applied, significantly less mineralization could be verified from the cells cultured on BNC surfaces (Figure 56). This can imply that the BNC surface does not support cell differentiation, however that is in conflict with what was observed in Figure 50, where cells on BNC surfaces produced higher levels of ALP after 14 days, compared to cells grown on the CNF surfaces in osteogenic medium. An-

other interesting result important to mention in this context is the following; BNC surfaces does not bind crystal violet stain as shown in Figure 31 from the multiscale imaging. A question is therefore if the BNC surface somehow block the ARS stain from binding to calcium deposits present? Whether or not the BNC surface supports cell differentiation requires more research to conclude, as this was only the result from one experiment.

5.2.5 Summary of cytocompatibility studies

In order to get an overlook of all the results obtained from the cytocompatibility studies, the results have been compared towards the behaviour of the control groups and summarized in Table 9. The three CNF qualities behaved overall similar to each other, while differed significantly from both the BNC and TCP samples in some analyses.

The cells cultured on the TO-CNF and TO-O-CNF surfaces showed higher viability than the cells cultured on TCPs, seen from the alamarBlue and LDH assay, respectively. The cells cultured on the TO-R-CNF quality showed similar viability compared to the cells cultured on TCPs. In addition, the BNC sample showed similar viability as the control group, when disregarding the size of the cells grown on BNC surfaces observed with live/dead staining. The morphology assay showed that cells cultured on both the TO-O-CNF and BNC surfaces had smaller surface area than the control group. No significant difference was detected for the surface area of cells cultured on the TO-CNF and TO-R-CNF surface, compared to the control group. The other analyses conducted; proliferation, ALP and ARS staining all showed significant differences between all the nanocellulose qualities and the control group. For the proliferation and ALP analyses, the BNC sample behaved most similar to the TCP sample, compared to the CNF samples, and opposite in the ARS analysis. As previously discussed, it is desired to re-conduct the proliferation, ALP and ARS analyses using a higher seeding density in order to see if a low seeding density affected the results obtained.

Seeding density is mentioned as a possible explanation to why the cells cultured on CNF surfaces experienced less cell proliferation and cell differentiation compared to the cells cultured on the TCP surfaces. The credibility of the other analyses conducted, cell viability and cell morphology, is not subjected to the same distrust as the proliferation and differentiation analyses. That is because the proliferation, ALP and ARS assays are analyses where seeding density can be a problem. In the indirect cytotoxicity assay, all cells were grown on TCP surfaces, while the mediums differed. All groups thus experienced the TCP surface roughness and had the same possibility to grow when regarding surface roughness as a possible obstacle to cell proliferation. In the morphology and L/D assays, no evaluation of the cell number was conducted, the seeding density was therefore not as important.

One of the aims of this master thesis was to evaluate whether or not removal of aldehyde groups in TEMPO-oxidized nanocellulose affected the cytocompatibility of the materials, *in vitro*. From this study, it can be verified that none of the nanocellulose materials were toxic to the cells, however it seems as if the TO-O-CNF and BNC samples limited normal cell morphology. From Table 8, no obvious correlation between the TO-O-CNF and BNC samples was noticed. It is therefore unclear why cells grown on these surfaces had a poorer cell morphology. When it comes to the materials' effect on cell proliferation and cell differentiation, the analyses

will be done once more before concluding on anything. However, in the proliferation and differentiation analyses, the three CNF qualities behaved similar to each other. This implies that it is not necessary to remove the aldehyde groups from TEMPO-oxidized cellulose, as little difference in cell behaviour was observed when they were removed.

Another interesting result from this study was that preparing CNF qualities with differences in aldehyde content lead to differences in other materials properties, as seen in Table 8. Carboxyl contents changed and the degree of fibrillation of sample TO-O-CNF was affected. In addition, the CNF samples obtained different contact angle and protein adsorption properties. However, for now it seems as if the differences observed between the materials have all been within ranges of what the stem cells can tolerate.

The BNC sample was included to show the behaviour of a material widely accepted as biocompatible [99]. The BNC material can not be regarded as toxic, judging by the cell viability results. However, the CNF qualities seemed to provide a better surface for normal cell attachment and cell morphology. In addition, the CNF samples provided better surfaces for mineralization.

5.3 Functionalization of the TO-CNF material

5.3.1 Effect of NaOH dipping

FTIR was used to evaluate the grafting of βCD to the TO-CNF material. When using FTIR, it is important to keep in mind that the infrared band positions of the carboxylic acid group and ester group are close to one another. In order to see the contribution of the carboxylic acid group at the infrared band position of the ester group (around 1740 cm^{-1}), films were analyzed both before and after dipping in NaOH. The NaOH dipping was conducted to convert the carboxylic acid groups to carboxylate groups, as acid had been added during the film-production in order to initiate the esterification reaction.

As can be seen from Figure 57, both films evaluated before and after dipping in NaOH showed a decrease in the peak around 1740 cm^{-1} while the peaks around 1600 cm^{-1} increased. As 1600 cm^{-1} is around the infrared band position of the carboxylate group, it was expected that the 1600 cm^{-1} peak increased when the 1740 cm^{-1} peak decreased. However, it was not possible to determine if the remaining peaks around 1740 cm^{-1} were due to more carboxylic acid groups or the ester groups.

5.3.2 Films with and without βCD

In order to ensure that films without βCD could be separated from films with βCD, film 0%βCD was prepared and compared to film 10%βCD, as can be seen in Figure 58. Also, film 0%βCD/100C/V was compared to film 10%βCD/100C/V, seen in Figure 59.

The films in Figure 58 had both been dipped in NaOH, unfortunately it could still be observed small peaks around 1720-1740 cm^{-1} for both films, even though none of the films had been through any esterification process, and only film 10%βCD contained βCD. The films in Figure 59 had both been dipped in NaOH after esterification at 100°C over night in V-oven. It was observed more difference between film 0%βCD/100C/V which did not contain βCD and film

10%βCD/100C/V which did contain βCD. This indicated that it was possible to observe differences between films with and without βCD after esterification had been conducted. However, there might be other methods which could be better suited to verify presence of βCD grafted to CNFs, compared to FTIR. This will be discussed in Section 5.3.5.

5.3.3 Effect of esterification conditions

In literature, heating for 24 hours at 70°C using a V-oven had provided promising results in regards to grafting of βCD to CNF samples [77]. However, as can be seen from Figure 60, no esterification could be verified after such a treatment (film 10%βCD/70C/V) and similarly after esterification at 70°C using R-oven (film 10%βCD/70C/R). A higher esterification temperature than 70°C was assumed necessary in order to achieve ester bond formation.

Figure 60 of film 10%βCD/100C/V, which had been treated at 100°C in V-oven over night, showed promising results (as a peak around 1740 cm^{-1} could be seen). In order to see if it was necessary to use a V-oven, where fewer samples could be run in parallel compared to R-oven, film 10%βCD/100C/R was produced where the esterification process conducted was at 100°C in R-oven. By observing the FTIR spectra, the treatment using V-oven seemed to be more efficient in evaporating the water and shifting the esterification reaction towards the desired ester bond formation between βCD and the TO-CNFs.

5.3.4 Effect of grafting method

From Figure 61, the peak around 1720-1740 cm^{-1} for film 10%βCD/100C/V was more narrow and shifted towards 1740 cm^{-1}, compared to the other films. Film 10%βCD/100C/V was made through the direct covalent bulk grafting method. As the films in Figure 61 only differ by grafting method, it seemed as the direct covalent bulk grafting method was most efficient. However, the spectra were obtained using FTIR which is a method that has a penetration depth at micrometer scale. As the other films in the figure were produced through surface grafting methods, covalently bound βCDs might not be visible even if it were present, as the FTIR do not scan the top surface of the samples. X-ray photoelectron spectroscopy, XPS, is another spectroscopy technique which analyzes the top 1-10 nm of a sample, which might be a more suitable method to evaluate surface grafting.

5.3.5 Future work

The grafting of βCD to the TO-CNF material was tested in collaboration with Julien Bras and Bastien Michel from LGP2 in Grenoble, as a part of the Cyclocell project. The collaboration lasted for one month and the Cyclocell project had started a couple of months prior to this. As the Cyclocell project was only in the start-up phase, methods for how to graft and verify the grafting of βCD to CNFs had not been determined. During the stay, it became clear that the verification of grafting, using FTIR, might not be accurate enough to ensure that there were ester bonds observed and not carboxylic acid groups. However, it was not enough time to start with new grafting or verification methods.

One suggested verification method which will be explored further by Bastien Michel, is the use of XPS instead of FTIR. As the peaks observed around 1740 cm^{-1} for the films made through

one of the surface grafting methods were smaller than what was observed using the direct covalent bulk grafting method, it was hypothesised that FTIR analysed the film too far within the material to be able to see possible ester bonds at the surface (top 1-10 nm of the film). It is therefore suggested to use XPS in order to evaluate the surface layer more thoroughly. Nuclear Magnetic Resonance (NMR) is also considered a good option to determine the chemical structure of the CNFs before and after addition of βCD. Another option can be to test indirect methods to verify the presence of βCD, such as the complexation with phenolphtalein [100]. However, indirect methods can be inaccurate, and it will not be possible to distinguish between absorbed or covalently bound βCD. If the time had allowed, it would also have been interesting to test other grafting methods, such as grafting through the use of an amine linker. An amine linker, such as hexamethylenediamine, can be used to covalently bind βCD to carboxymethylated CNFs in a similar procedure as described in literature [76].

6 Conclusion

In the present study, surface properties of nanocellulose gels as a scaffold material were explored for BTE applications. The study consisted of three parts; characterizing the nanocellulose qualities used, evaluation of the cytocompatibility of three CNF qualities in regards to *in vitro* cell viability, morphology, proliferation and osteogenic differentiation, and functionalization of TEMPO-oxidized CNFs by βCD grafting. The three CNF samples differed in pretreatment methods, where all qualities were TEMPO-oxidized and two of them were further treated (oxidized and reduced, respectively) to remove the aldehyde groups. The aldehyde groups were removed in order to evaluate the effect of aldehyde groups on the cytocompatibility of the materials. For the cytocompatibility studies, a BNC sample was also evaluated in order to compare the CNF qualities towards a material which have shown good properties as a scaffold material for different TE applications [84, 85].

A spectrophotometric method was used to confirm the differences in aldehyde contents for the three different CNF samples, where no aldehyde groups were detected for the two further treated CNF qualities. The BNC sample showed no traces of aldehyde groups either, while the TO-CNF sample contained 280 ± 14 μmol/g aldehyde groups. In addition, other material properties were characterized, such as the carboxyl content, degree of fibrillation, ζ-potential, contact angle and protein adsorption properties. Unsurprisingly, the TO-O-CNF sample contained the highest amount of carboxyl groups as the aldehyde groups removed for this sample had been oxidized to carboxyl groups. The TO-O-CNF quality was also significantly less fibrillated compared to the other two CNF samples. The ζ-potentials of the three CNF qualities in water were similar to each other, while the BNC sample had a lower ζ-potential due to no carboxylic groups present on the material surface. The BNC sample had a lower measured contact angle compared to the CNF samples, in addition to poorer protein adsorption properties when 10 % FBS in α-MEM medium was used as a protein solution.

The cytocompatibility assays showed that all of the nanocellulose qualities supported good cell viability of rBMSCs cultured on nanocellulose coated TCPs. For cells cultured on TO-O-CNF and BNC surfaces, poorer cell morphology was observed. However, this was not observed for the other CNF samples. The cell proliferation properties were significantly poorer for the cells

cultured on any of the nanocellulose surfaces, compared to the control group, especially when cultured in regular (α-MEM) growth medium. The osteogenic cell differentiation properties were evaluated by investigating both the ALP and mineralization activity of the cells. From the ALP assay, all nanocellulose groups showed poorer ALP expression compared to the control group, while the mineralization assay showed that the CNF qualities can initiate osteogenic differentiation without the presence of osteogenic medium. However, it is hypothesized that the proliferation and differentiation analyses were conducted with a too low seeding density to obtain proper results. It is considered necessary to re-perform those analyses before concluding on how cell proliferation and differentiation are affected by the nanocellulose qualities.

Even though cells cultured on the CNF surfaces did not show the desired cell proliferation and differentiation potential, the cells on the different CNF qualities behaved overall similar to each other. As the cells cultured on the CNF surfaces showed similar properties in regards to cell viability and morphology too, this implies that it does not make a significant difference of removing the aldehyde groups from TEMPO-oxidized CNFs.

The determination on how to graft βCD to the TO-CNF and how to verify the grafting was not finished during the one month collaboration with Julien Bras and Bastien Michel at LGP2 in Grenoble. The work started by producing the different types of films and continued with trying to verify the grafting of βCD. FTIR analysis indicated presence of ester bonds for film 10%βCD/100C/V, which had been esterified over night at 100°C in V-oven. For the films produced using other grafting methods, narrow peaks around 1740 cm^{-1} was not observed. In order to evaluate the produced films further, it was desired to use XPS and NMR. Future work will test grafting using an amine linker, to see if this increases the grafting efficiency and possibly opens up for new verification methods. This work will be continued by Bastien Michel in his PhD project.

References

[1] O'Brien, F. J. (2011) Biomaterials & scaffolds for tissue engineering. *Materials Today,* **14**(3), 88–95.

[2] U.S. Government Information on Organ Donation and Transplantation. Organ Donation Statistics [Internet]. [Updated in 2017; cited: 09.12.2018]. Available from: `https://www.organdonor.gov/statistics-stories/statistics.html`.

[3] Rashad, A., Mustafa, K., Heggset, E. B., and Syverud, K. (2017) Cytocompatibility of Wood-Derived Cellulose Nanofibril Hydrogels with Different Surface Chemistry. *Biomacromolecules,* **18**, 1238–1248.

[4] Sokolsky-Papkov, M., Domb, A. J., and Golenser, J. (2006) Impact of aldehyde content on amphotericin B - Dextran imine conjugate toxicity. *Biomacromolecules,* **7**(5), 1529–1535.

[5] Syverud, K. Tissue Engineering Using Plant-Derived Cellulose Nanofibrils (CNF) as Scaffold Material. In: Agarwal, U. P., Atalla, R. H. and Isogai, A. (editors). Nanocelluloses: Their preparation, Properties, and Applications. Washington DC: American Chemical Society; 2017.

[6] Engel, J. and Chiquet, M. An Overview of Extracellular Matrix Structure and Function. In: Mecham, R. P (editor). The Extracellular Matrix: and Overview. 1st ed. Berlin: Springer; 2011.

[7] Williams, D. F. (2014) There is no such thing as a biocompatible material. *Biomaterials,* **35**(38), 10009–10014.

[8] Arima, Y. and Iwata, H. (2007) Effect of wettability and surface functional groups on protein adsorption and cell adhesion using well-defined mixed self-assembled monolayers. *Biomaterials,* **28**(20), 3074–3082.

[9] Kim, U. J., Kuga, S., Wada, M., Okano, T., and Kondo, T. (2000) Periodate oxidation of crystalline cellulose. *Biomacromolecules,* **1**(3), 488–492.

[10] Singh, M., Ray, A. R., and Vasudevan, P. (1982) Biodegradation studies on periodate oxidized cellulose. *Biomaterials,* **3**(1), 16–20.

[11] Khang, D., Choi, J., Im, Y. M., Kim, Y. J., Jang, J. H., Kang, S. S., Nam, T. H., Song, J., and Park, J. W. (2012) Role of subnano-, nano- and submicron-surface features on osteoblast differentiation of bone marrow mesenchymal stem cells. *Biomaterials,* **33**(26), 5997–6007.

[12] Rodionova, G., Eriksen, , and Gregersen, (2012) TEMPO-oxidized cellulose nanofiber films: Effect of surface morphology on water resistance. *Cellulose,* **19**(4), 1115–1123.

[13] Ikada, Y. (2006) Chapter 1: Scope of Tissue Engineering. *Interface Science and Technology,* **8**(C), 1–469.

[14] Ratner, B. D. and Hoffman, A. S. Synthetic Hydrogels for Biomedical Applications. In: Andrade, J. D. (editor). Hydrogels for Medical and Related Applications. Washington DC: American Chemical Society; 1976.

[15] Roseti, L., Parisi, V., Petretta, M., Cavallo, C., Desando, G., Bartolotti, I., and Grigolo, B. (2017) Scaffolds for Bone Tissue Engineering: State of the art and new perspectives. *Materials Science and Engineering C,* **78**, 1246–1262.

[16] Henriksson, G. and Lennholm, H. Cellulose and Carbohydrate Chemistry. In: Ek, M., Gellerstedt, G. and Henriksson, G. (editors). Pulp and Paper Chemistry and Technology: Wood Chemistry and Wood Biotechnology. Berlin: Walter de Gruyter; 2009. pp. 71-99.

[17] Christensen, B. E. Compendium TBT4135 Biopolymers [Internet]. [Updated in 2016; cited: 10.10.2018]. Available from: `https://www.ntnu.no/trykk/publikasjoner/Biopolymers/files/assets/common/downloads/Biopolymers.pdf`.

[18] Klemm, D., Philipp, B., Heinze, T., Heinze, U. and Wagenknecht, W. General Considerations on Structure and Reactivity of Cellulose. 1st ed. Weinheim: Wiley-VCH Verlag GmbH; 1998. pp. 10-15.

[19] Tommila, M., Jokilammi, A., Penttinen, R. and Ekholm, E. Cellulose - A Biomaterial with Cell-Guiding Property. In: Ven, T. and Godbout, L. (editors). Cellulose - Medical, Pharmaceutical and Electronic Applications. London: IntechOpen; 2013.

[20] Klemm, D., Kramer, F., Moritz, S., Lindström, T., Ankerfors, M., Gray, D., and Dorris, A. (2011) Nanocelluloses: A new family of nature-based materials. *Angewandte Chemie - International Edition,* **50**(24), 5438–5466.

[21] Karppinen, A. Microfibrillated cellulose, cellulose fibrils or nanocellulose? [Internet]. [Updated in 2018; cited: 19.10.2018]. Available from: `https://blog.exilva.com/microfibrillated-cellulose-or-nanocellulose`.

[22] Homogenizers. High-pressure Homogenization [Internet]. [Cited: 19.10.2018]. Available from: `https://homogenizers.net/pages/ac-high-pressure-homogenization`.

[23] Jozala, A. F., de Lencastre-Novaes, L. C., Lopes, A. M., de Carvalho Santos-Ebinuma, V., Mazzola, P. G., Pessoa-Jr, A., Grotto, D., Gerenutti, M., and Chaud, M. V. (2016) Bacterial nanocellulose production and application: a 10-year overview. *Applied Microbiology and Biotechnology,* **100**(5), 2063–2072.

[24] Dufresne, A. (2013) Nanocellulose: a new ageless bionanomaterial. *Materials Today,* **16**(6), 220–227.

[25] Curvello, R., Raghuwanshi, V. S., and Garnier, G. (2019) Engineering nanocellulose hydrogels for biomedical applications. *Advances in Colloid and Interface Science,* **267**, 47–61.

[26] Syverud, K., Kirsebom, H., Hajizadeh, S., and Chinga-Carrasco, G. (2011) Cross-linking cellulose nanofibrils for potential elastic cryo-structured gels. *Nanoscale Research Letters,* **6**(1), 1–6.

[27] Borregaard. EXILVA [Internet]. [Cited: 03.12.2018]. Available from: https://www.exilva.com/.

[28] Lou, Y.-R., Kanninen, L., Kuisma, T., Niklander, J., Noon, L. A., Burks, D., Urtti, A., and Yliperttula, M. (2014) The Use of Nanofibrillar Cellulose Hydrogel As a Flexible Three-Dimensional Model to Culture Human Pluripotent Stem Cells. *Stem Cells and Development,* **23**(4), 380–392.

[29] Hu, Y. and Catchmark, J. M. (2011) In vitro biodegradability and mechanical properties of bioabsorbable bacterial cellulose incorporating cellulases. *Acta Biomaterialia,* **7**(7), 2835–2845.

[30] Isogai, A., Saito, T., and Fukuzumi, H. (2011) TEMPO-oxidized cellulose nanofibers. *Nanoscale,* **3**(1), 71–85.

[31] Syverud, K., Pettersen, S. R., Draget, K., and Chinga-Carrasco, G. (2015) Controlling the elastic modulus of cellulose nanofibril hydrogels – scaffolds with potential in tissue engineering. *Cellulose,* **22**(1), 473–481.

[32] Sigma-Aldrich. TEMPO Catalyzed Oxidations [Internet]. [Cited: 15.09.2018]. Available from: https://www.sigmaaldrich.com/technical-documents/articles/chemistry/tempo-catalyzed-oxidations.html.

[33] Saito, T. and Isogai, A. (2004) TEMPO-mediated oxidation of native cellulose. The effect of oxidation conditions on chemical and crystal structures of the water-insoluble fractions. *Biomacromolecules,* **5**(5), 1983–1989.

[34] Saito, T. and Isogai, A. (2006) Introduction of aldehyde groups on surfaces of native cellulose fibers by TEMPO-mediated oxidation. *Colloids and Surfaces A: Physicochemical and Engineering Aspects,* **289**, 219–225.

[35] Bruice, P. Y. Ch 20: More about oxidation-reduction reactions and amines. In: Folchetti, N. (editor). Organic Chemistry. 6st ed. USA: Pearson/Prentice Hall; 2011. p. 891.

[36] Master Organic Chemistry. Reagent Friday: Sodium Borohydride ($NaBH_4$) [Internet]. [Cited: 08.12.2018]. Available from: https://www.masterorganicchemistry.com/2011/08/12/reagent-friday-sodium-borohydride-nabh4/.

[37] Kürti, L. and Czakó, B. Strategic Applications of Named Reactions in Organic Synthesis. 1st ed. UK: Elsevier Inc; 2005. p. 354.

[38] Jaušovec, D., Vogrinčič, R., and Kokol, V. (2015) Introduction of aldehyde vs. carboxylic groups to cellulose nanofibers using laccase/TEMPO mediated oxidation. *Carbohydrate Polymers,* **116**, 74–85.

[39] Koyama, D., Coulter, P., Grubb, M. P., Greetham, G. M., Clark, I. P., and Orr-Ewing, A. J. (2015) Reaction Dynamics of CN Radicals in Acetonitrile Solutions. *Journal of Physical Chemistry A,* **119**(52), 12924–12934.

[40] Chinga-Carrasco, G. (2013) Optical methods for the quantification of the fibrillation degree of bleached MFC materials. *Micron,* **48**, 42–48.

[41] Chinga-Carrasco, G. (2011) Cellulose fibres, nanofibrils and microfibrils: The morphological sequence of MFC components from a plant physiology and fibre technology point of view. *Nanoscale Research Letters,* **6**, 1–7.

[42] Chinga-Carrasco, G., Averianova, N., Kondalenko, O., Garaeva, M., Petrov, V., Leinsvang, B., and Karlsen, T. (2013) The effect of residual fibres on the microtopography of cellulose nanopaper. *Micron,* **56**, 80–84.

[43] Haugstad G. Atomic Force Microscopy: Understanding Basic Modes and Advanced Applications. New Jersey: John Wiley Sons, Inc.; 2012.

[44] Rubert Co Ltd. ROUGHNESS PARAMETERS, MEAN ROUGHNESS [Internet]. [Cited: 16.04.2019]. Available from: `http://www.rubert.co.uk/faqs/roughness-parameters/`.

[45] Fairhurst D. An Overview of the Zeta Potential - Part 1: The Concept [Internet]. [Updated in 2013; cited: 26.03.2019]. Available from: `https://www.americanpharmaceuticalreview.com/Featured-Articles/133232-An-Overview-of-the-Zeta-Potential-Part-1-The-Concept/`.

[46] Coriolis Pharma. Zeta Potential [Internet]. [Cited: 26.03.2019]. Available from: `https://www.coriolis-pharma.com/contract-analytical-services/zeta-potential/`.

[47] Wikipedia. Zeta potential [Internet]. [Cited: 26.03.2019]. Available from: `https://en.wikipedia.org/wiki/Zeta_potential`.

[48] Wu, C. N., Saito, T., Yang, Q., Fukuzumi, H., and Isogai, A. (2014) Increase in the water contact angle of composite film surfaces caused by the assembly of hydrophilic nanocellulose fibrils and nanoclay platelets. *ACS Applied Materials and Interfaces,* **6**(15), 12707–12712.

[49] FMPS. Contact Angle platform [Internet]. [Cited: 03.05.2019]. Available from: `https://fmps.fbk.eu/contact-angle-platform`.

[50] Schmidt D.R, Waldeck H., Kao W.K. Ch 1: Protein Adsorption to Biomaterials. In: Puleo D.A., Bizios R. (editors). Biological Interactions on Materials Surfaces. 1st ed. New York: Springer; 2009.

[51] Wertz, J-L, Bedué, O. Lignocellulosic Biorefineries. 1st ed. Lausanne: EPFL Press; 2013. p.300.

[52] Shokri, J., Adibkia, K. Application of Cellulose and Cellulose Derivatives in Pharmaceutical Industries. In: Ven, T. and Godbout, L. (editors). Cellulose - Medical, Pharmaceutical and Electronic Applications. London: IntechOpen; 2013.

[53] Murphy, D. B. and Davidson, M. W. (2012) Fundamentals of Light Microscopy and Electronic Imaging, Vol. 83, John Wiley & Sons, Incorporated, 2nd edition.

[54] Lumen. Instruments of Microscopy [Internet]. [Cited: 27.03.2019]. Available from: https://courses.lumenlearning.com/microbiology/chapter/instruments-of-microscopy/.

[55] Kubitscheck, U., Dobrucki, J.W. Fluorescence Microscopy. In: Kubitscheck, U. (editor). Fluorescence Microscopy: From Principles to Biological Applications. 2nd ed. Weinheim: Wiley-VCH Verlag GmbH Co; 2017.

[56] Wikipedia. Fluorescence microscope [Internet]. [Cited: 27.03.2019]. Available from: https://en.wikipedia.org/wiki/Fluorescence_microscope.

[57] Evans, N. D., Gentleman, E., and Polak, J. M. (2006) Scaffolds for stem cells. *Materials Today,* **9**(12).

[58] Pittenger, M. F., Mackay, A. M., Beck, S. C., Jaiswal, R. K., Douglas, R., and Mosca, J. D. (1999) Multilineage potential of adult human mesenchymal stem cells. *Science,* **284**, 143–147.

[59] Neuhuber, B., Swanger, S. A., Howard, L., Mackay, A., and Fischer, I. (2009) Effects of plating density and culture time on bone marrow stromal cell characteristics. *Experimental Hematology,* **36**(9), 1176–1185.

[60] Abcam. Live and Dead Cell Assay [Internet]. [Updated in 2019; cited: 01.04.2019]. Available from: https://www.abcam.com/live-and-dead-cell-assay-ab115347.html.

[61] Thermo Fisher Scientific. alamarBlue™ Cell Viability Reagent [Internet]. [Cited: 10.05.2019]. Available from: https://www.thermofisher.com/order/catalog/product/DAL1025.

[62] Abcam. Lactate Dehydrogenase (LDH) Assay Kit (Colorimetric) [Internet]. [Updated in 2014; cited: 01.04.2019]. Available from: https://www.abcam.com/ldh-assay-kit--lactate-dehydrogenase-assay-kit-colorimetric-ab102526.html.

[63] Thermo Fisher Scientific. Cell morphology [Internet]. [Cited: 03.05.2019]. Available from: https://www.thermofisher.com/no/en/home/references/gibco-cell-culture-basics/cell-morphology.html.

[64] Thermo Fisher Scientific Cell Culture Basics Handbook [Internet]. [Updated in 2016; cited: 12.05.2019]. Available from: https://www.thermofisher.com/content/dam/LifeTech/Documents/PDFs/PG1563-PJT1267-COL31122-Gibco-Cell-Culture-Basics-Handbook-Global-FLR.pdf.

[65] Invitrogen. Quant-iT™ PicoGreen ® dsDNA Reagent and Kits [Internet]. [Cited: 10.05.2019]. Available from: https://www.thermofisher.com/order/catalog/product/P7581.

[66] Buttery, L. D. K., Bourne, S., Xynos, J. D., Wood, H., Hughes, F. J., Hughes, S. P. F., Episkopou, V., and Polak, J. M. (2002) Differentiation of Osteoblasts and in Vitro Bone Formation from Murine Embryonic Stem Cells . *Tissue Engineering,* **7**(1), 89–99.

[67] Golub, E. E. and Boesze-Battaglia, K. (2007) The role of alkaline phosphatase in mineralization. *Current Opinion in Orthopaedics,* **18**(5), 444–448.

[68] Rashad, A., Mohamed-Ahmed, S., Ojansivu, M., Berstad, K., Yassin, M. A., Kivijärvi, T., Heggset, E. B., Syverud, K., and Mustafa, K. (2018) Coating 3D Printed Polycaprolactone Scaffolds with Nanocellulose Promotes Growth and Differentiation of Mesenchymal Stem Cells. *Biomacromolecules,* **19**(11), 4307–4319.

[69] Havlik, R. J. (2002) Hydroxyapatite. *Plastic & Reconstructive surgery,* **110**(4), 1176–1179.

[70] Gregory, C. A., Gunn, W. G., Peister, A., and Prockop, D. J. (2004) An Alizarin red-based assay of mineralization by adherent cells in culture: Comparison with cetylpyridinium chloride extraction. *Analytical Biochemistry,* **329**(1), 77–84.

[71] Abcam. Alkaline Phosphatase Assay Kit (Colorimetric) (ab83369) [Internet]. [Cited: 10.05.2019]. Available from: `https://www.abcam.com/alkaline-phosphatase-assay-kit-colorimetric-ab83369-protocols.html#top-509`.

[72] King W.J., K. P. (2013) NIH Public Access. *Advanced Drug Delivery Reviews,* **64**(12), 734–763.

[73] Sigma Aldrich. Beta-Cyclodextrin [Internet]. [Cited: 18.01.2019]. Available from: `https://www.sigmaaldrich.com/catalog/product/sigma/c4767?lang=en&region=NO`.

[74] Crini, G., Fourmenin, S., Fenyvesi, E., Torri, G., Fourmentin, M. and Morin-Crini, N. Fundamentals and Applications of Cyclodextrins. In: Fourmentin, S., Crini, G., and Lichtfouse, E. (editors). Cyclodextrin Fundamentals, Reactivity and Analysis. Cham: Springer; 2018.

[75] Indiamart. Beta Cyclodextrin [Internet]. [Cited: 18.01.2019]. Available from: `https://www.indiamart.com/proddetail/beta-cyclodextrin-12387538873.html`.

[76] Ruiz-Palomero, C., Soriano, M. L., and Valcárcel, M. (2015) β-Cyclodextrin decorated nanocellulose: A smart approach towards the selective fluorimetric determination of danofloxacin in milk samples. *Analyst,* **140**(10), 3431–3438.

[77] Saini, S., Quinot, D., Lavoine, N., Belgacem, M. N., and Bras, J. (2017) β-Cyclodextrin-grafted TEMPO-oxidized cellulose nanofibers for sustained release of essential oil. *Journal of Materials Science,* **52**(7), 3849–3861.

[78] Master Organic Chemistry. Conversion of carboxylic acids to esters using acid and alcohols (Fischer Esterification) [Internet]. [Cited: 07.02.2019]. Available from: `https://www.masterorganicchemistry.com/reaction-guide/`

conversion-of-carboxylic-acids-to-esters-using-acid-and-alcohols-fischer-esterification/.

[79] Castro, D. O., Tabary, N., Martel, B., Gandini, A., Belgacem, N., and Bras, J. (2016) Effect of different carboxylic acids in cyclodextrin functionalization of cellulose nanocrystals for prolonged release of carvacrol. *Materials Science & Engineering C,* **69**, 1018–1025.

[80] Thermo Fisher. FTIR Spectroscopy Academy [Internet]. [Cited: 06.02.2019]. Available from: www.thermofisher.com/FTIRlearning.

[81] Wikipedia. Attenuated total reflectance [Internet]. [Cited: 24.01.2019]. Available from: https://en.wikipedia.org/wiki/Attenuated_total_reflectance.

[82] Bradley M. A Gift for You: An FTIR Basic Organic Functional Group Reference Chart [Internet]. [Updated in 2015; cited: 08.02.2019]. Available from: https://www.thermofisher.com/blog/materials/a-gift-for-you-an-ftir-basic-organic-functional-group-reference-chart/.

[83] Hirn, U. and Bauer, W. (2006) a Review of Image Analysis Based Methods To Evaluate Fiber Properties. *Scanning,* **86**, 96–105.

[84] de Oliveira Barud, H. G., da Silva, R. R., da Silva Barud, H., Tercjak, A., Gutierrez, J., Lustri, W. R., de Oliveira, O. B., and Ribeiro, S. J. (2016) A multipurpose natural and renewable polymer in medical applications: Bacterial cellulose. *Carbohydrate Polymers,* **153**, 406–420.

[85] Helenius, G., Bäckdahl, H., Bodin, A., Nannmark, U., Gatenholm, P., and Risberg, B. (2006) In vivo biocompatibility of bacterial cellulose. *Journal of Biomedical Materials Research - Part A,* **76**(2), 431–438.

[86] Serra, A., González, I., Oliver-Ortega, H., Tarrès, Q., Delgado-Aguilar, M., and Mutjé, P. (2017) Reducing the amount of catalyst in TEMPO-oxidized cellulose nanofibers: Effect on properties and cost. *Polymers,* **9**(11).

[87] Sigma Aldrich. Fetal Bovine Serum [Internet]. [Cited: 08.05.2019]. Available from: https://www.sigmaaldrich.com/catalog/product/sigma/f2442?lang=en&region=NO.

[88] Pirich, C. L., de Freitas, R. A., Woehl, M. A., Picheth, G. F., Petri, D. F., and Sierakowski, M. R. (2015) Bacterial cellulose nanocrystals: impact of the sulfate content on the interaction with xyloglucan. *Cellulose,* **22**(3), 1773–1787.

[89] Pertile, R. A., Andrade, F. K., Alves, C., and Gama, M. (2010) Surface modification of bacterial cellulose by nitrogen-containing plasma for improved interaction with cells. *Carbohydrate Polymers,* **82**(3), 692–698.

[90] Thibault, R. A., Scott Baggett, L., Mikos, A. G., and Kasper, F. K. (2009) Osteogenic Differentiation of Mesenchymal Stem Cells on Pregenerated Extracellular Matrix Scaffolds in the Absence of Osteogenic Cell Culture Supplements. *Tissue Engineering Part A,* **16**(2), 431–440.

[91] Taira, M., Nakao, H., Takahashi, J., and Araki, Y. (2003) Effects of two vitamins, two growth factors and dexamethasone on the proliferation of rat bone marrow stromal cells and osteoblastic MC3T3-E1 cells. *Journal of Oral Rehabilitation,* **30**(7), 697–701.

[92] Langenbach, F. and Handschel, J. (2013) Effects of dexamethasone, ascorbic acid and β-glycerophosphate on the osteogenic differentiation of stem cells in vitro. *Stem Cell Research and Therapy,* **4**(5), 1.

[93] Bott, K., Upton, Z., Schrobback, K., Ehrbar, M., Hubbell, J. A., Lutolf, M. P., and Rizzi, S. C. (2010) The effect of matrix characteristics on fibroblast proliferation in 3D gels. *Biomaterials,* **31**(32), 8454–8464.

[94] Tirkkonen, L., Haimi, S., Huttunen, S., Wolff, J., Pirhonen, E., Sándor, G., and Miettinen, S. (2016) Osteogenic medium is superior to growth factors in differentiation of human adipose stem cells towards bone-forming cells in 3D culture. *European Cells and Materials,* **25**, 144–158.

[95] Kumar, G., Tison, C. K., Chatterjee, K., Pine, P. S., McDaniel, J. H., Salit, M. L., Young, M. F., and Simon, C. G. (2011) The determination of stem cell fate by 3D scaffold structures through the control of cell shape. *Biomaterials,* **32**(35), 9188–9196.

[96] Faia-Torres, A. B., Charnley, M., Goren, T., Guimond-Lischer, S., Rottmar, M., Maniura-Weber, K., Spencer, N. D., Reis, R. L., Textor, M., and Neves, N. M. (2015) Osteogenic differentiation of human mesenchymal stem cells in the absence of osteogenic supplements: A surface-roughness gradient study. *Acta Biomaterialia,* **28**, 64–75.

[97] Javazon, E. H., Colter, D. C., Schwarz, E. J., and Prockop, D. J. (2004) Rat Marrow Stromal Cells are More Sensitive to Plating Density and Expand More Rapidly from Single-Cell-Derived Colonies than Human Marrow Stromal Cells. *Stem Cells,* **19**(3), 219–225.

[98] Vielreicher, M., Kralisch, D., Völkl, S., Sternal, F., Arkudas, A., and Friedrich, O. (2018) Bacterial nanocellulose stimulates mesenchymal stem cell expansion and formation of stable collagen-I networks as a novel biomaterial in tissue engineering. *Scientific Reports,* **8**(1), 1–14.

[99] Petersen, N. and Gatenholm, P. (2011) Bacterial cellulose-based materials and medical devices: Current state and perspectives. *Applied Microbiology and Biotechnology,* **91**(5), 1277–1286.

[100] Mäkelä, M., Korpela, T., and Laakso, S. (1987) Colorimetric determination of β-cyclodextrin: two assay modifications based on molecular complexation of phenolphatalein. *Journal of Biochemical and Biophysical Methods,* **14**(2), 85–92.

[101] Manivaskam, N. Industrial Water Analysis Handbook. 1st ed. USA: Chemical Publishing Company Inc; 2011. pp. 300-302.

[102] Desmaisons, J., Boutonnet, E., Rueff, M., Dufresne, A., and Bras, J. (2017) A new quality index for benchmarking of different cellulose nanofibrils. *Carbohydrate Polymers,* **174**, 318–329.

[103] Study.com. Transmission Electron Microscopy, Theory and Applications [Internet]. [Cited: 24.01.2019]. Available from: https://study.com/academy/lesson/transmission-electron-microscopy-theory-applications.html.

[104] Wikipedia. Transmission electron microscopy [Internet]. [Cited: 24.01.2019]. Available from: https://en.wikipedia.org/wiki/Transmission_electron_microscopy.

A Appendix

A.1 Determine carboxylate contents

The conductivity curve of sample TO-CNF, parallel 1, is shown in Figure 1. To calculate the amount of NaOH consumed in phase 2, points B and C must be known. These points can be found by fitting three separate, straight lines to the curve in phase 1, 2 and 3. By calculating the intersection between the phase 1 curve and phase 2 curve, as well as the intersection between the phase 2 curve and phase 3 curve, points B and C can be determined.

Where each phase start and end is determined manually by observing the conductivity curve shown in Figure 1. The following procedures described have been performed in matlab, however, excel is also suitable for the task. The list of data points presented in Figure 1 are divided into three separate txt.-files. The curves for each phase are shown in Figure 2. The curved areas around point B and C in Figure 1 are not included, because these parts represents transitions between two phases.

The curves for each phase are further fitted through linear regression, and these straight lines are shown in Figure 3. The intersection between the lines representing phase 1 and phase 2 is calculated, as well as the intersection between the lines representing phase 2 and phase 3. This is done in MATLAB and the script is shown in Figure 4. It is important that the concentration of the strong base is known.

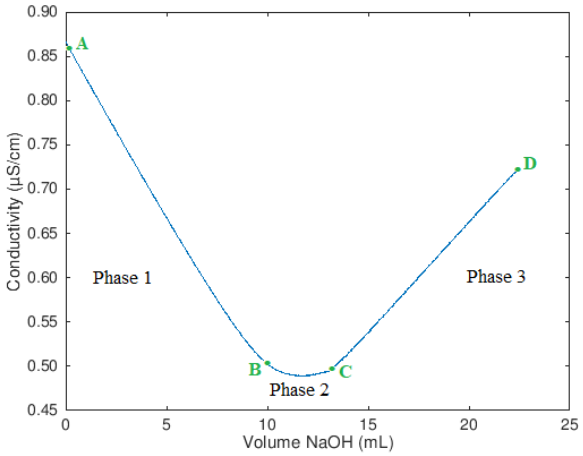

Figure 1: Conductivity curve of sample TO-CNF, parallel 1.

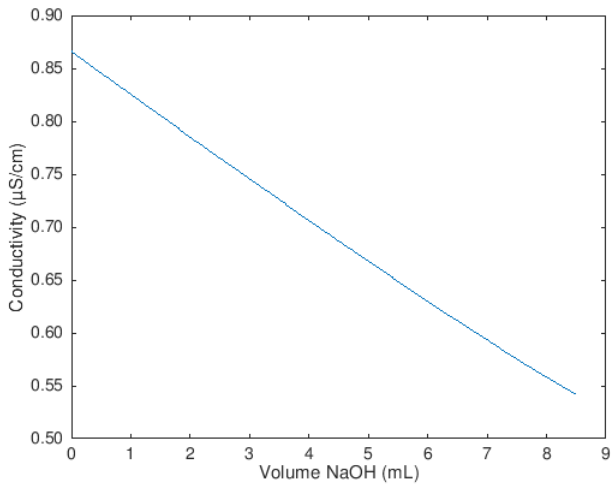

()

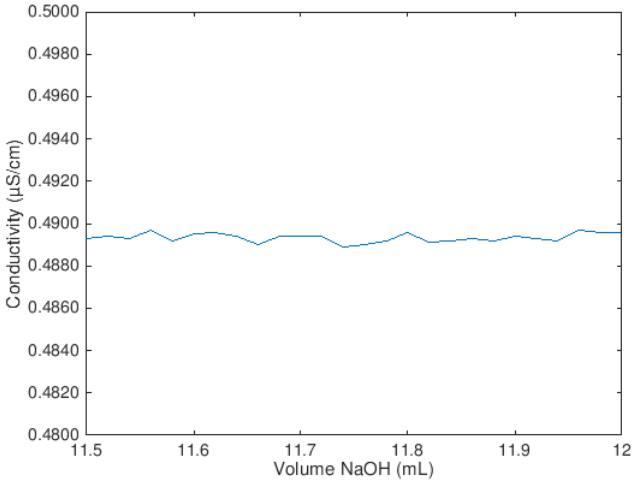

()

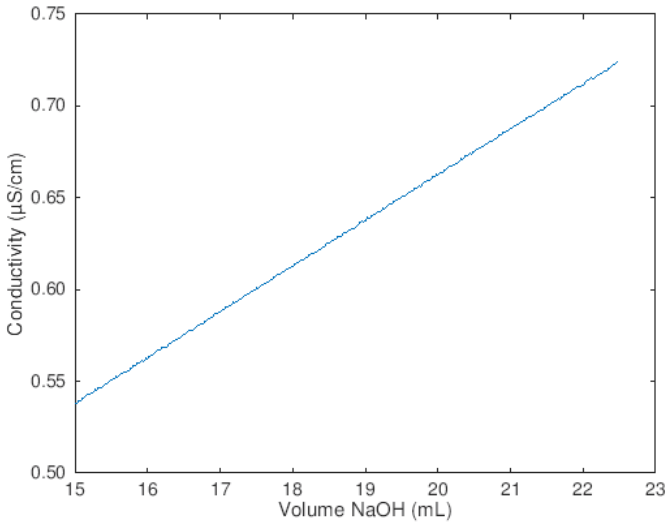

()

Figure 2: The figure shows the curves of phase 1 (a), phase 2 (b) and phase 3 (c) for sample TO-CNF, parallel 1. The data points making up these curves have manually been chosen by observing Figure 1 of where the different phases start and stop.

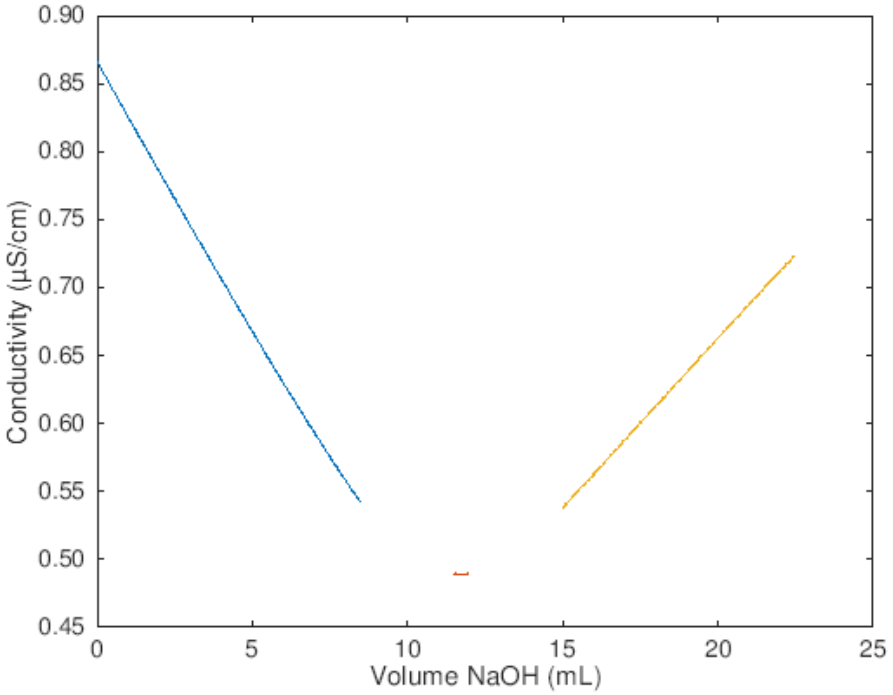

Figure 3: Straight lines fitted with linear regression for each of the three phases of sample TO-CNF, parallel 1.

```
% Determination of carboxylate content
close all
clear all
clc
%% Determining each phase manually and save in
txt-files
%Each txt-file is further opened and called b, c
and d.
b=input('Hvilken tekstfil skal opnes? Svar
filnavn (phase 1) etterfulgt av .txt','s');
c=input('Hvilken tekstfil skal opnes? Svar
filnavn (phase 2) etterfulgt av .txt','s');
d=input('Hvilken tekstfil skal opnes? Svar
filnavn (phase 3) etterfulgt av .txt','s');
%% Organizing each txt-file to matrix's and
extract the useful information
B= dlmread(b);
C= dlmread(c);
D=dlmread(d);
x1=B(:,1); %Extracting all numbers from the first
column (Volume NaOH added)
y1=B(:,2); %Extracting all numbers from the
second column (Conductivity)
x2=C(:,1);
y2=C(:,2);
x3=D(:,1);
y3=D(:,2);
%% Plotting the three curves separatly
figure
plot(x1,y1);
hold on
plot(x2,y2);
hold on
plot(x3,y3);
xlabel('Volume NaOH (mL)');
ylabel('Conductivity (µS/cm)');
ytickformat('%.2f');
```

```
%% Using linear regression to fit straight lines
to each curve
e=polyfit(x1,y1,1); %Phase 1
f=polyfit(x2,y2,1); %Phase 2
g=polyfit(x3,y3,1); %Phase 3
%% Finding the intersection between the phase 1
and phase 2 lines, and between the phase 2 and
phase 3 lines.
syms x y
eqn1 = e(1)*x-y == -e(2);
eqn2 = f(1)*x-y == -f(2);
eqn3 = g(1)*x-y == -g(2);
sol = solve([eqn1,eqn2],[x,y]);
xsol1 = sol.x;
ysol1 = sol.y;
sol = solve([eqn2,eqn3],[x,y]);
xsol2 = sol.x;
ysol2 = sol.y;
xsol1=double(xsol1); % X-value in intersection
between phase 1 and phase 2 lines.
ysol1=double(ysol1);
xsol2=double(xsol2); % X-value in intersection
between phase 2 and phase 3 lines.
ysol2=double(ysol2);
%% Calculating the volume of NaOH used in the
titration
V_NaOH=xsol2-xsol1; % In mL
C_NaOH=(0.0488+0.0483)/2;%mol/L
n_NaOH=V_NaOH*C_NaOH;%mmol NaOH = mmol karboksyl
%% Calculating the carboxyl content of the sample
A=input('Hvor mange g dry cellulosemasse ble
brukt?','s');
B=str2num(A);
C=n_NaOH/B; %mmol carboxyl/g dry cellulose mass
```

Figure 4: MATLAB script used to calculate the carboxylate content of the different samples. The script is read from the left column to the right column.

A.1.1 Determine NaOH concentration

Determining the concentration of NaOH was done using conductometric titration where NaOH was added to known amounts of HCl in an aqueous solution. A general conductivity curve from such a titration is shown in Figure 5. The intersection between the curve from phase 1 and phase 2 is equal to the volume of NaOH used to neutralise the acid. As one molecule of NaOH neutralises one molecule of HCl, and the amount of HCl added is known, the concentration of NaOH can be calculated. The calculations were done using MATLAB and the script is shown in Figure 6.

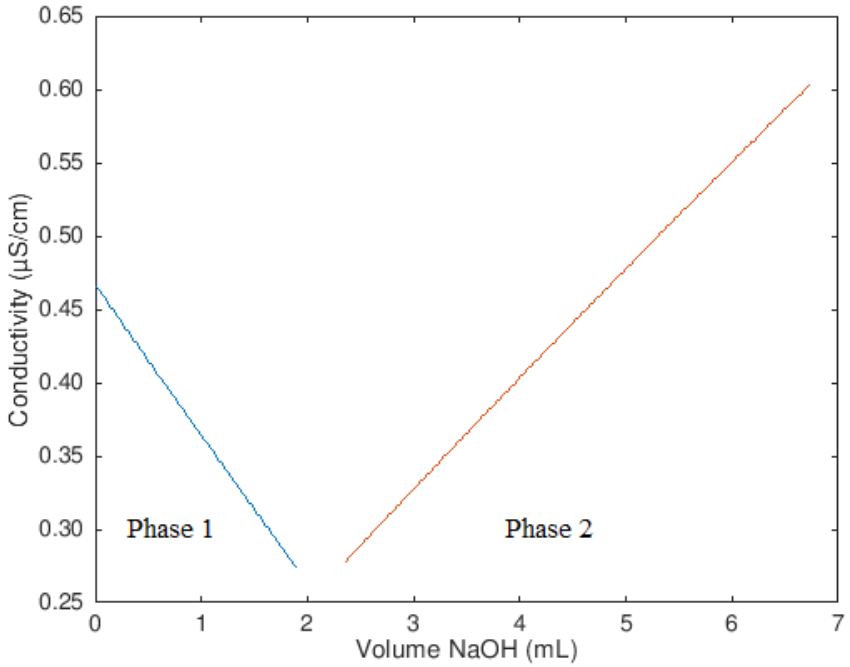

Figure 5: The curves show the conductivity measured for a HCl solution titrated against an NaOH solution.

```
close all
clear all
clc
%% Extract the datapoints for each phase
b=input('Hvilken tekstfil skal opnes? Svar
filnavn (phase 1) etterfulgt av .txt','s');
c=input('Hvilken tekstfil skal opnes? Svar
filnavn (phase 2) etterfulgt av .txt','s');
B= dlmread(b);
C= dlmread(c);
x1=B(:,1);
y1=B(:,2);
x2=C(:,1);
y2=C(:,2);
%% Plot the datapoints for each phase
figure
plot(x1,y1);
hold on
plot(x2,y2);
xlabel('Volume NaOH (mL)');
ylabel('Conductivity (µS/cm)');
ytickformat('%.2f');
```

```
%% Use linear regression to fit straight lines to
each phase
d=polyfit(x1,y1,1);
e=polyfit(x2,y2,1);
%% Find intersection between the two straight
lines
syms x y
eqn1 = d(1)*x-y == -d(2);
eqn2 = e(1)*x-y == -e(2);
sol = solve([eqn1,eqn2],[x,y]);
xsol = sol.x;
ysol = sol.y;
xsol=double(xsol); % Number of interest. Equal to
the volume of NaOH added to neutralize all the
acid.
ysol=double(ysol);
%% Calculate NaOH-concentration:
%Antar at HCl kons. er kjent og lik 0.1M.
HCl=0.1*10^(-3); %mol H+
NaOH=(HCl/xsol)*10^3;%For ?  f?  i mol/L
```

Figure 6: MATLAB script used to calculate the concentration of the strong base used in the conductometric titrations. The script is read from the left column to the right.

A.2 Determine aldehyde contents

The absorbance of the nanocellulose qualities after reaction with TTC were measured and the mean absorbance are listed in Table 1, along with standard deviation. The values presented in Table 1 have been corrected by subtracting the absorbance of the blank samples.

Table 1: Absorbance after reaction between the nanocellulose qualities and TTC.

Sample	**Average absorbance**
TO-CNF	1.077 $\pm$0.081
TO-O-CNF	0.035 $\pm$0.010
TO-R-CNF	0.038 $\pm$0.028
BNC	0.033 $\pm$0.016

The calibration curve used to determine the aldehyde (CHO) contents are shown in Figure 7. In this figure, the absorbance measured for a sample after reaction with TTC is related to glucose concentration. The calibration curve was related to glucose concentration for simplicity reasons, as glucose at different concentrations were used to make the calibration curve.

To show how the CHO content of a nanocellulose sample can be determined from the calibration curve, the measured absorbance of sample TO-CNF after reacting with TTC is used. The

mean absorbance from the TO-CNF reactions performed was equal to 1.077±0.081 (Table 1). From the calibration curve, the glucose concentration that corresponds to this absorbance can be calculated as shown in Equation (10).

$$1.077 = 81.631x - 0.5727, x = 0.0202\% \tag{10}$$

For all reactions between either the glucose suspensions or the nanocellulose qualities and the TTC, 4 g of suspension was used. For a 0.0202% glucose suspension, this means that $8.084 \cdot 10^{-4}$ g glucose reacts with TTC. With a molecular weight of 180.156 g/mol, $8.084 \cdot 10^{-4}$ g glucose equals $4.49 \cdot 10^{-6}$ mol glucose. As there is 1 mol CHO per mol glucose, $4.49 \cdot 10^{-6}$ mol CHO has reacted with TTC.

The concentration of the nanocellulose suspensions used in the TTC reactions was equal to 0.4%. As 4 g 0.4% suspension was used, this equals 0.016 g dry cellulose. The CHO content of the TO-CNF sample is thus equal to 280 μmol CHO/ g dry cellulose.

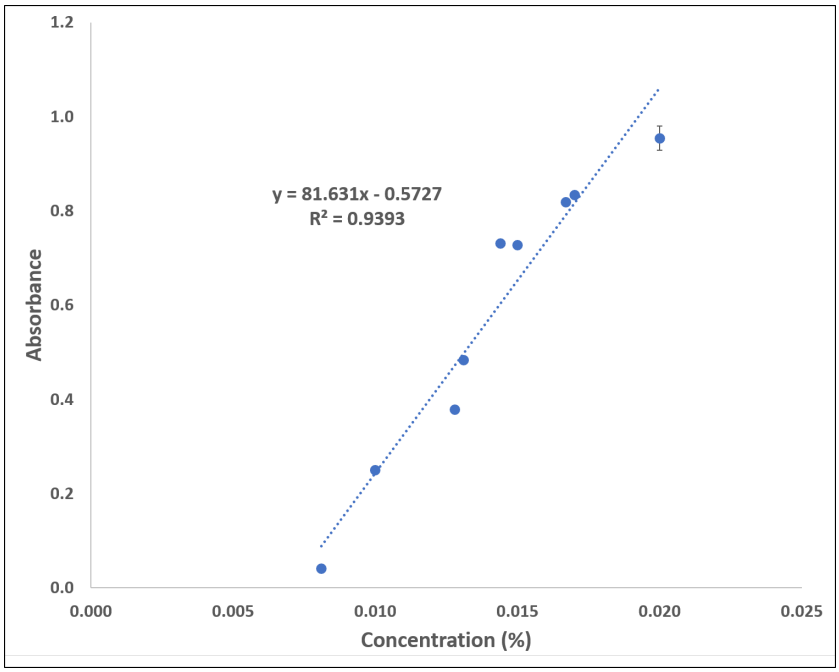

Figure 7: The absorbance measured as a function of glucose concentration in reaction with TTC.

A.3 Standard deviation

The standard deviation, SD, between two or more parallels can be calculated from Equation (11). In the equation, x_i is the determined value of parallel i, $\bar{x}$ is the average value of all the parallels and n is the number of parallels measured.

$$SD = \sqrt{\frac{\sum_{i=1}^{n} (x_i - \bar{x})^2}{n}} \tag{11}$$

A.4 Normalization procedure

Normalization of some results was conducted in order to facilitate comparison between the control group and the nanocellulose groups. The example calculation shown here is from the indirect cytotoxicity assay, for the control group. As shown in Figure 8, the mean absorbance result for the control group after the first time point was calculated and each of the control group results were normalized by dividing each absorbance on the mean. A new mean for the control group was calculated (equal to 1) as well as the standard deviation (not shown in the figure). For the other nanocellulose groups, and for the control group at the second time point, the absorbance results were divided on the mean of the control group at the first time point (here equal to 58.02) and a new mean + standard deviation was calculated.

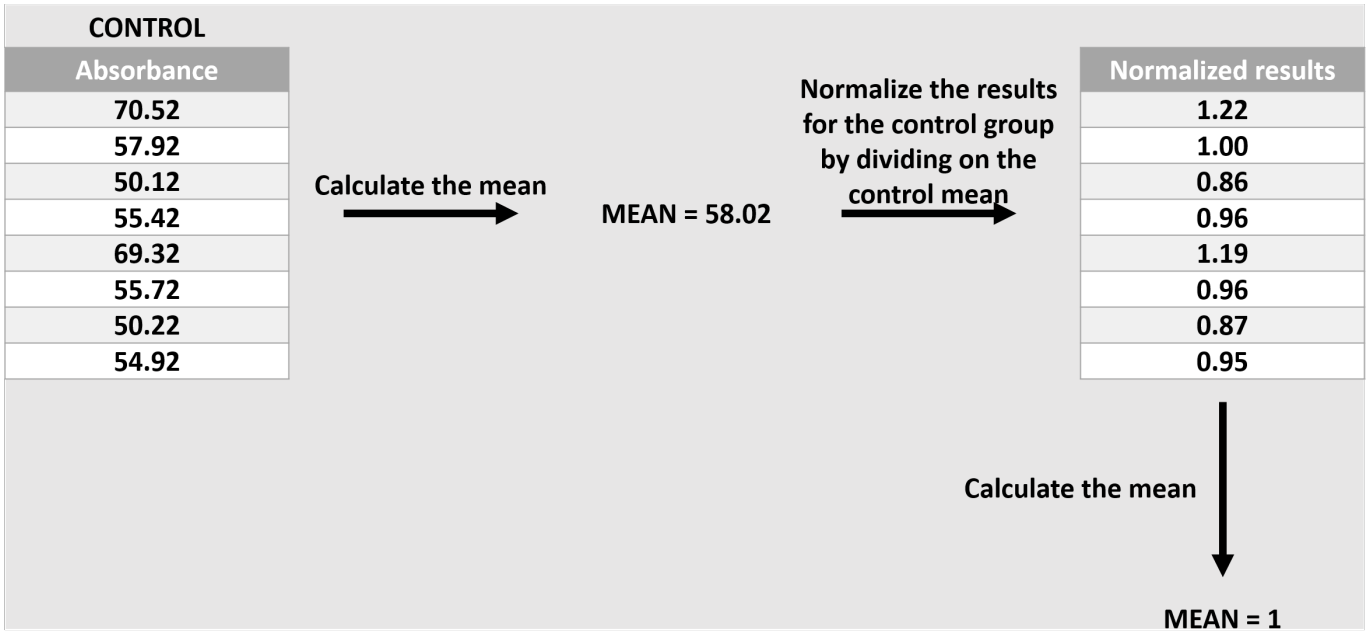

Figure 8: Schematic of how to normalize the results.

A.5 Amount of residual fibers in the CNF samples

Extracts of raw data from the fiber tester analysis of sample TO-CNF, parallel 1, is shown in Figure 9 and 10.

Length weighted (ISO)

Variable	Value	Difference
Mean length	0.324 mm	-0.013 mm
Mean width	37.8 µm	-0.5 µm
Mean shape	80.9 %	0.6 %
Mean fibril area	18.3 %	-3.9 %
Mean fibril perimeter	37.8 %	-3.2 %
Mean fines	87.0 %	

Figure 9: Extracts of raw data for sample TO-CNF, parallel 1, from the fiber tester analysis using the Fiber Tester 912 Plus apparatus.

Number of fibers	6586 (384807)
Number of images	7864
Temperature	29.7 °C

Figure 10: Extracts part two of raw data for sample TO-CNF, parallel 1, from the fiber tester analysis using the Fiber Tester 912 Plus apparatus.

The apparatus reports amongst others the number of fiber residues detected, n, their mean length, l and mean width, b, which can be obtained from Figure 9 and 10. As shown in Equation (12), b can be used to calculate the mean cross-sectional fiber residue area, A, and by multiplying A with l, the mean fiber residue volume, V, is estimated as shown in Equation (13).

$$A = \pi \cdot (b/2)^2 = \pi \cdot \left(\frac{37.8\mu m}{2}\right)^2 = 1122\mu m^2 = 1.122 \cdot 10^{-3} mm^2 \tag{12}$$

$$V = A \cdot l = 1.122 \cdot 10^{-3} mm^2 \cdot 0.324mm = 3.636 \cdot 10^{-4} mm^3 \tag{13}$$

From the mean fiber residue volume and by using an estimate for the density of the cellulose fibers (1.55 g/cm^3, [42]), the average weight of one fiber, $\overline{w_f}$ can be estimated, see Equation (14). In Equation (15), the apparent residual fiber content, R_f, is estimated, where w_s is the dry weight of the sample investigated [42]. The dry weight used for each parallel, of every sample, was equal to 0.1 g.

$$\overline{w_f} = V \cdot 1.55 = 3.636 \cdot 10^{-4} mm^3 \cdot 1.55 g/cm^3 \cdot 10^{-3} cm^3/mm^3 = 5.636 \cdot 10^{-7} g \tag{14}$$

$$R_f(\%) = \frac{\overline{w_f} n}{w_s} \cdot 100 = \frac{5.636 \cdot 10^{-7} g \cdot 6586}{0.1g} \cdot 100 = 3.7 \tag{15}$$

A.6 Complete figures

A.6.1 Proliferation

The proliferation of rBMSCs grown on the nanocellulose coated TCP were compared to cells grown on uncoated TCPs, by a dsDNA based assay. The assay was conducted using both regular medium (Figure 11) and osteogenic medium (Figure 12). Statistical analysis have been performed and all the bars indicating significant differences are included in the figures.

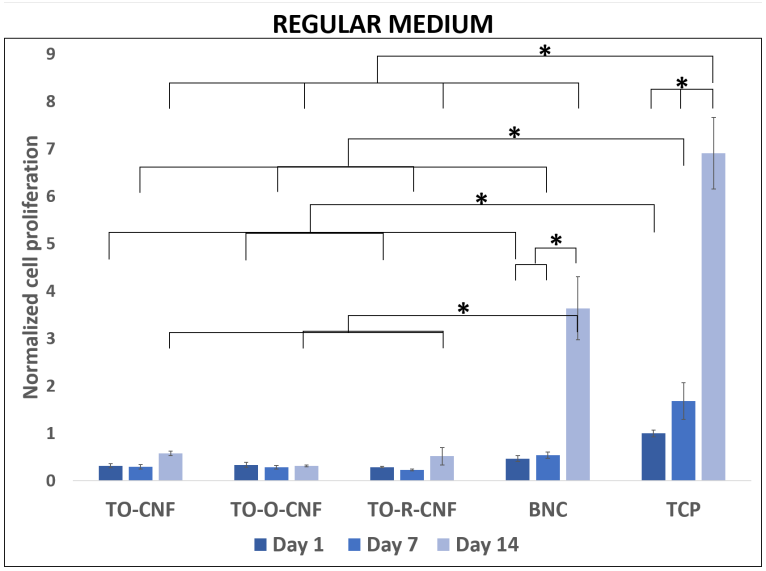

Figure 11: The proliferation of rBMSCs cultured on different surfaces with regular medium. Results are presented as normalized means ± SD.

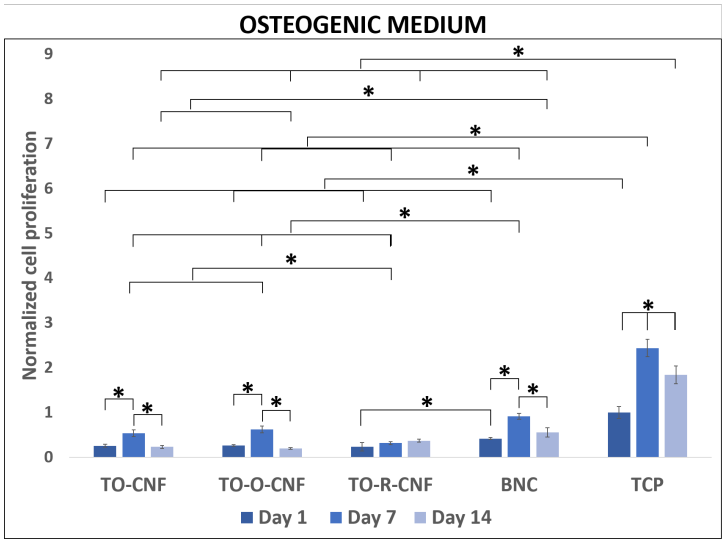

Figure 12: The proliferation of rBMSCs cultured on different surfaces with osteogenic medium. Results are presented as normalized means ± SD.

A.6.2 Differentiation

The differentiation of stem cells are crucial for tissue regeneration. Osteogenic differentiation of rBMSCs were evaluated by investigating the ALP activity of the cells. ALP activity is an early marker for osteogenic differentiation and the ALP levels were measured after 1, 7 and 14 days, in regular medium (Figure 13) and osteogenic medium (Figure 14). Statistical analysis have been performed and all the bars indicating significant differences are included in the figures.

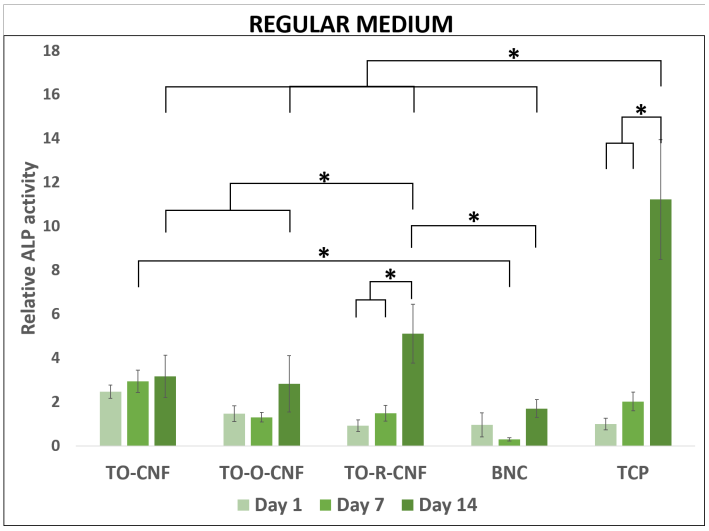

Figure 13: ALP activity after 1, 7 and 14 days for rBMSCs cultured on different surfaces with regular medium. Results are presented as relative means ± SD.

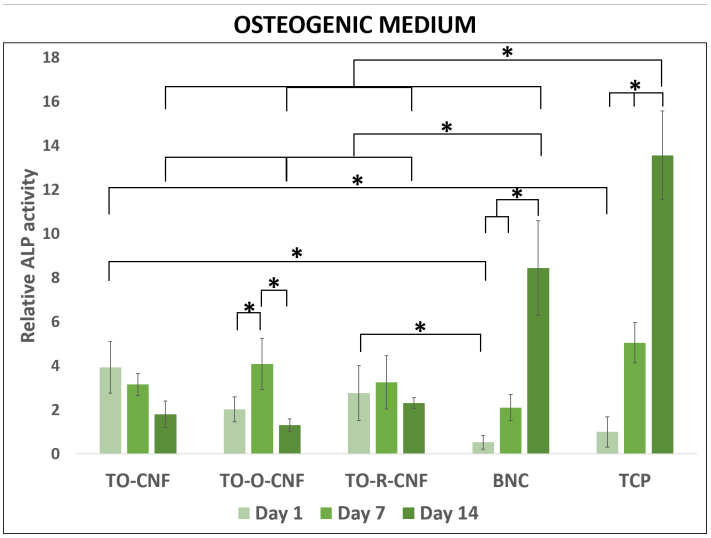

Figure 14: ALP activity after 1, 7 and 14 days for rBMSCs cultured on different surfaces with osteogenic medium. Results are presented as relative means ± SD.

A.7 Characterizations conducted in Grenoble of sample TO-CNF

It was only the TO-CNF sample that was brought to LGP2 to test grafting of βCD to the CNFs. In order to compare the TO-CNF material to other nanocellulose qualities used at LGP2, several properties were investigated. Some theory behind these methods, the experimental methods and results from these characterizations are presented below including a brief discusion of the results obtained.

A.7.1 Theory

Turbidity
Turbidity is an optical property which describes the transparency of a suspension, where highly transparent samples are less turbid [101]. Turbidimeters can be used to measure the turbidity of a suspension by measuring the amount of light that is transmitted through the suspension. Samples containing insoluble material scatter light sent through the sample which results in a higher turbidity value. Turbidity can be used as a measure to assess nanocellulose quality, as more fibrillated suspensions will be more transparent and thus yield a low turbidity. Less fibrillated fibers result in an increase in turbidity [102].

Transmission electron microscopy
Transmission Electron Microscope (TEM) is an electron microscope which can create high resolution images at nanometer level. The TEM apparatus generally consist of an electron source, electromagnetic lenses, aperture and sample holder, and the TEM imaging is operated under vacuum. A general TEM apparatus is shown in Figure 62.

The electron source produces accelerated electrons which are focused by the electromagnetic lenses. The beam of electrons are transmitted through the sample and further focused onto the imaging screen by electromagnetic projection lenses. Not all electrons will pass through the sample, and non-uniform samples contain areas that transmit more electrons than others. The areas with less transmittance of electrons will be seen as darker spots in TEM images [103]. Compared to SEM, with the sample holder at the bottom of the microscope, the sample holder in TEM is located above the imaging screen. This means that the entire sample is imaged in TEM, compared to surface structure which is evaluated in SEM.

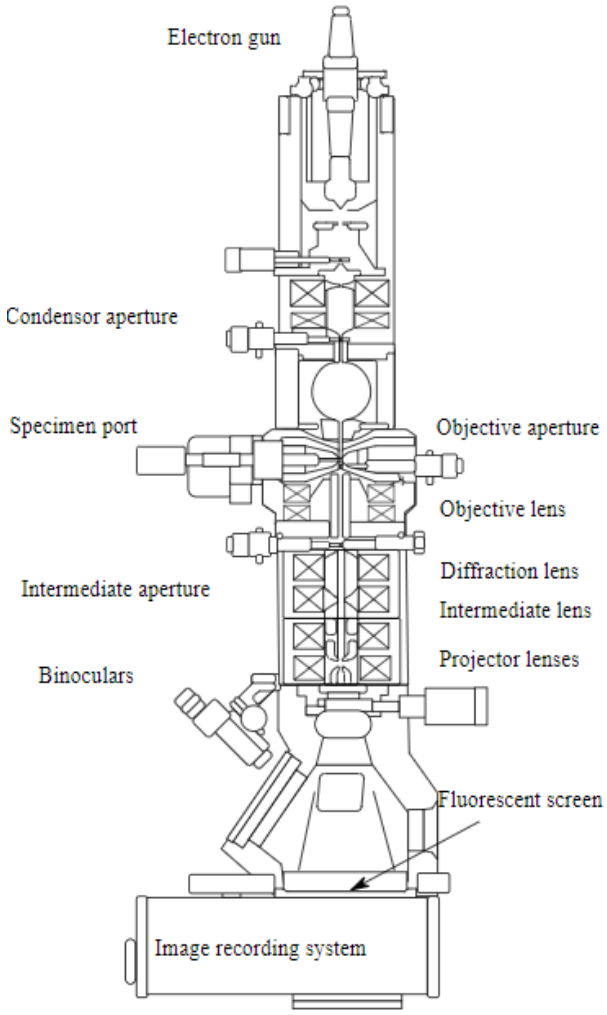

Figure 62: General apparatus for a Transmission Electron Microscopy. Figure collected from [104].

A.7.2 Methods

Nanosized fraction

The nanosized fraction of the TO-CNF material was determined as described in literature [102]. For the measurements, 0.02% TO-CNF was prepared and stirred for 10 minutes using the T25 Ultra Turrax (IKA). 90 mL of the suspension was centrifuged at 1000G for 15 minutes using the 6-16KS centrifuge (Sigma). Around 20 g of the supernatant was added to aluminium foil petri dishes before and after centrifugation and dried at 105°C. The solid content was determined and the nanosized fraction was calculated as the ratio between the solid content after and before centrifugation, see example calculation in Appendix A.7.5. The procedure was performed in two parallels, by Bastien Michel.

Fiber analysis

The amount and size of residual fibers were evaluated using the MORFI LB-01 (TechPap) apparatus. For the analysis, 5% (200 g) TO-CNF suspension was stirred for 10 minutes using the T25 Ultra Turrax (IKA) and mixed with 2 L of water before analysis.

Turbidity
0.1% TO-CNF (400 mL) was stirred for 10 minutes using the T25 Ultra Turrax (IKA) and the turbidity of the suspension was evaluated using the AL250T-IR (AQUALYTIC) turbidimeter. Eight samples were measured in two parallels.

Optical microscopy
The macroscopic size of the fiber residues, measured in μm^2, as well as the fiber area, in %, were determined using the AX10 optical microscope (ZEISS) and the ImageJ software. 0.5% TO-CNF suspension was stirred for 10 minutes using the T25 Ultra Turrax (IKA) prior to the analysis. A drop of the TO-CNF suspension was placed between an object glass and a cover glass and images were taken at 10x magnification. ImageJ was used to calculate the average size of the residual fibers and the fiber area by transforming the images taken with optical microscope to 8-bit and adjusting the treshold. A scale bar was further added and the size of the black particles was estimated as well as the % area of the particles. The ImageJ treatment was conducted by Bastien Michel.

Transmission electron microscopy
To obtain high resolution images of the TO-CNF suspension at nanometer level, TEM was conducted using a JEM-2100 Plus Transmission Electron Microscope (JEOL). The TO-CNF suspension was diluted and a drop was deposited on a carbon coated copper grid, which previously had been made hydrophilic by glow discharge. Uranyl acetate was also added to the sample as the TEM was conducted through negative staining using uranyl acetate. An accelerating voltage of 200 kV was applied and the imaging was conducted by Christine Lancelon-Pin from Cermav.

A.7.3 Results

The different results obtained are presented below and summed up in Table 2.

Nanosized fraction
The nanosized fraction is a measure of the amount of nanosized particles in a suspension, by the use of a gravimetric approach. The mean nanosized fraction, calculated from two parallels, was equal to 46.1 $\pm$ 2.9%, indicating that around 50% of the solid matter in the TO-CNF suspension are CNFs and nanofibril aggregates that are not separated out through the use of centrifugal force [102].

Fiber analysis
The results from the fiber analysis have been used to estimate the apparent residual fiber fraction equal to 2.4 % for the TO-CNF sample. The MORFI apparatus also provided information about the fines content, measured both in % area and % length. The fines content in % area was equal to 37.8 $\pm$ 0.6 and is a measure of the amount of fibers with a surface area smaller than 3000 μm^2. The fines content in % length was equal to 71.7 $\pm$ 0.2 and is the amount of fibers with fiber length below 200 μm. Example calculation of the apparent residual fibre fraction is shown in Appendix A.5.

Optical microscopy
Six images were taken using an optical microscope and analysed using the ImageJ software. The average macroscopic size, meaning the average surface area of visible particles in the TO-CNF suspension, was estimated to 11.4 $\pm$ 2.7 μm^2. The ImageJ software was also used to calculate the % area of visible particles in each image, and the mean value was equal to 3.3 $\pm$ 1.5 %.

Turbidity
The turbidity of a 0.05% TO-CNF suspension was measured as 49.4 $\pm$ 11.1 NTU, implying that the suspension has a relatively high composition of nanoscaled materials.

Transmission Electron Microscopy
TEM images of the TO-CNF quality was conducted in order to investigate and confirm the presence of nanoscaled fibrils. The images are shown in Figure 15 and 16.

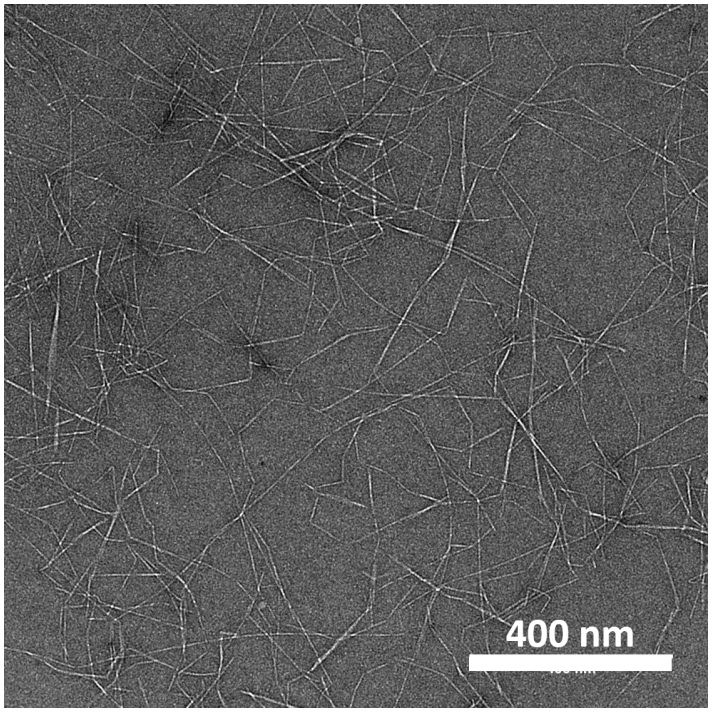

Figure 15: TEM images of sample TO-CNF.

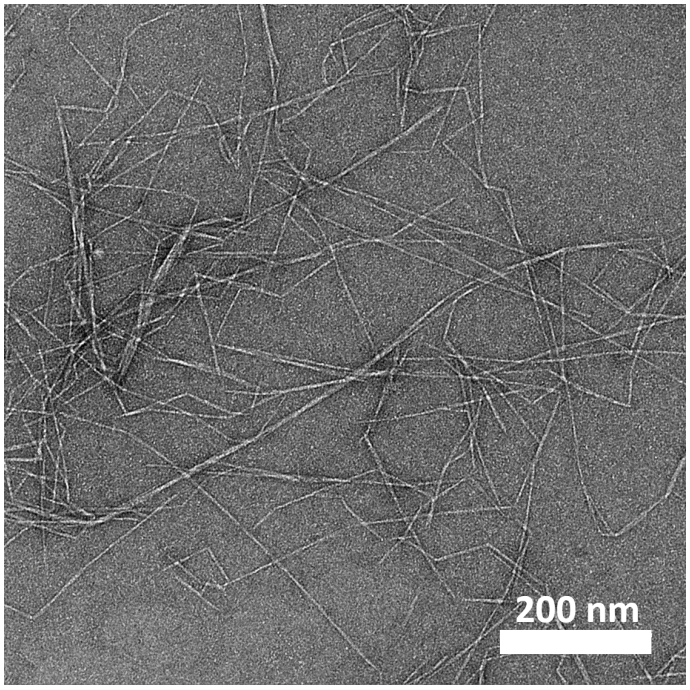

Figure 16: TEM images of sample TO-CNF showing the nanoscale fibrils.

Table 2: Results from the characterisation of sample TO-CNF.

Property	**Result**
Nanosized fraction	46.1 ± 2.9 [%]
Residual fiber fraction	2.4 %
Fines content	37.8 ± 0.6 [% in area]
Fines content	71.7 ± 0.2 [% in length]
Average macroscopic size	11.4 ± 2.7 [μm^2]
Average particle area	3.3 ± 1.5 [%]
Turbidity	49.4 ± 11.1 [NTU]
TEM	Nanoscaled fibrils confirmed

A.7.4 Discussion

The work conducted at LGP2 was performed using only the TO-CNF quality. To be able to compare the results obtained using the TO-CNFs to other CNFs used at LGP2, characterisations were conducted. These characterisations included determining the nanosized fraction, the amount and size of residual fibers and the turbidity. TEM was also performed to obtain high resolution images at nanometer level of the TO-CNF quality.

The results from the characterization of the TO-CNF sample summed up in Table 2 shows that the sample contained both nanosized fibrils as well as fiber residues. This was expected, both due to the results obtained during the specialization project, as well as the fact that generally, fibrillated cellulose samples will contain nanofibrils, fibrillar fines, fiber fragments and fibers [41]. Still, the estimated residual fiber fraction of 2.4% indicated that most parts of the CNF suspension consisted of nanofibrils, which also was confirmed by the low average particle area.

A.7.5 Example calculation

Nanosized fraction
The nanosized fraction is calculated as the ratio between the dry matter, %DM, of the supernatant after centrifugation and before centrifugation. The %DM can be calculated as shown in Equation (16), where M_f is the weight of the aluminium petri dish and the solid material after heating over night at 105°C, while M_i is the weight of the aluminium petri dish and the added sample before heating. M_p is the mass of the aluminium petri dish. The values measured for one of the parallels are used in the calculations to exemplify.

$$\%DM = \frac{M_f - M_p}{M_i - M_p} \cdot 100 = \frac{1.1815g - 1.1761g}{21.9584g - 1.1761g} \cdot 100 = 0.026 \tag{16}$$

By measuring the %DM before and after centrifugation, the nanosized fraction in percent, $\%NF$, can be calculated as shown in Equation (17), where $\%DM_a$ is the calculated dry matter after centrifugation, and $\%DM_b$ is the calculated dry matted before centrifugation. The %DM of 0.026% calculated above was the dry matter before centrifugation for one of the parallels. The %DM after centrifugation was equal to 0.011%.

$$\%NF = \frac{\%DM_a}{\%DM_b} \cdot 100 = \frac{0.011\%}{0.026\%} \cdot 100 = 42.3 \tag{17}$$

A.8 Effect of dipping films in NaOH

FTIR was used to evaluate the grafting of βCD to the TO-CNF material. When using FTIR, it is important to keep in mind that the infrared bond positions of the carboxylic acid group and ester group are close to one another. In order to see the contribution of the carboxylic acid group at the infrared band position of the ester group (around 1740 cm^{-1}), films were analyzed both before and after dipping in NaOH. The NaOH dipping was conducted to convert the carboxylic acid groups to carboxylate groups, as acid had been added during the film-production in order to initiate the esterification reaction.

Figures showing the effect of dipping films in NaOH prior to FTIR analysis for film 'onestep-surface/100C/V' and 'twosteps-surface/100C/V' are included in figure 63 and 64. These films have been produced through the surface grafting method by the use of fumaric acid as a crosslinker in one and two steps, respectively.

As can be seen from Figure 63 and 64, the films show a decrease in the peak around 1740 cm^{-1} while the peaks around 1600 cm^{-1} increased after dipping in NaOH. As 1600 cm^{-1} is around the infrared band position of the carboxylate group, it is expected that the 1600 cm^{-1} peak increases when the 1740 cm^{-1} peak decreases.

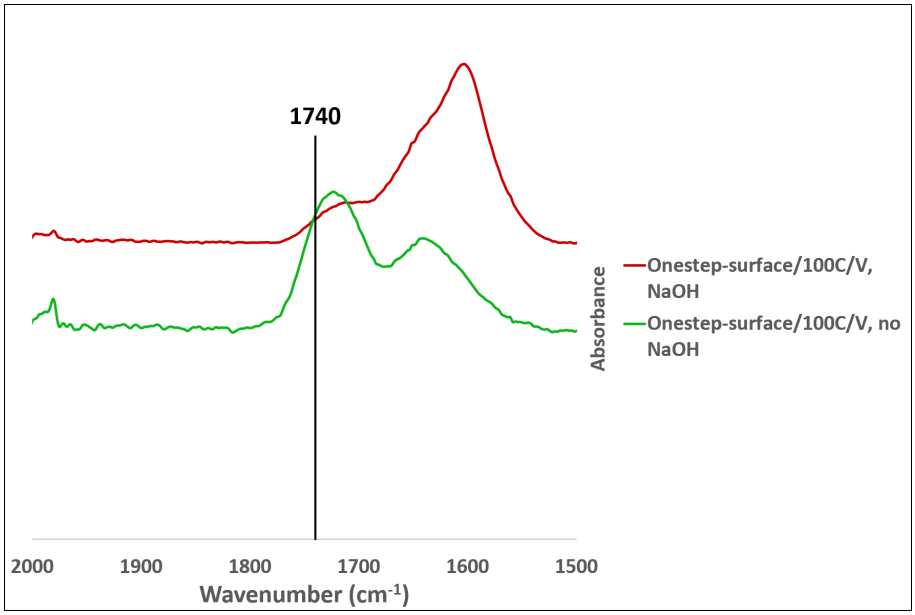

Figure 63: FTIR spectra before and after NaOH dipping for film onestep-surface/100C/V. The red curve has been dipped in NaOH, while the green curve has not.

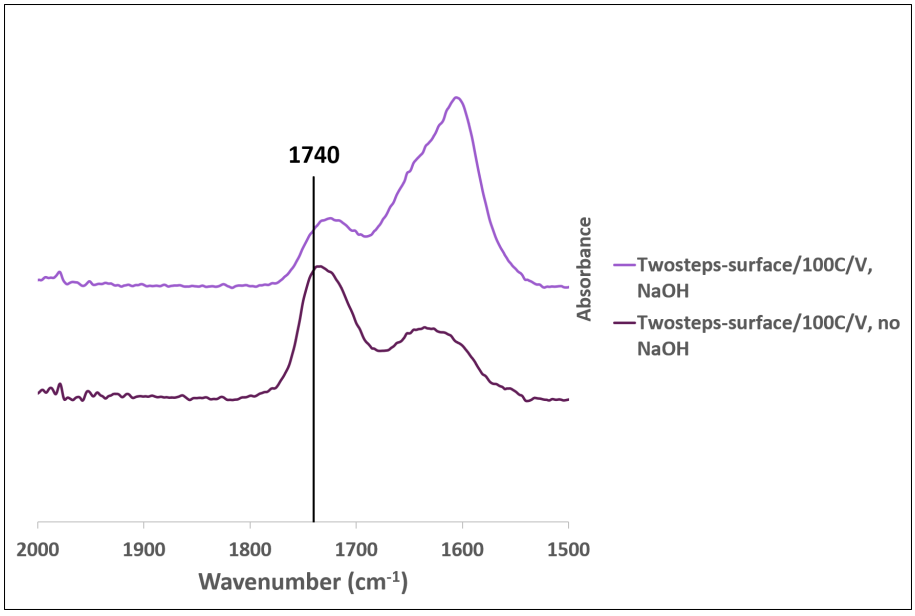

Figure 64: FTIR spectra before and after NaOH dipping for film twosteps-surface/100C/V. The upper curve shows the film after dipping in NaOH, while the bottom curve presents the film without NaOH.

Martha Grøndahl

Cytocompatibility and Functionalization of Nanocellulose for Bone Tissue Engineering Applications

NTNU
Norwegian University of
Science and Technology

PFI
PART OF RI.SE